

https://dspace.org/

Structural analysis and geological modelling of a stratiform copper-cobalt deposit at Konkola, Central African Copper Belt, Zambia

Mulonda, Sitwala

2024

https://hdl.handle.net/10539/37455

Downloaded from a DSpace repository. https://dspace.org/



NAME: SITWALA MULONDA

STUDENT NUMBER: 2018796

MSc ECONONIC GEOLOGY

Research Report

Structural Analysis and Geological Modelling of a Stratiform Copper-Cobalt Deposit at Konkola, Central African Copper Belt, Zambia

University of the Witwatersrand, Johannesburg

School of Geosciences

SENATE PLAGIARISM POLICY

Declaration by Students

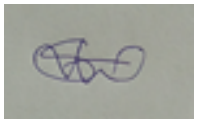
I Sitwala Mulonda (Student number: 2018796) am a student registered for _Master of Science in Economic Geology CW/RR in the year 2023. I hereby declare the following:

I am aware that plagiarism (the use of someone else's work without their permission and/or without acknowledging the original source) is wrong.

I confirm that ALL the work submitted for assessment for the above course is my own unaided work except where I have explicitly indicated otherwise.

I have followed the required conventions in referencing the thoughts and ideas of others.

I understand that the University of the Witwatersrand may take disciplinary action against me if there is a belief that this is not my own unaided work or that I have failed to acknowledge the source of the ideas or words in my writing.

Signature: _____ Date: _____14/06/2023_____

Abstract

The Konkola east mining block is one of the six mining blocks at Konkola mine owned by Konkola Copper Mines (KCM) in Chililabombwe Zambia. A structural analysis was carried out on the Konkola east mining block that assessed the main geological structures in the area and how they fit into the regional deformation history. The impact of the geological structures on short term mine planning was also assessed. The second part of this study involved creating a geological model and documenting the steps taken to create a workflow that can be applied to other parts of the mine.

Geological mapping was carried out on underground crosscuts and 23 boreholes were logged. Ten thin sections were studied using an Olympus BX53M/DP74 microscope. Old mine working plans containing historical geological information were scanned and digitized. A database was created and validated data was used to create a geological model of the ore bearing rock; the ore shale unit using Surpac mining software.

This study established that Konkola east has major normal faults striking north-south and low angle reverse faults striking east-west and sub- parallel to the regional fold axis. Parasitic folds were also identified. This configuration led to the interpretation of Konkola east as part of a larger dextral strike-slip fault system formed by north-south directed compression and east-west extension. Three main deformation phases were identified in this study and correlated with previous regional work. The earliest deformation resulted in the development of a bedding-parallel foliation due to burial. The second phase of deformation included the development of bedding parallel veins and the main folding event. The third phase involved the development of brittle structures including faults and three main joint sets. The main faults identified in this third deformation phase are thrust faults where the hangingwall block is observed to have moved up relative to the footwall block and normal faults where the hangingwall is observed to have moved down relative to the footwall.

These structures were found to have major implications for the short-term mining plan especially regarding ground stability and the mine hydrogeological environment. A geological model was successfully created and the total volume of the ore shale unit was estimated to be 1,032,199 m^3.

Acknowledgement

I would like to thank Konkola Copper Mines management through my line managers, Mr. Allam Kasanda (Manager Technical services), Mr. Kelvin Mwamba (Head of Geology- KCM) and Mr. Davy Mubita (General Manager Technical Services) for according me the opportunity to conduct this research. I would further like to acknowledge the input and guidance from my immediate manager, Mr. Jasper Manyika (Konkola Head of Geology department). My supervisor, Professor Paul Nex is also greatly appreciated for the guidance throughout this study and whose lecture notes inspired this research.

Secondly many thanks go to Mr. Zifa Tembo (Head - Mineral resources) for immense support in various ways to ensure this study was successfully done. My colleagues at Konkola Copper mines, Luma Evans, Masinge Banda, Sakala Vincent and Musa Gama are thanked for both direct input and enlightening discussions around the research project. I'm also thankful to my parents, Joseph Mulonda and Dorothy Mulonda, my brother Bennie Mulonda and the rest of my family for the support.

Finally, special thanks go to my lovely wife Akemata Katebe for the support and encouragement throughout my studies.

Table of Contents

1. Contents

Abstract i

Acknowledgement ii

Table of Contents iii

List of Figures v

List of Tables viii

1 Introduction 1

1.1 Location and Research Area 1

1.2 Konkola East Mining Block 2

1.3 Research Problem 3

1.4 Aim 4

1.4.1 Objectives 4

2 Literature Review 5

2.1 Konkola Modelling History 5

2.2 Geology of the Zambian Copperbelt 5

2.2.1 Regional Geological Setting 5

2.2.2 Basement Complex 6

2.2.3 The Katanga Supergroup 7

2.2.4 Mineralization 7

2.2.5 Deformation 9

2.3 Local Geology of the Konkola Area 10

2.3.1 Stratigraphy of Konkola 11

2.3.2 Structure 14

2.3.3 Hydrogeological Setup 15

3 Methodology 16

4 Geology of Konkola East 20

4.1 Footwall Quartzite 20

4.2 Argillaceous Sandstone. 21

4.3 Porous Conglomerate 22
4.4 Footwall Sandstone 24
4.5 Footwall Conglomerate 25
4.6 Ore Shale Unit 26
5 Petrographic Analysis 28
5.1 Description of the Footwall Conglomerate Under cross polarized and under plane polarized light. 28
5.2 Description of the Footwall Conglomerate under reflected light Microscopy 30
5.3 Description of Ore Shale Under Cross polarized and transmitted light Microscopy. 31
5.4 Description Ore Shale Unit Under reflected light microscopy 32
6 Structural Elements of Konkola East. 34
6.1 Bedding and Foliation 35
6.2 Folds 38
6.3 Faults 40
6.4 Joints 45
6.5 Structure and Mineralization 47
7 Geological Modelling of Konkola East 49
7.1 Available Data 49
7.2 Data Validation 49
7.3 Modelling Process 50
7.4 Model Results 52
7.5 Model validation 54
8 Discussion 55
8.1 Deformation history 56
8.2 Geotechnical Implications 57
9 Conclusion 61
10 Recommendations 62
11 Bibliography 63
12 Appendices 66
12.1 Appendix A: Konkola structural Mapping data for Konkola 66
12.2 Appendix B: Part of the collar table used in the database 78
12.3 Appendix C: Part of the survey table used in the database creation 79
12.4 Appendix D: Part of the geology table used in the database creation 80

12.5 Appendix E: Validation report for the geology table 81
12.6 Appendix F: Volume report of the ore shale in each block modeled 82
12.7 Appendix G: Validation report of the created solids for the ore shale lithology 83

List of Figures

Figure 1-1: Map of Africa and Zambia showing the location of Konkola mine, Chililabombwe, Copperbelt province(Konkola Copper Mines, 2020a) 1
Figure 1-2: Plan view of the Konkola deposit from surface showing the Konkola East mining block and other mining blocks with their resource schedule (Konkola Copper Mines, 2020b) 2
Figure 1-3: 3D view of the mine development (Excavations) in Konkola east 2520mW retreat showing the areas which were mapped in this study. The upper level 760 ml is shown in blue and the lower level, 780 ml is shown in pink color. 3
Figure 2-1: Simplified geological maps showing the tectonic setting and structural architecture of the Lufilian arc (Selley et al., 2005) 6
Figure 2-2: Lithostratigraphy of the Zambian Copperbelt showing the distribution of copper-cobalt mineralization (Selley et al., 2005). The figure also shows the stratigraphic position of the Copperbelt Orebody Member (highlighted in red) 8
Figure 2-3: Generalized geological Map of the Zambian Copperbelt showing the Kafue anticline as the dominant structure (Hitzman et al., 2012). The numbers, 1 to 34 denote the numerous deposits of the Zambian Copperbelt. Konkola deposit, the study area is represented by the number 20. 9
Figure 2-4: South to north cross section across the Lufilian arc showing the four subdivisions including the domes region where Konkola east lies (Zientek et al., 2010) 10
Figure 2-5: Geological Map of the Konkola area also showing the location of Konkola East.(Konkola Copper Mines, 2013) 11
Figure 2-6: stratigraphic column for Konkola Mine also showing the part of the stratigraphy that is exposed by mine developments at Konkola east (Greyling, 2009) 13
Figure 2-7: Map of structural elements associated with the Konkola ore deposit showing the surface trace of the Krilabombwe anticline (Torremans et al., 2012) 14
Figure 3-1 Microstation (dgn) mine plans of Konkola East mining block showing the two levels which were mapped during this study. (a) 760mL showing the mine development in relation to the general strike (b) 780mL showing the mine development in relation to the general strike. 16
Figure 6-2:Location of some of the boreholes used in this study shown in plan-view on underground working levels. (a) 760 mL showing the collar position and orientation of some of the boreholes drilled on this level. (b) 780 mL showing boreholes drilled on this level and used in this study. Samples for petrographic analysis were gotten from BPN 881 and BPN 881. 18
Figure 6-3: Scanned plan of (a) 1850 ft. level plan and (b) 2340 ft. level plan showing the geological structures which were digitized. 19
Figure 4-1: Geological map of Konkola East showing the major lithologies and structural features of Konkola east. The area was subdivided into 3 zones, Zone A, Zone B and Zone C based on the average dip and strike of the bedding of the Ore Shale Unit (red). 20
Figure 4-2: Underground picture showing massive and jointed Footwall Quartzite. 21

Figure 4-3: Underground picture of Argillaceous Sandstone exposure showing argillite bands interbedded with sandstone. The picture was taken from 760mL, 2400mW (Figure 1-3) crosscut facing north. 22
Figure 4-4: Underground picture taken from 2400mW crosscut facing east showing the Porous Conglomerate with malachite staining along the joints. 23
Figure 4-5: Underground picture showing the contact between the Porous Conglomerate and the Footwall Sandstone. Note pen for scale. Picture taken on 780 mL, 2400 MW crosscut (Figure 1-3). 24
Figure 4-6: Underground face mapping. 760mL 2400mW access to orebody showing the top part of the Footwall Conglomerate where it makes contact with the Ore Shale unit. This contact is also called the Geological Footwall (GFW). 25
Figure 4-7: Underground picture from 2400mW showing distinct bedding in the Ore shale Unit. 26
Figure 4-8: Hand specimen of the Ore Shale Unit showing bornite mineralization occurring in layer parallel veins 27
Figure 5-1: Core samples showing where the photomicrographs discussed in this chapter were prepared from. (a) SM 02 sample of footwall conglomerate from borehole BPN 881 (b) SM 04 sample of the Ore Shale Unit. 28
Figure 5-2: Photomicrographs of the footwall Conglomerate, SM02 showing sinusoidal mica. (A) Viewed under cross polarized light. (B) Viewed under plane polarized light. 29
Figure 5-3: Photomicrograph of SM 02 (Footwall conglomerate) viewed under reflected light showing chalcocite (whitish grey) being replaced by malachite (green) along the grain boundaries. 30
Figure 5-4: Photomicrograph of SM 04 as observed under (a) cross polarized light and (b) plane polarized light. Ore minerals appear dark in both cross polarized light and plane polarized light and occur mainly along layers. 31
Figure 5-5: Photomicrograph of SM 04 viewed under Reflected light showing the major ore minerals being bornite (pinkish brown), chalcocite (whitish grey) and chalcopyrite (yellow). In insert A in the bottom, chalcocite is observed to be replacing the relic bornite grains. 32
Figure 5-6 : Part of the photomicrograph (SM04), an extract from figure 8.3 showing textural relationship between bornite (BN), chalcocite (CC) and malachite (MLT) 33
Figure 6-1: Eastern Sidewall mapping of 2400mW showing the lithologies and joints observed in the cross cut. Two drives, hanging wall drive (HW/DR) and foot wall drive (FW/DR) are shown by the dotted lines. 34
Figure 6-2: Geological map of 780 ml produced after mapping the mining excavations. 34
Figure 6-3: (A) 780mL 2400mw pillar cross cut 6 showing the S_1 fabric strongly developed in the ore shale and the fairly to poorly developed S_2 fabric. (B) Strongly developed S_1 fabric in ore shale as observed in core. 35
Figure 6-4 : Cross polarized light thin section of SM 04 showing S_o/S_1 fabric and S_2 fabric shown by the elongation of sulphide minerals appearing black. The yellow line represents S_2 and the yellow arrows shows the elongation direction. 36
Figure 6-5: Lower hemisphere Stereo plots of S_1 on the 3 zones identified as shown in Figure 7-1 36
Figure 6-6: Photomicrograph SM 02, of the footwall conglomerate viewed under plane polarized showing mica fish developed and interpreted as a shear sense indicator of a left lateral shear. 37
Figure 6-7: Schematic map of the Kirilabombwe anticline (not to scale) showing the location of Konkola east and the parasitic fold along the main fold. 38
Figure 6-8: A relatively open fold observed from borehole BPN 881. 39

Figure 6-9: Folds observed in core logged. (a) Ore shale with well moderately open parasitic fold. Two generations of folds are observed here. F1 fold is refolded in folding event F2. (b) Folding observed in ore Hangingwall quartzite. (c) Folds in highly weathered ore shale unit with malachite mineralization (d) moderately open to tight folds developed in ore shale unit with chalcocite mineralization. 39
Figure 6-10: 780mL geological map showing the major structures and the ellipse demonstrating zones of extension and zones of compression 40
Figure 6-11: High angle faults observed in Konkola east. (a) Steep reverse fault with a releasing bend (circled in red) observed facing east. (b) A normal fault with a restraining bend (circled in red) as observed on the 2400mW pillar cross cut 3 facing northwest. 41
Figure 6-12 Mapped fault zones from underground. (a) Minor fault zone with a reverse shear sense and minor displacement. (b) Medium sized fault zone with a normal shear sense and displacement above 5 meters. 42
Figure 6-13: Observed brecciated Fault zone in DVN 1592 with relatively low intensity of cataclasis. 43
Figure 6-14: Underground photo from 2400mW Konkola east showing a normal fault with relatively high intensity of cataclasis. 43
Figure 6-15: Minor fault structures observed at Konkola East. (a) Minor strike slip fault observed in BPN 893. (b) Slickensides observed in a quartz filled faulting surface. Kinematic analysis on this site based on the smoothening direction indicated the fault to be a low angle reverse fault . (c) Slickensides observed along bedding planes in BPN 883. This confirmed the existence of bedding concordant faults that contributed to creation of saddles. (d) A fault indicated by a sharp contact between the oreshale Unit and the footwall sandstone. In this borehole and at this site the footwall conglomerate is missing indicating a stratigraphic gap caused by faulting. (e) Minor normal fault observed from BPN 876. 44
Figure 6-16 Jointing pattern in Konkola East. (a) General map showing the location of Konkola east. (b) Underground photo showing the relationship between S1 and J1. (c) Geological map of Konkola East showing the general trend of the identified major joint sets, J1, J2 and J3. (d) Underground picture showing the Orientation of J3 and J2 in relation to the bedding parallel S1. 45
Figure 6-17: Lower hemisphere plot of the orientation of the established joint sets. 46
Figure 6-18: Photo from BPN 891 showing crescentic saddles created through flexural slip and hinge dilation through the folding process. Malachite mineralization is observed to be concentrated on the fold hinge. Schematic illustration done after(Cox et al., 1991) 47
Figure 6-19: Core photo from BPN 881 showing bedding discordant fault resulting from flexural slip on one limb that goes through and breaks across the fold hinge. Schematic illustration done after (Cox et al., 1991) 48
Figure 6-20: Grade maps showing grade in relation to the four major faults modelled on 609m level elevation. The circled areas show range associated with the faults. 48
Figure 7-1: Workflow followed in generating the short term geological model. 50
Figure 7-2: Surpac plan view of 780 m level showing the 4 blocks and the 4 major faults. The lines indicate lithological contacts. 51
Figure 7-3: Plan view of the created geological model showing the four faults and the 4 blocks. 52
Figure 7-4: Section along A-A' showing the four major faults identified in the study and the ore shale lithology 53
Figure 7-5: Isometric view of the created model facing south-west the four main faults identified (in brown) and the ore shale unit lithology in red. 53

Figure 7-6 : Random section of the created model used for validation purposes showing the ore shale lithology displaced in a normal way along fault 1. 54
Figure 8-1: Structural pattern of Konkola East compared to the expected structural pattern of a typical dextral strike slip fault. (a) structural pattern observed and mapped at Konkola east in this study. (b) Structural pattern of a typical dextral strike slip fault (Eggers, 2016) 55
Figure 8-2: Cross section view (facing east) illustrating formation of wedge failure as a result of the interaction of the bedding planes and the joint orientation. 58
Figure 8-3: Picture of rock dislodged due to wedge failure on 760mL 2400mW access to the ore body. . 59
Figure 8-4: Picture of an underground mine accident that involved fall of ground (rock fall) in weak zones attributed to geological structures. 60

List of Tables

Table 1: Hydro stratigraphy of Konkola ((Konkola Copper Mines, 2020a) 15
Table 2: Borehole collar information for Konkola East boreholes logged for this study. (Local mine coordinates) 17
Table 3: Range of joint spacing per lithology in Konkola East 46
Table 4 : Available data that was used in the creation of the short-term geological model..... 49
Table 5: Table showing major deformation events noted in Konkola east and correlated to other previous work done on a regional scale. Modified after (Kampunzu and Cailteux, 1999)..... 57

1 Introduction

A structural analysis followed by geological modelling was carried out at Konkola East at Konkola mine. Konkola East is one of the 6 mining blocks at the Konkola Mine in the Central African Copperbelt of Zambia. The study focused on understanding the structural configuration of the area and the implications on short term mine planning. The influence of the geological structures on the geotechnical and hydrogeological conditions are closely looked at.

1.1 Location and Research Area

Konkola mine is located in the border town of Chililabombwe in the Copperbelt province of Zambia in Central Africa (Figure 1-1). Chililabombwe is accessed by the Great North Road from the capital Lusaka.

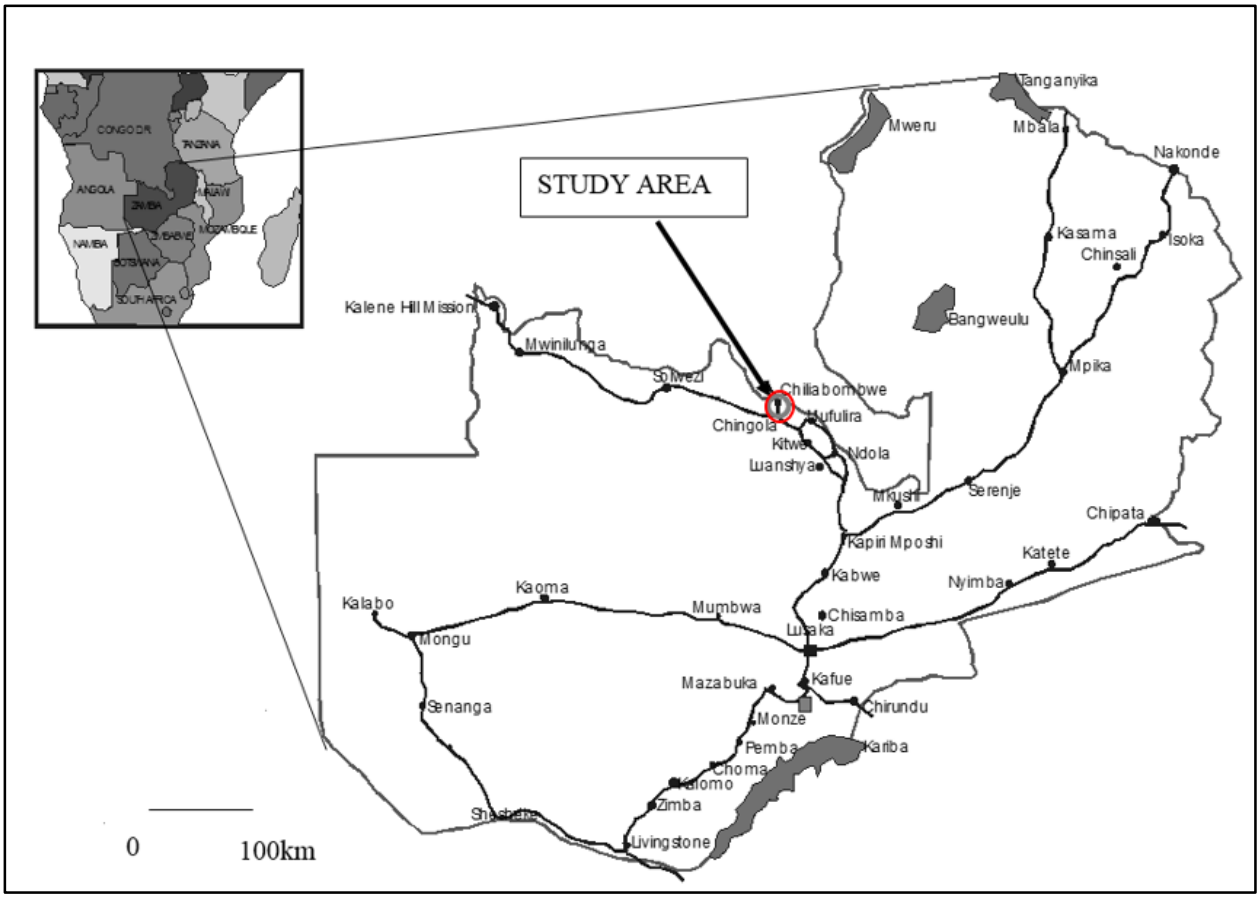


Figure 1-1: Map of Africa and Zambia showing the location of Konkola mine, Chililabombwe, Copperbelt province(Konkola Copper Mines, 2020a).

The Konkola deposit is located in the eastern part of the Zambian Copperbelt. The Zambian Copperbelt is part of the Central African Copperbelt which is the richest and largest known sediment-hosted copper province (Brems et al., 2009). Konkola is a high grade copper-cobalt deposit with grades averaging 3.6 wt% Cu (Torremans et al., 2013). The mine is owned and operated by Konkola Copper Mines (KCM) and is exploited using three shafts (1, 3, and 4). The mine is further subdivided into six mining blocks; Bancroft

deeps, Bancroft central, Bancroft North, Konkola Extension, Konkola Flats and Konkola East. This study focuses on the Konkola East mining block located on the northern limb of the Konkola deposit (Figure 1-2).

1.2 Konkola East Mining Block

The Konkola East mining block is located in the north-eastern part of the Konkola deposit (Figure 1-2). It makes up almost the entire northern limb of the Kirilabombwe anticline. It stretches from 0 meter west (mW) to 4000 meter west (mW), a total strike length of approximately 4 km. With an estimated resource of over 2 million tonnes (Konkola Copper Mines, 2020b) contained copper, Konkola east is largely seen as the future of Konkola mine.

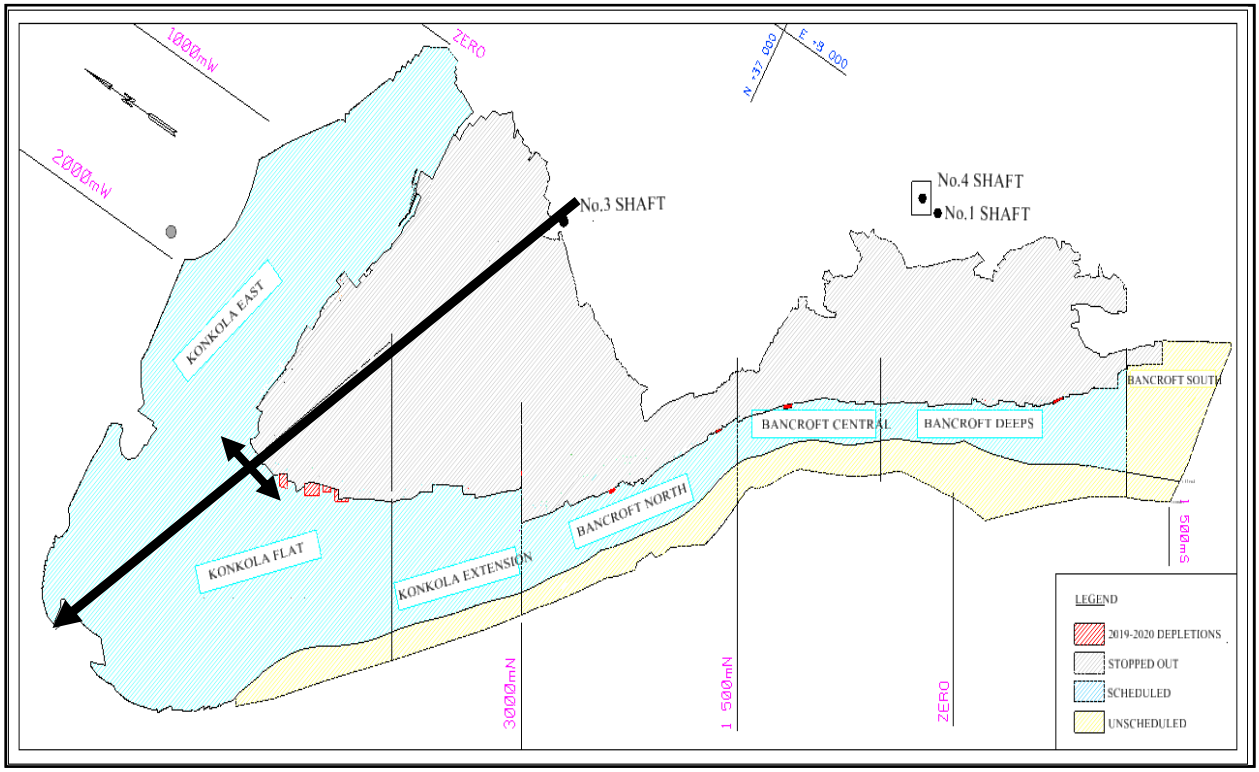


Figure 1-2: Plan view of the Konkola deposit from surface showing the Konkola East mining block and other mining blocks with their resource schedule (Konkola Copper Mines, 2020b)

Mining in the study area has been carried out down to the 800 m level below the surface. However, this study focused on orebody exposures on the 760 m and 780 m depth levels (Figure 1-3). On these two levels, Mechanized Sublevel Open Stopping (MSLOS) and Post Pillar Cut and Fill (PPCF) are the two main mining methods used. The PPCF mining method is used around the hinge zone where the ore body is shallow dipping and has a relatively thicker apparent thickness. In the area where the orebody is steeper (above 45˚ dip), the MSLOS mining method is used. The two mining methods both involve the mining of cross cuts across the strike of the orebody at intervals of 7 m (PPCF) and 30 m (MSLOS) (Figure 1-3). There are also drives mined along the strike of the ore body. One orebody drive is mined in the MSLOS and two or more ore body drives in the PPCF depending on the apparent thickness of the orebody. The cross cuts

and hanging wall drives mined using these two mining methods allowed for detailed geological mapping to be carried out.

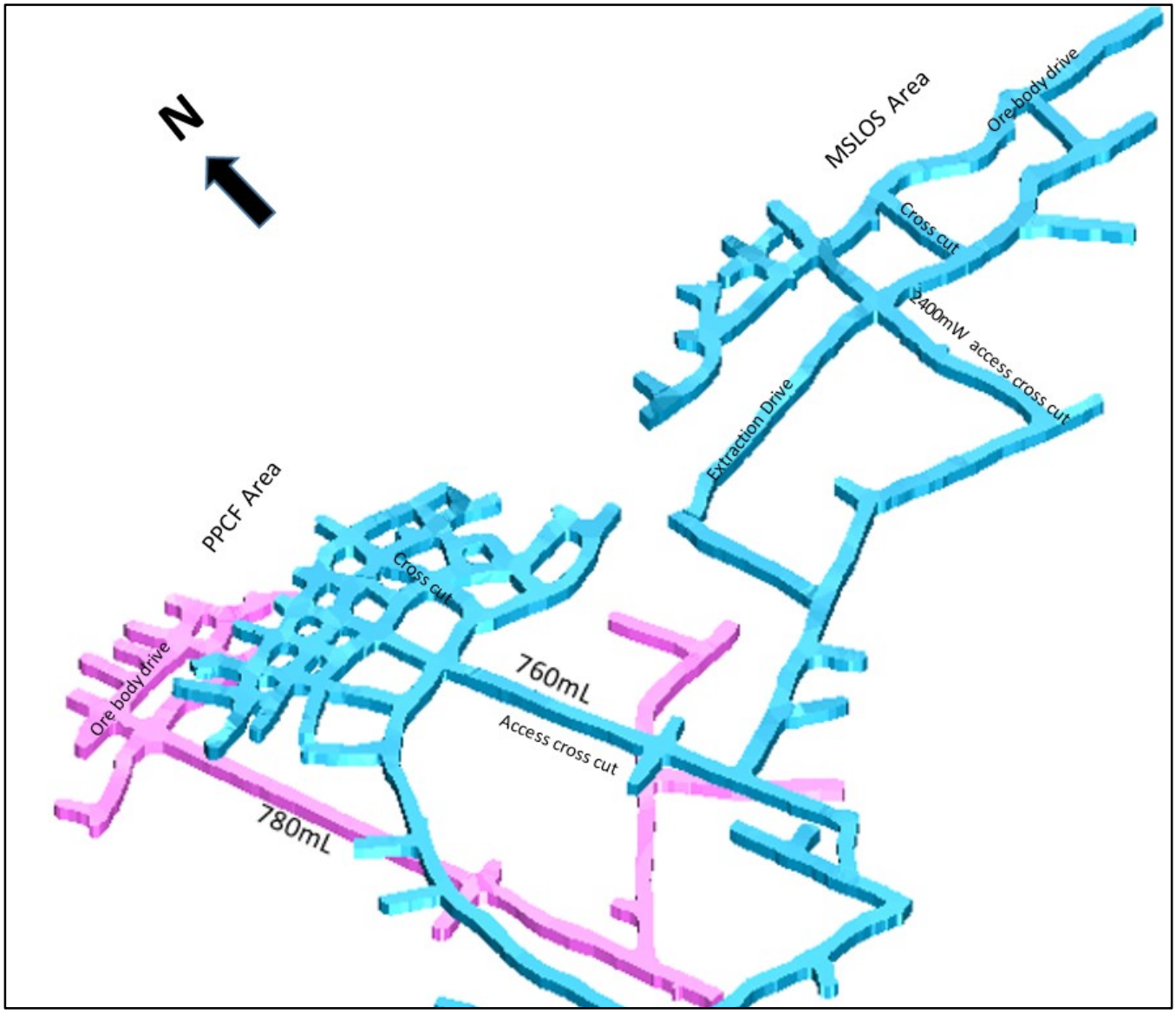


Figure 1-3: 3D view of the mine development (Excavations) in Konkola east 2520mW retreat showing the areas which were mapped in this study. The upper level 760 ml is shown in blue and the lower level, 780 ml is shown in pink color.

1.3 Research Problem

A good understanding of the geological and structural configuration of any mine is a prerequisite to economical and safe mining. Konkola mine which includes Konkola East currently operates with a long term three dimensional (3D) geological model. This model is updated annually and mainly used for the generation of annual resource model reports. However, the model lacks sufficient structural detail as it only captures lithological variation in terms of surfaces and also major faults and folds. Critical but relatively small scale geological structures are not part of this model. This data includes but is not limited to, major joint orientations, stope scale faults and folds. The current geological model therefore does not

sufficiently support the requirements of short term mine planning like grade control, stope delineation and prediction of weak ground conditions. Furthermore, the current model does not incorporate data generated on a day to day basis from mapping and drilling as it is currently only updated annually.

1.4 Aim

The aim of this research project is to investigate and evaluate the structural configuration of the Konkola East mining block at Konkola deposit and to generate a geological model that can be used for both short term and long term mine planning based on the results.

1.4.1 Objectives

- Conduct a detailed analysis of the structural configuration and deformation history of the Konkola East area.
- Identify geological structures that may influence geotechnical stability, hydrogeological conditions and overall short term mine planning.
- Generate a work flow and standard procedure for geological modelling that can be replicated in other parts of the mine.
- Produce a 3D geological model that can be used for both short term and long term mine planning.

2 Literature Review

Konkola mine has been exploiting the Kirilabombwe orebody from 1957 by underground methods through shaft 1 on the west limb and the north limb through shaft 3. In June 2006 KCM commenced sinking of the No. 4 shaft on the west limb of the Konkola deposit as part of the Konkola Deep Mining Project (KDMP).

Historically, the No 1 and 3 shafts have been managed separately. Underground haulages connecting the two mines were developed mainly for dewatering purposes and cross tramming. The separate treatment of the two mines was due to the presence of a barren gap in the orebody that physically divided the ore reserves. The barren gap extended from the surface down to about 720 meter level (mL) (Konkola Copper Mines, 2020a).

Currently mining is taking place from the number four shaft which accesses the orebody at a deeper level on the west limb and the number three shaft which extends its depth through the use of ramps on the north limb. The deepest levels at present are 1040 mL and 820 mL at number four shaft and number three shaft respectively.

2.1 Konkola Modelling History

The first geological model for the Konkola deposit was created in 1989 by MRDL led by Dr. Harry Parker. This was updated twice between 1990 and 1995. Upon take over by Anglo-American Corporation, the modeling work was taken over by the Mineral Resource Department of Anglo-American Corporation based in Johannesburg (MINRED) and a revised model update was done in 2001. In order to integrate geology and mine planning requirements, GEMS from GEMCOM was set up in September 2001. Thereafter there was a break in model updates with the changeover from ANGLO to Vedanta Resources (PLC). Upon takeover of KCM operations, Vedanta Resources (PLC) set an objective to produce a 3-D model that would form a foundation for a dynamic mine planning model that could be updated at more regular intervals using a set of macros / scripts to be developed as part of the modelling process. In 2011, SRK Consulting of South Africa completed the first 3D model (Konkola Copper Mines, 2013) which they subsequently updated in 2016 and used to inform the life of mine of the 2017/2018 financial year. The latest model update attempt was done in 2021 but did not pass the audits due to poor QAQC and poor honoring of primary data. These models were robust, dynamic and meeting their objective of supporting the life of mine plan but not the short term mine plan. Therefore, there was need to create short term geological models that will support the short term grade control models by incorporating stope scale geological structures.

2.2 Geology of the Zambian Copperbelt

The study area lies within the Central African Copperbelt which consists of the Zambian Copperbelt, the Congolese Copperbelt and deposits in the north west province of Zambia, together making up the world's largest and highest-grade sedimentary copper province (Hitzman et al., 2012).

2.2.1 Regional Geological Setting

The Konkola deposit lies within the Lufilian fold belt which is one of the Pan-African mobile belts separating the Congo and the Kalahari Craton (Figure 2-1). The Lufilian belt formed due to the late Neoproterozoic to early Phanerozoic collision, deformation and metamorphism of the precursor basin formed during a prior extensional phase (Muchez et al., 2010). It is a north-directed fold-and-thrust belt stretching for 700 km from the west to the south east with a width of more than 150 km (Cailteux et al.,

2005). Four distinct tectonic zones are present in the Lufilian fold belt, each exhibiting a unique deformation style (Muchez et al., 2010). These are from south to north: the Katanga high, the Synclinorial belt, the Domes region, and the External fold and thrust belt (Turlin et al., 2016). The Zambian Copperbelt is situated within the Domes region which attained a green schist to amphibolite facies metamorphic grade (Muchez et al., 2010).

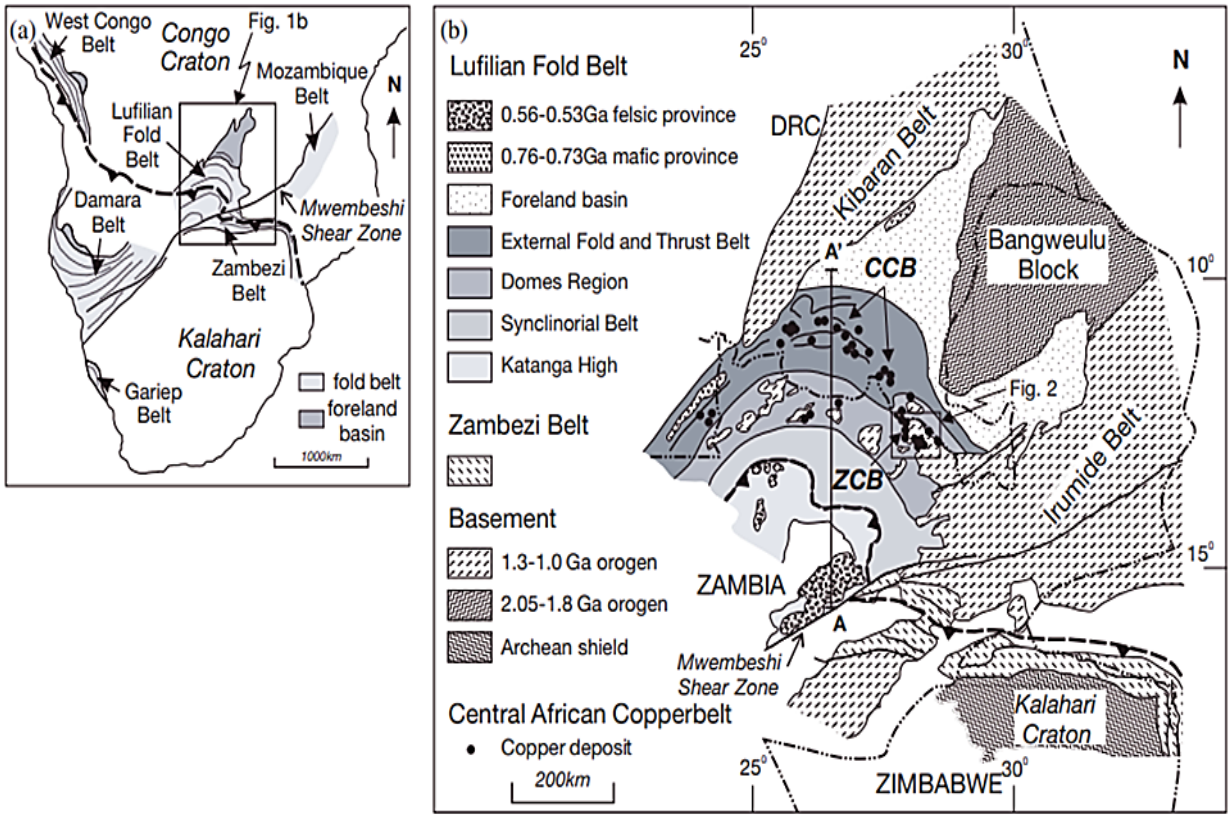


Figure 2-1: Simplified geological maps showing the tectonic setting and structural architecture of the Lufilian arc (Selley et al., 2005)

Three main tectonic events are noted in the Zambian Copperbelt (Hitzman et al., 2012). The earliest extension is linked to initial rifting along master faults which resulted in the formation of fault-controlled basins. A second rifting stage occurred during the period from the deposition of the upper portion of the Mwanshya Subgroup to the deposition of the lower Nguba Group and was associated with mafic magmatism. Subsequently the Lufilian orogeny led to basin inversion and compressive deformation and the attainment of green schist facies metamorphism (Hitzman et al., 2012).

2.2.2 Basement Complex

The basement strata consists of the Lufubu and the Muva Supergroups intruded by various pre-Katanga granites and they are exposed principally in the Kafue basement inlier and smaller surrounding inliers (Torremans et al., 2018). It comprises Archean to Mesoproterozoic reworked metagranites, migmatites

and metavolcanic and metasedimentary units and relatively weakly reworked metagranites (Selley et al., 2019). The Basement Complex is suggested to be at least of Eburnean age (McGowan et al., 2006).

2.2.3 The Katanga Supergroup

The Katanga Supergroup is a supracrustal sedimentary succession which is approximately 5-10 km thick (Cailteux et al., 2005). The earliest deposition of the Katanga Supergroup is constrained by the 883 ± 10 Ma age of the Nchanga Granite (Cailteux et al., 2005; Batumike et al., 2007; Twite et al., 2019). Most of the Katangan sediments were sourced from the Paleoproterozoic basement and the Nchanga granite (Master et al., 2005; Master, 2021). The Katanga Supergroup is sub divided into the Roan, Nguba and Kundelungu groups on the basis of two regionally correlative glaciogenic diamictites (Muchez et al., 2015).

The Roan Group which is just above the basement includes initial rift stage clastic rocks, post rift evaporitic carbonate rocks and second rifting stage clastic rocks and igneous mafic rocks (Hitzman et al., 2012). At the base of the Roan Group is the siliciclastic Mindola Subgroup which is overlain by the Kitwe Subgroup formed by a mixed association of siliciclastic and carbonate strata containing the Ore Shale Formation (Master, 2021)(Figure 2-2). This abrupt transition from continental to marine conditions marked by the Ore Shale Formation is inferred to have occurred in response to linkage of a subset of the pre-existing normal faults connected to master structures (Bull et al., 2011).The Upper Roan Supergroup contains platform carbonates which are stratiform to discordant and also breccias which are most likely after evaporite dissolution. This is overlain by the Nguba Group, which contains the glaciogenic Grand Conglomerate at its base which is a regional marker throughout the Central African Copperbelt. On top of the Nguba Group, another glaciogenic unit, the Petit Conglomerate marks the beginning of the Kundelungu group (Hitzman et al., 2012). Sedimentary characteristics of the rocks of each of these groups indicate a widening of the basin due to extension (Cailteux et al., 2007).

2.2.4 Mineralization

In the Eastern Zambian Copperbelt most major deposits are hosted within the lower Roan Subgroup (Turlin et al., 2016). The deposits are stratiform and are differentiated into argillite-hosted and arenite-hosted deposits. Argillite-hosted deposits occur mostly in carbonaceous dolomitic siltstones and shales while arenite-hosted deposits occur both in the hanging wall and footwall of the ore shale unit (Figure 2-2).

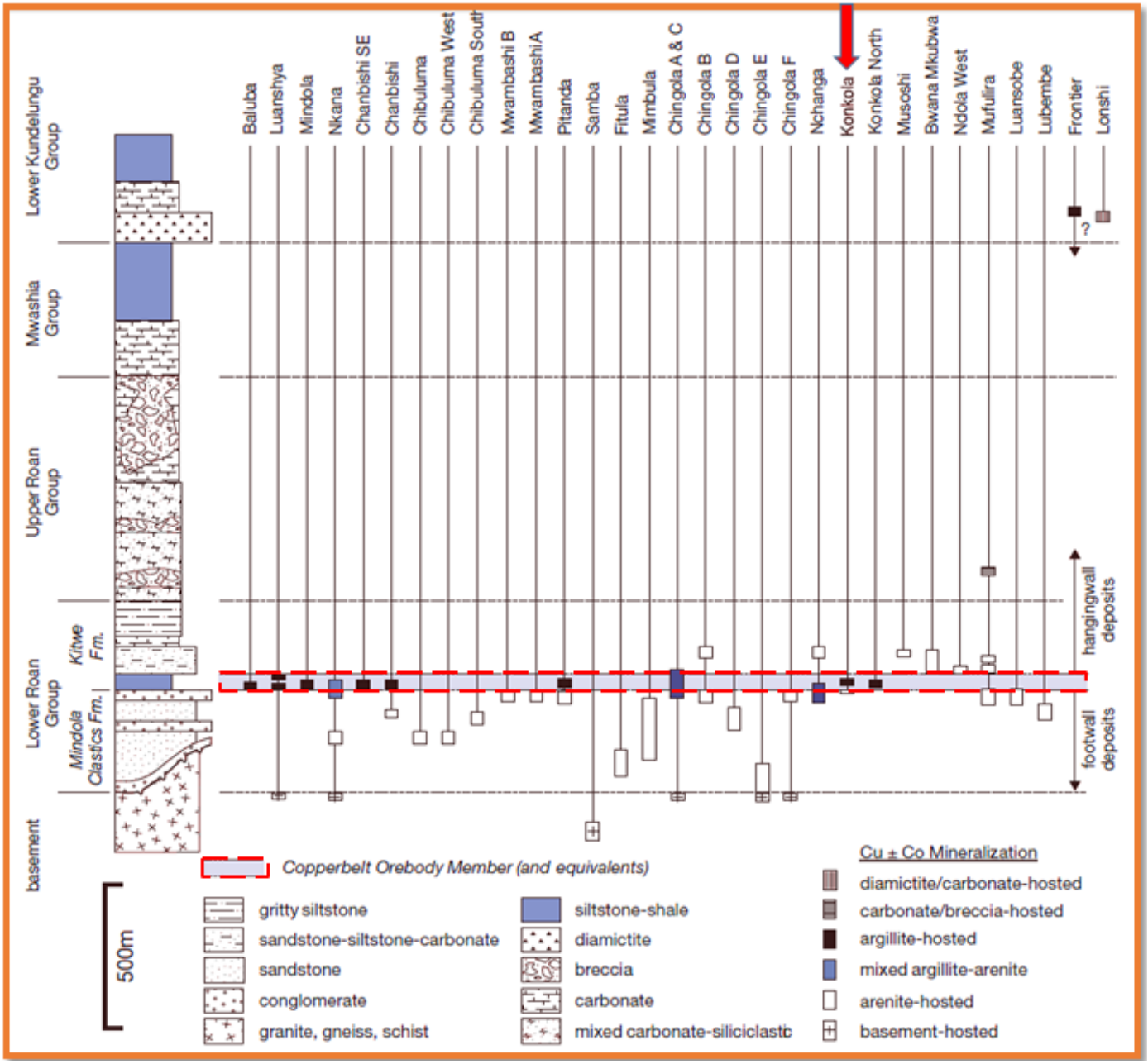


Figure 2-2: Lithostratigraphy of the Zambian Copperbelt showing the distribution of copper-cobalt mineralization (Selley et al., 2005)*. The figure also shows the stratigraphic position of the Copperbelt Orebody Member (highlighted in red).*

Generally, argillite-hosted deposits tend to have a longer strike length compared to arenite-hosted deposits (Hitzman et al., 2012). The shape, size and distribution of the deposits is highly influenced by the sub-basin fault architecture and the presence of reductants (Hitzman et al., 2012). The Konkola deposit, shown as deposit 20 in Figure 2-3 is argillite-hosted and part of the shale belt.

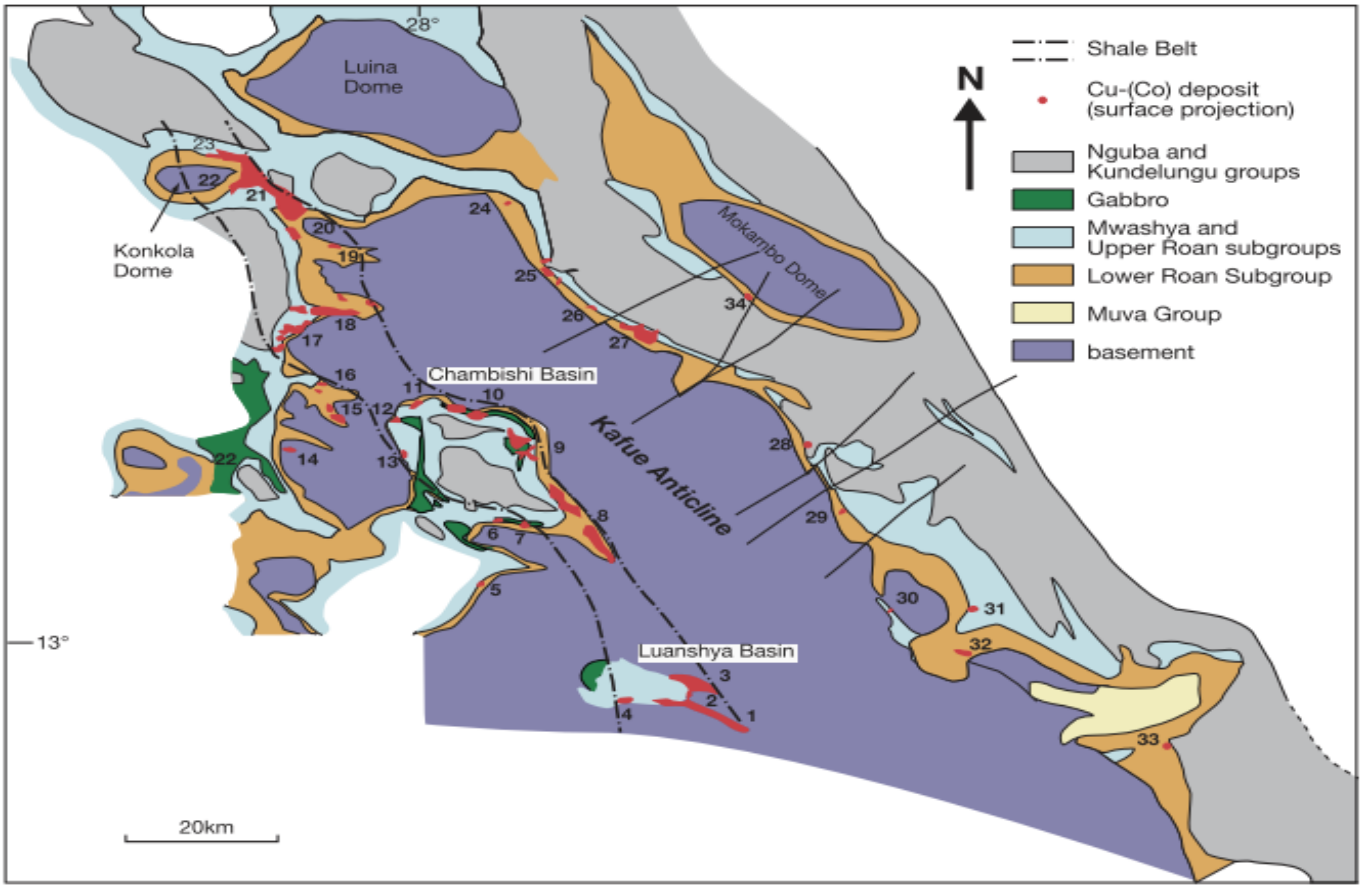


Figure 2-3: Generalized geological Map of the Zambian Copperbelt showing the Kafue anticline as the dominant structure (Hitzman et al., 2012). The numbers, 1 to 34 denote the numerous deposits of the Zambian Copperbelt. Konkola deposit, the study area is represented by the number 20.

2.2.5 Deformation

The Konkola deposit lies within the domes region of the Lufilian arc. The Lufilian arc formed from the deformation of the Katanga Super group by collision of the Congo craton and the Kalahari craton during the assembly of Gondwana (Master, 2021). The domes region is one of the four distinct tectonic zones with others being the Katanga high, the synclinorial belt and the external fold and thrust belt (Figure 2-4).

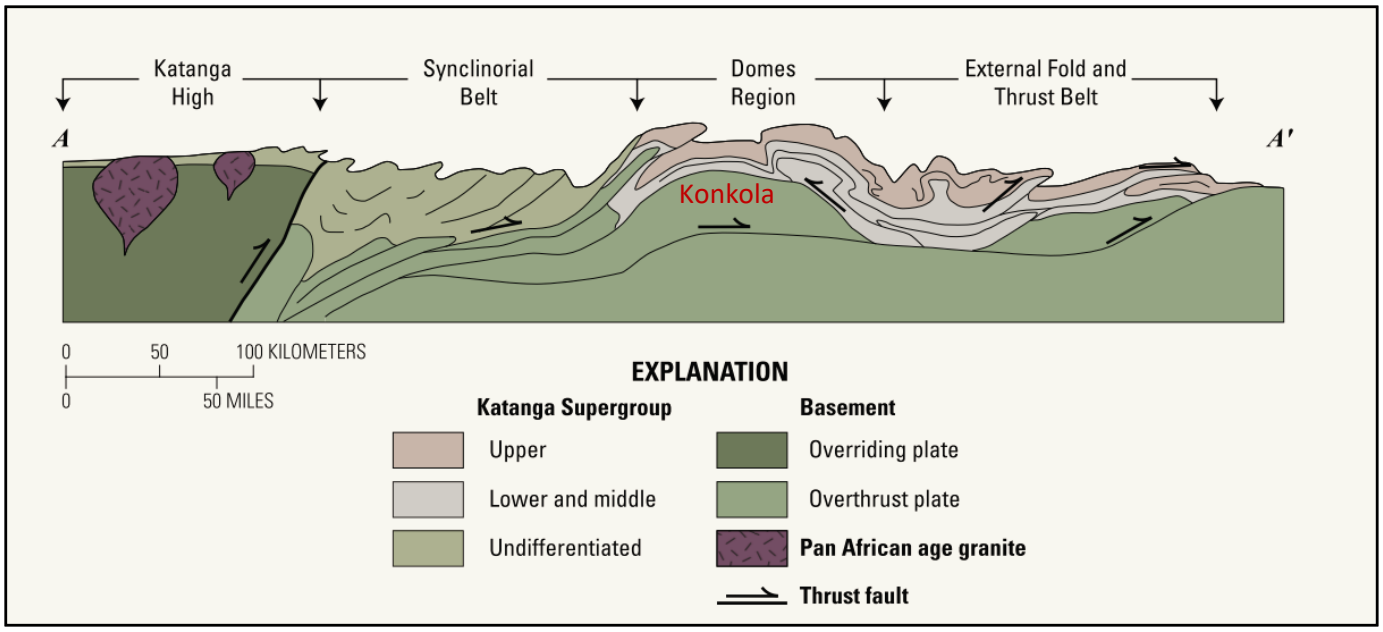


Figure 2-4: South to north cross section across the Lufilian arc showing the four subdivisions including the domes region where Konkola east lies (Zientek et al., 2010).

The Domes Region is characterized by thick- to thin-skinned tectonics. It is made up of basement domes that represent culminations on top of thrust ramps and granitoid bodies that probably intruded late to post orogenesis (Jackson et al., 2003). The exposed basement domes are generally aligned west to east. These domes include the Kabompo, Mwombezhi, Solwezi and Luswishi Domes and the Kafue Anticline where the Konkola deposit is located (Koegelenberg et al., 2019).

2.3 Local Geology of the Konkola Area

Formerly known as the Bancroft deposit, the Konkola deposit is a high-grade copper-cobalt (average 3.6 wt% Cu) argillite-hosted deposit with a strike length of more than 10 km (Torremans et al., 2013). Also known as the Konkola deep, it is part of the Konkola-Musoshi deposit that also includes Konkola North and Musoshi in the DRC (Hitzman et al., 2012) which straddles the Zambia-DRC border. It is made up of several orebodies which were previously thought to be separate but now understood to be continuous making it the single largest deposit in Zambia (Hitzman et al., 2012). This study focuses only on the Konkola deposit (Konkola deep) which is draped around the Kirilabombwe anticline (Figure 2-5).

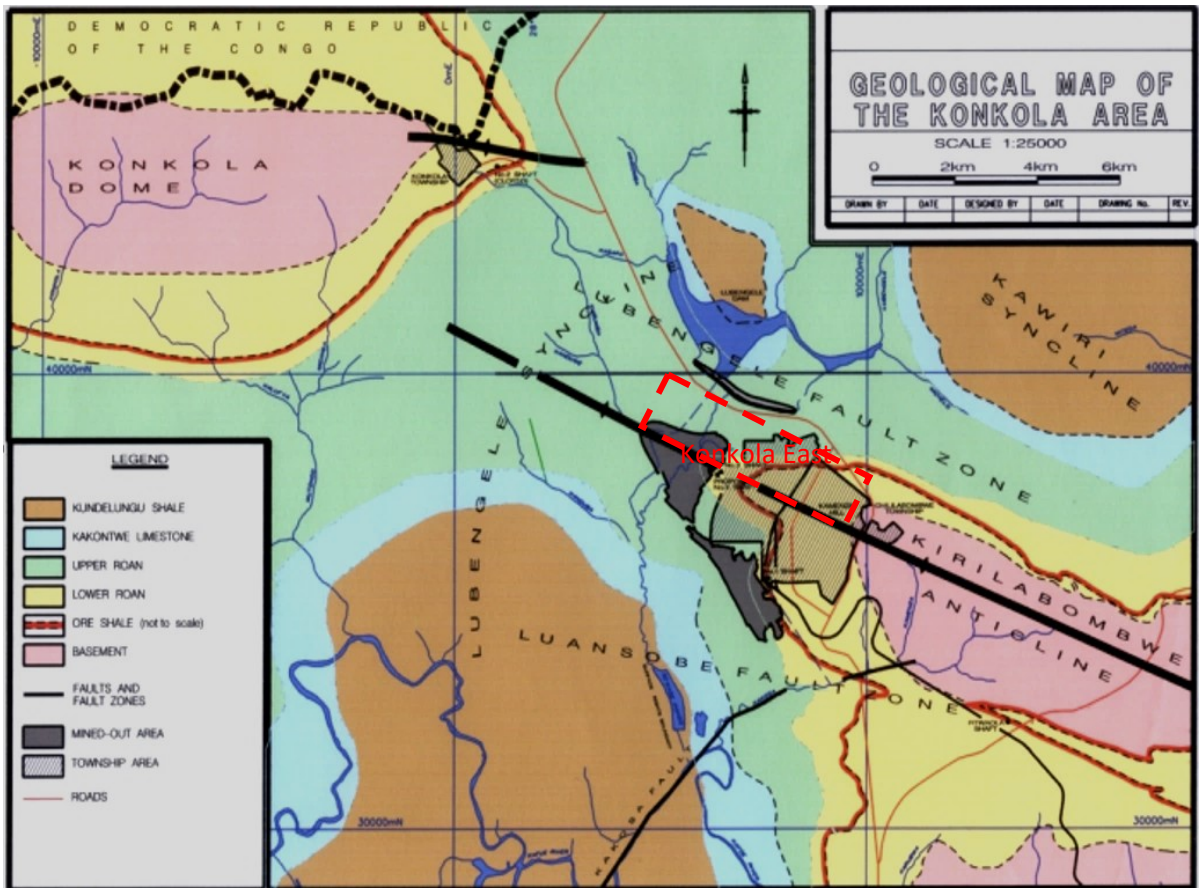


Figure 2-5: Geological Map of the Konkola area also showing the location of Konkola East.(Konkola Copper Mines, 2013)

2.3.1 Stratigraphy of Konkola

Konkola mine is located on the western limb of the Kafue Anticline which consists of rocks of the Basement Complex as the lowest unit which is uncomformably overlain by Roan Group, Nguba and Kundelungu sediments as shown in Figure 2-6.

2.3.1.1 Basement Complex

The oldest rocks in the area are the Proterozoic basement rocks of the Kirilabombwe dome (Figure 2-6) that form the core of the Kirilabombwe anticline. The Basement Complex comprises schists, gneisses, quartzites and granites intruded by the Muliashi Porphyry.

2.3.1.2 Katanga Supergroup

The Katanga Supergroup rocks lie uncomformably above the basement rocks and have been deformed together with the basement rocks (Torremans et al., 2013). The lowest formation of the Katanga Supergroup at Konkola is the Boulder Conglomerate (Figure 2-6). It is a coarse-grained boulder conglomerate, with the boulders comprising quartz and granite. It is vuggy and loosely cemented.

The Boulder Conglomerate is overlain by the Pebble Conglomerate. It is a coarse quarzitic conglomerate which is well-cemented. At the top, it is leached and porous. This top part is locally referred to as the

Lower Porous Conglomerate (Konkola Copper Mines, 2020b). Overlying the Pebble Conglomerate is the Footwall Quartzite. It consists of massive cross-beds, grey, medium grained quartzite with minor grits and arkose, with occasional bands of conglomerate. The Argillaceous Sandstone, a well-bedded sandstone with argillite intercalations overlies the Footwall Quartzite. It is greyish in color and has a medium-grained texture.

Overlying the Argillaceous Sandstone is the Footwall Aquifer Formation which comprises the Porous Conglomerate, the Footwall Sandstone and the Footwall Conglomerate. The Footwall and Porous Conglomerates both consist of pebbles of feldspar, quartzite and granite material imbedded in a fine-grained, grey feldspathic quartzite matrix. The Footwall Conglomerate is however not continuous and is poorly cemented. The Footwall Sandstone, sandwiched between the two conglomerates is a medium-grained, feldspathic sandstone (Konkola Copper Mines, 2020a).

The Ore Shale Unit, also commonly known as the Copperbelt Orebody Member (Sillitoe et al., 2017) overlies the Footwall Aquifer. It is a finely laminated dolomitic siltstone, with lesser carbonaceous shale, and massive to microbially laminated dolomite. The rest of the overlying Lower Roan Group comprises the Hangingwall Quartzite, Hangingwall Aquifer, and Shale with Grit (Greyling, 2009).

The Upper Roan Subgroup is dominated by dolomites and evaporites (anhydrite and gypsum), with few siliciclastic rocks. The Upper Roan dolomite is overlain by the Mwanshya subgroup. The Mwanshya is followed by a diamictite called the Grand Conglomerate which is a regional marker unit. The youngest formation overlying the Grand Conglomerate is the Kakontwe Limestone Formation.

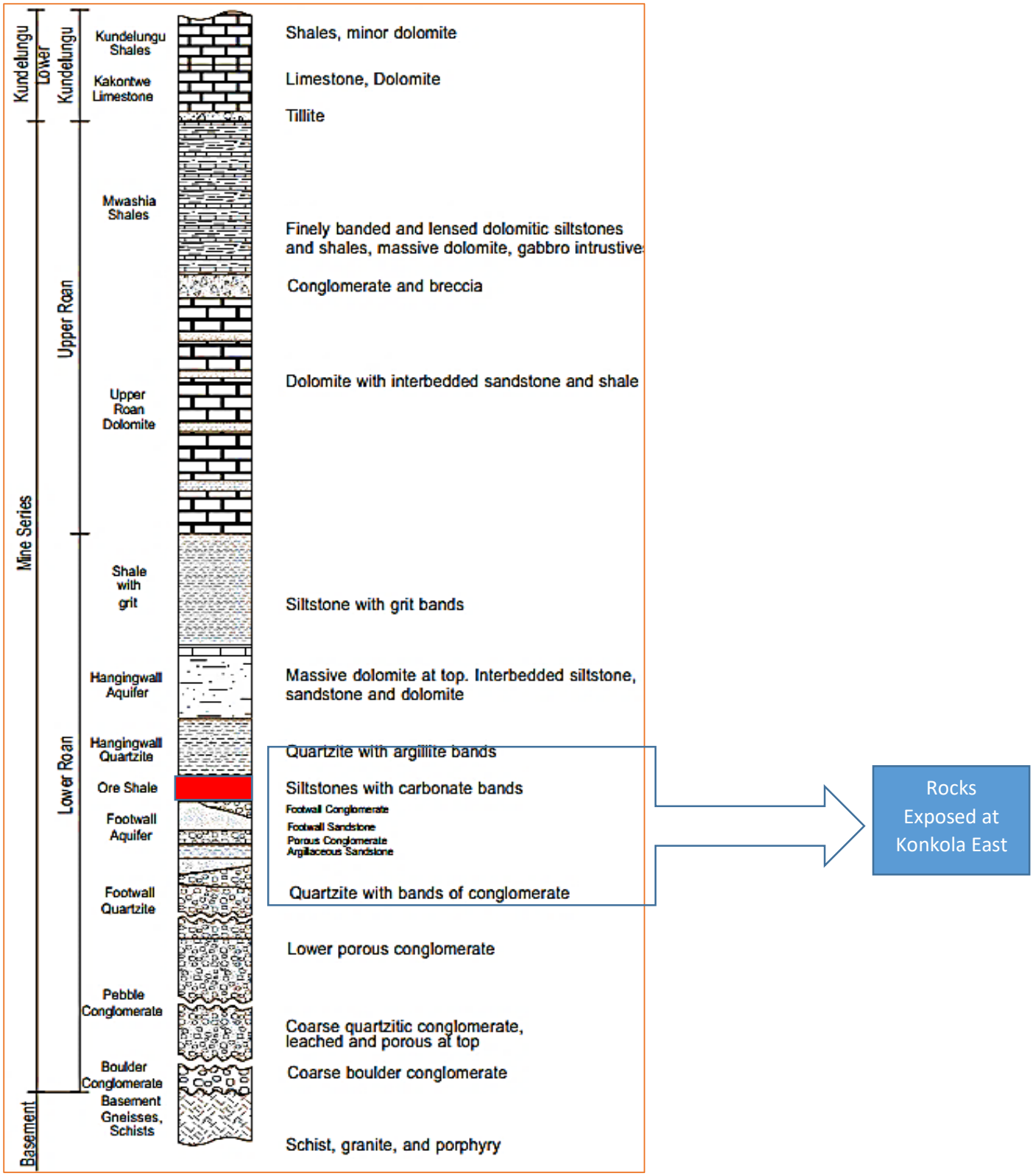


Figure 2-6: stratigraphic column for Konkola Mine also showing the part of the stratigraphy that is exposed by mine developments at Konkola east (Greyling, 2009)

2.3.2 Structure

The main structural feature in the Konkola area is the Kirilabombwe anticline around which the Konkola ore deposit is draped (Torremans et al., 2012). The Kirilabombwe anticline represents the north-western extremity of the major Kafue anticline (Figure 2-3). The Kirilabombwe anticline has a southeast to northwest trend with numerous minor folds occurring on the flanks (Figure 2-7). Torremans et al., (2012) analyzed boreholes along the axis of the Kirilabombwe anticline and concluded that it is a tight and upright anticline with a subvertical axial plane and an interlimb angle of 35-45° plunging at 10-15° to the northwest with a N75W trend of the fold axis.

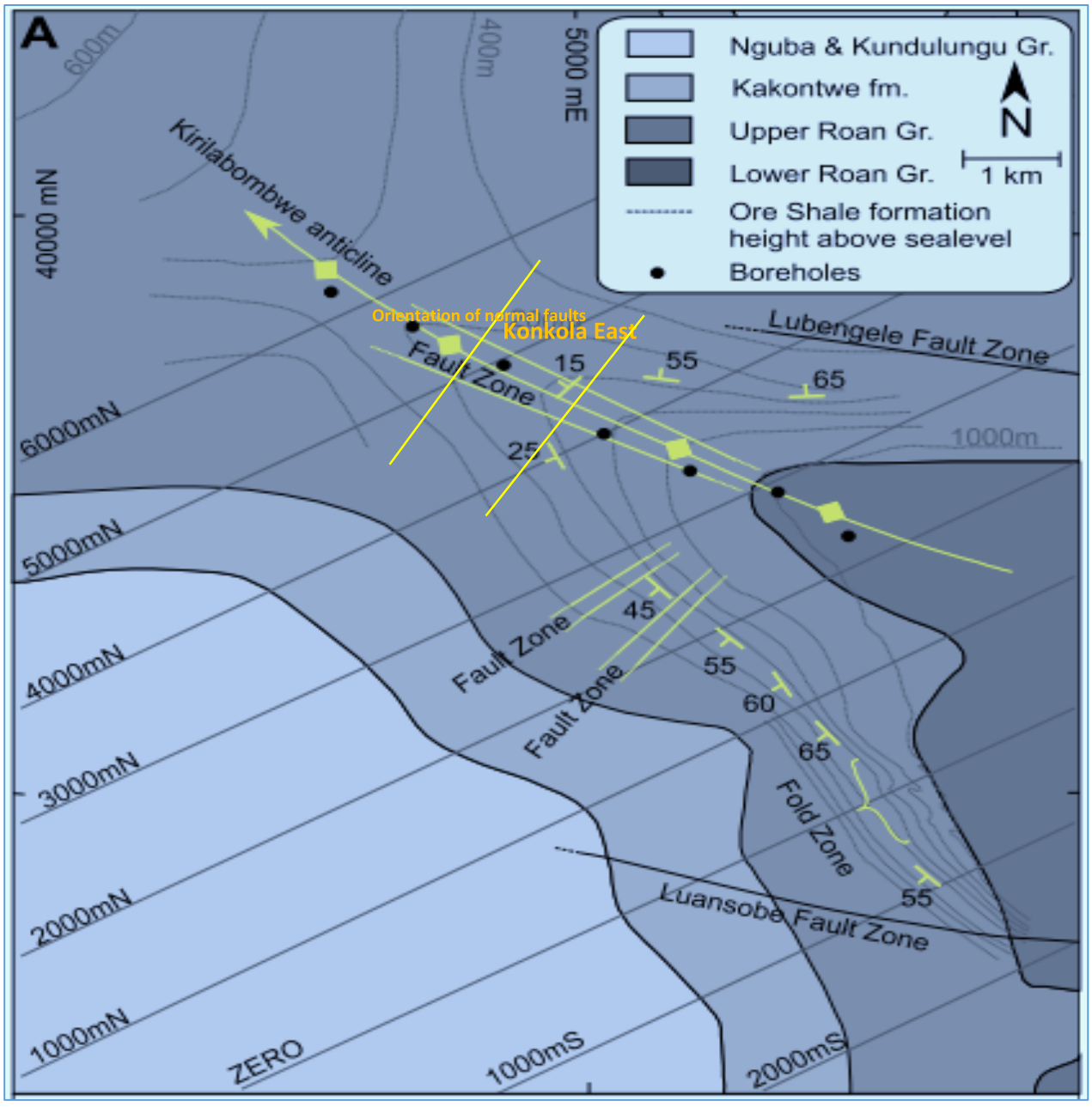


Figure 2-7: Map of structural elements associated with the Konkola ore deposit showing the surface trace of the Krilabombwe anticline (Torremans et al., 2012)

Major fault zones in the area are the Lubengele fault to the north and the Luansobe fault to the south which coincide approximately with a thickness change in the Mindola Clastic Formation and are inferred to be syndepositional faults (Hitzman et al., 2012). Another major fault runs parallel to the axial plane of the Kirilabombwe anticline and it is termed the Kirilabombwe fault (Torremans et al., 2012). Several other important fault zones occur in the limbs of the anticline.

To the south of the deposit (Figure 2-7) there is a zone of secondary folding that consists of multiple upright low amplitude gently north to northwest plunging folds(Torremans et al., 2012).

2.3.3 Hydrogeological Setup

Konkola deposit is sandwiched between two major aquifers making it one of the wettest mines in the world pumping an average of 300,000m^3 of water per day(Sixtus, 1991). The two aquifers are the Footwall aquifer below the orebody and the Hangingwall aquifer above the orebody (Table 1). The Footwall aquifer comprises mainly siliciclastic rocks while the Hangingwall aquifer is dominated by carbonate-rich rocks. The footwall aquifer provides approximately 65% of total mine inflows while the hanging wall aquifer provides about 35% of the total mine inflow(Sixtus, 1991).

Table 1: Hydro stratigraphy of Konkola ((Konkola Copper Mines, 2020a)

Stratigraphic Column of Konkola Mine					
Super Group	**Group**	**Formation**	**Lithology**	**Thickness (m)**	**Aquifer Zones**
Kundelungu	Lower Kundelungu	Kundelungu Shales [KUS]	Shales, minor dolomite	Unknown	
		Kakontwe Limestone [KAL]	Limestone, dolomite with tillite at the contact with underlying Mwashia Shales.	250	Major aquifer
Roan	Upper Roan	Mwashia Shales [MW]	Finely banded and lensed dolomitic siltstones and shales, in place massive dolomite, also gabbro intrusive. Conglomerate and breccia at the base at the interface with the URD.	300-600	Aquitard semipervious
		Upper Roan Dolomite [URD]	Dolomite with interbedded sandstone and shale.	100-450	Major aquifer
	Lower Roan	Shale with Grit [SWG]	Siltstone with grit bands.	40-165	Major aquifer at the contact with the underlying HWA
		Hangingwall Aquifer [HWA]	Interbedded siltstone, sandstone and dolomite. Massive dolomite at the top.	15-75	Major aquifer at the interface with the overlying Shale with Grit
		Hangingwall Quartzite [HWQ]	Quartzite with argillite bands. Occasionally wet and fractured at the base.	30-150	Aquitard semipervious
		Ore Shale [OS]	Siltstones with carbonate bands.	5-20	Aquitard semipervious
		Footwall Aquifer [FWA]	Feldspatic sandstone with conglomerate bands (Footwall Conglomerate, Footwall Sandstone, and Porous Conglomerate)	20-40	Major aquifer
		Footwall Quartzite [FWQ]	Quartzite bands & argillaceous sandstone at the contact with Footwall Aquifer. Highly fractured, jointed and extremely wet at the base.	>400	Aquitard semipervious
		Pebble Conglomerate LPC PBC	Leached and porous at top at the contact with Footwall Quartzite, LPC and coarse quartzitic conglomerate and impermeable at the base, PBC.	>300 125m in #3 (50m LPC and 75m in PC)	LPC and fractured base section of the overlying FWQ (together approx. 150m thick) are major aquifer zone.
		Boulder Conglomerate	Coarse boulder conglomerate.	Unknown	
Basement		Basement Gneisses, Schists	Schist, granite and porphyry.	Unknown	

3 Methodology

The research methodology involved data collection through geological mapping, core logging, and a review of historical mapped plans. A geological database was created and validated. Digitization of old plans and sections was done. Finally, geological interpretation and geological modelling was done from a synthesis of all the data. This model was then validated and finally documentation of the steps followed into a work flowchart that can be replicated on other parts of the mine. These stages are:

1. Geological mapping.

   Detailed geological mapping was carried out in the study area. The purpose of this was to identify the rocks and geological structures in the in the study area. Mapping was conducted on a scale of 1:250 using underground survey pegs as reference points. A distometer was used for distance measurement and a geological compass was used for measuring dip direction and dip for geological structures. A total number of 3 access cross cuts, 23 advancing faces, and 8 pillar cross cuts were mapped. The mapping was conducted mainly on two mine levels, 760 mL and 780 mL (Figure 3-1). The mapped data was plotted on plans and sections using microstation software.

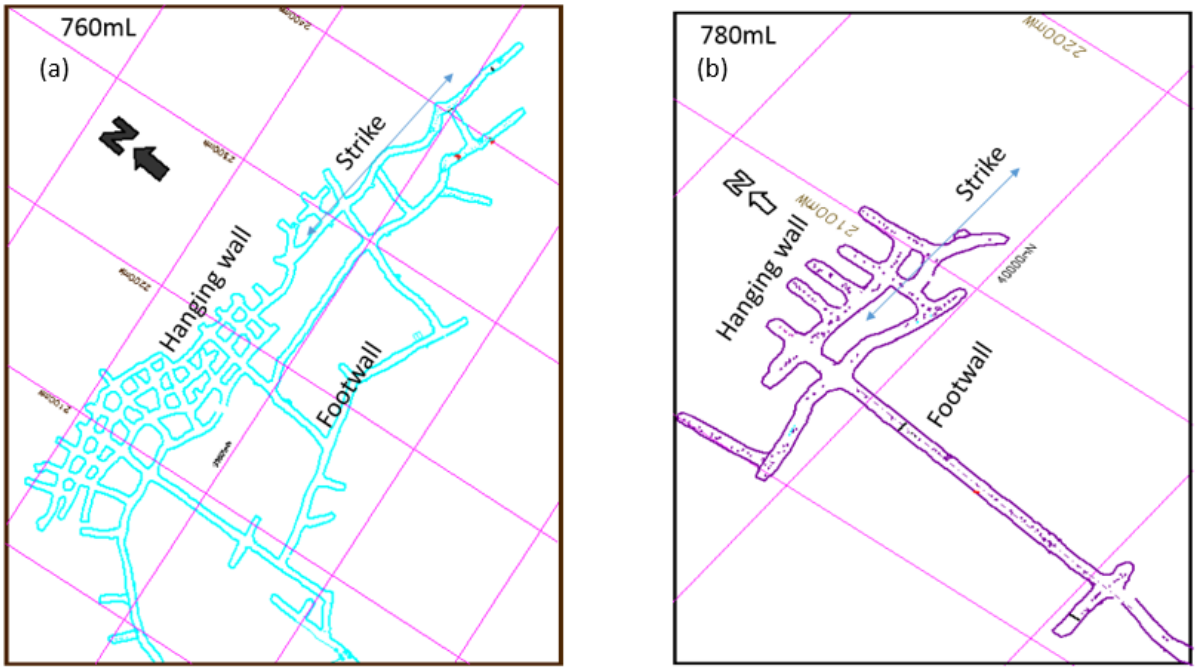


Figure 3-1 Microstation (dgn) mine plans of Konkola East mining block showing the two levels which were mapped during this study. (a) 760mL showing the mine development in relation to the general strike (b) 780mL showing the mine development in relation to the general strike.

2. Core logging

   This process involved close study and analysis of historical boreholes and recently drilled boreholes in the area. These boreholes include;

   - Surface exploration holes drilled in the early stages of exploration (1957-1974).

- Underground pilot boreholes that are drilled to help in ground selection when mining main haulages.
- Evaluation boreholes that are relatively short and restricted to only a few meters either side of the orebody

In total, 23 boreholes were logged and sampled. Table 2 lists the boreholes and their coordinates and Figure 3-2 shows the location of the boreholes on the two working level plans that were mapped for this study.

Table 2: Borehole collar information for Konkola East boreholes logged for this study. (Local mine coordinates)

Borehole ID	Level	Easting	Northing	Elevation	Hole Depth	Azimuth	Inclination
BPN 870	760mL	4135.631	39008.779	606.053	146.00	315	1.19
BPN 871	760mL	4134.978	39006.106	806.178	141.50	298	3.52
BPN 872	760mL	4135.458	39006.872	806.695	111.00	297	12.72
BPN 873	760mL	4135.697	39009.451	607.01	172.00	316	15.13
BPN 874	760mL	4135.574	38999.362	606.2	170.00	272	8.2
BPN 875	760mL	4136.544	39009.281	606.521	165.00	322	12.83
BPN 876	760mL	4135.796	39009.964	606.227	184.00	322	2.9
BPN 877	780mL	4026.412	38785.797	577.674	133.00	284	3.77
BPN 878	780mL	4027.877	38787.668	577.666	177.00	320	3.67
BPN 879	780mL	4036.949	38785.219	577.381	191.00	343	-0.44
BPN 880	780mL	4153.765	39063.541	606.739	178.50	7	-0.46
BPN 881	780mL	4148.75	39063.158	606.801	182.50	338	1.05
BPN 882	760mL	4173.089	39064.148	607.618	167.00	19	2.39
BPN 883	760mL	4177.245	39064.644	607.881	162.00	41	2.5
BPN 884	780mL	4073.06	39001.165	580.585	270.00	257	1.1
BPN 885	780mL	4073.21	39002.448	580.521	253.00	300	7.35
BPN 886	780mL	4114.368	39180.112	582.217	72.00	7	0.85
BPN 887	780mL	4108.815	39149.948	581.874	150.00	329	0.7
BPN 888	780mL	4113.437	39149.498	581.965	112.50	43	1.57
BPN 889	780mL	4089.663	39093.475	581.045	100.50	293	2.92
BPN 890	780mL	4060.846	39095.415	581.054	235.00	142	0
BPN 891	780mL	3923.302	38878.446	580.451	305.00	304	3
BPN 892	760mL	3906.768	38874.949	580.55	64.00	271	0
BPN 893	760mL	3954.53	38874.961	578.849	300.00	322	2
BPN 894	800mL	3973.612	38872.596	563.469	157.50	250	1
BPN 896	780mL	4244.538	39085.394	581.796	137.00	17	1
DVN 1596	800mL	4396.718	38081.102	524.698	102.00	254	1
BPN 897	780mL	4246.786	39084.709	581.967	244	52	1

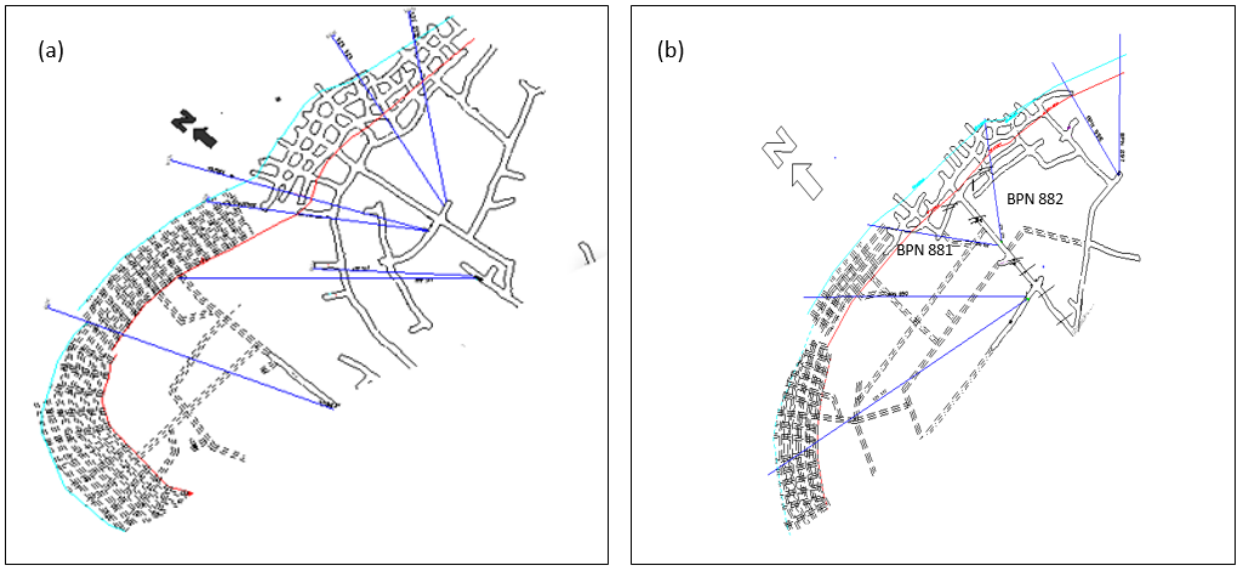


Figure 3-2:Location of some of the boreholes used in this study shown in plan-view on underground working levels. (a) 760 mL showing the collar position and orientation of some of the boreholes drilled on this level. (b) 780 mL showing boreholes drilled on this level and used in this study. Samples for petrographic analysis were gotten from BPN 881 and BPN 881.

3. Petrographic Analysis

Microscopic study of 10 samples was carried out on plane polarized light (PPL), cross polarized light (XPL) and reflected light. The purpose of the study was to observe and understand the structure of Konkola East at a microscopic scale. This was also used to observe mineralization in relation to structure at a microscopic scale.

The samples were obtained from two boreholes, BPN 881 and BPN 882 drilled on 780 m level (Figure 3-2). The samples were coded SM 01 –SM 11. From BPN 881, a sample was collected from the immediate footwall (SM-01) and 4 from the OSU (SM-03, SM-02, SM-05, and SM-06). Samples SM-04, SM-07, SM-08, SM-09, SM-10 and SM-11 were taken from borehole number BPN 882. The sampling from each borehole was done to cover mainly the ore shale unit, with also a sample from both the immediate footwall and the immediate hangingwall. The two boreholes were chosen for petrographic study because they were reasonably spaced and also they were very recent and easily accessible.

4. Database creation and Validation

For this study, a geological database was created from boreholes around the study area to be used to develop a geological model. The database was validated before being used to eliminate errors that can lead to ultimately wrong interpretation and modelling. Some of the common errors that were checked for include, but were not limited to, overlapping intervals, duplications, survey and collar errors and inconsistent nomenclature of lithological units.

The database had three Microsoft excel files; Collar, Survey and Geology. The collar survey contained the borehole name abbreviated as “BHID”, the coordinates, Eastings, Northings and Elevation abbreviated as “XCOLLAR”, “YCOLLAR” and “ZCOLLAR” respectively. “EOH” indicated the end of hole.

5. Digitization.

   At Konkola mine some of the geological data is in hard copy. This includes some level plans for old working areas, surface geological plans and selected sections of the mine (Figure 3-3). The historical sections were prepared at 100 m spacing. The digitization and incorporation of this information helped in creating a meaningful interpretation and a useful geological model.

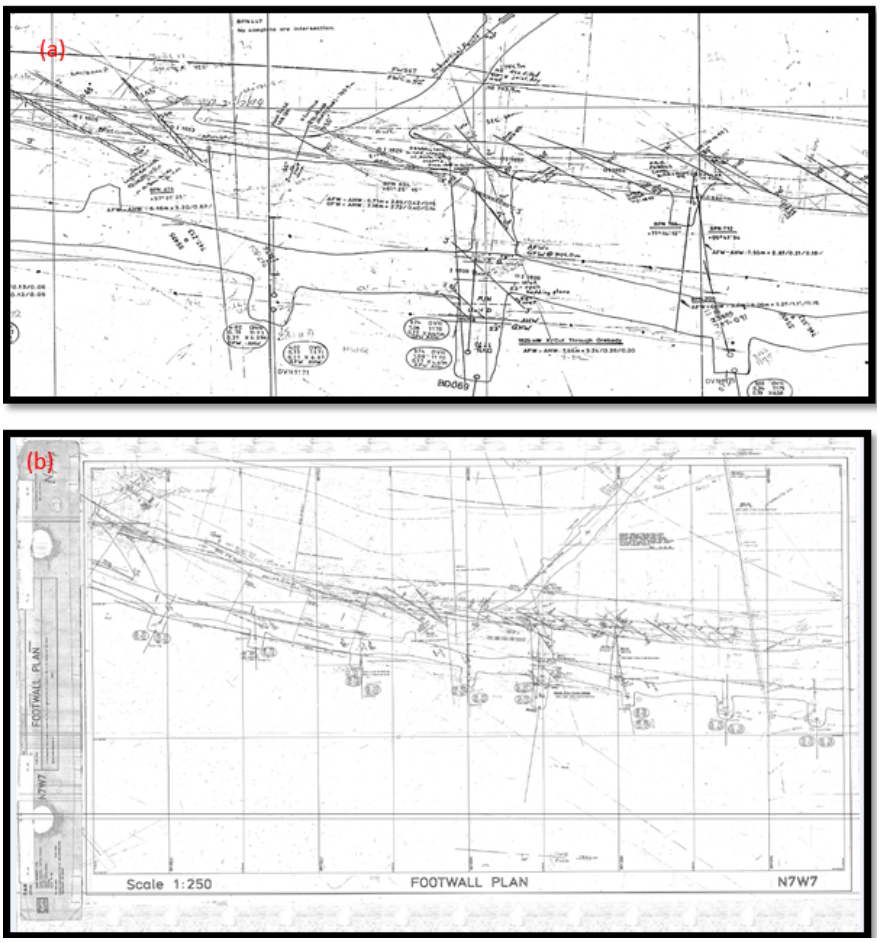


Figure 3-3: Scanned plan of (a) 1850 ft. level plan and (b) 2340 ft. level plan showing the geological structures which were digitized.

6. Geological Modelling and validation

   Geological interpretation of all the validated data was then carried out and compared to the regional tectonic setting and deformation history. Stereo plots and other structural visualization tools were used.

   This was followed by geological model creation. The geological model was created explicitly using Surpac software incorporating all the data. Validation of the geological model was done by inspection of random sections and by physical verification of selected areas. Comparisons were then made with the resource model surfaces.

7. Flow chart and Standard Procedure

   The steps taken in the creation of this model were documented in a workflow chart as a standard procedure to ensure that it can be replicated in other working areas of Konkola mine.

4 Geology of Konkola East

Mapping in the Konkola east exposed 7 main rock types. The rock formations are from the oldest to the youngest, Footwall Quartzite, Argillaceous Sandstone, Porous Conglomerate, Footwall Conglomerate, Ore Shale Unit, and the Hangingwall Quartzite (Figure 2-6). The lithologies in Konkola east are generally trending east to west and dip to the NE (Figure 4-1).

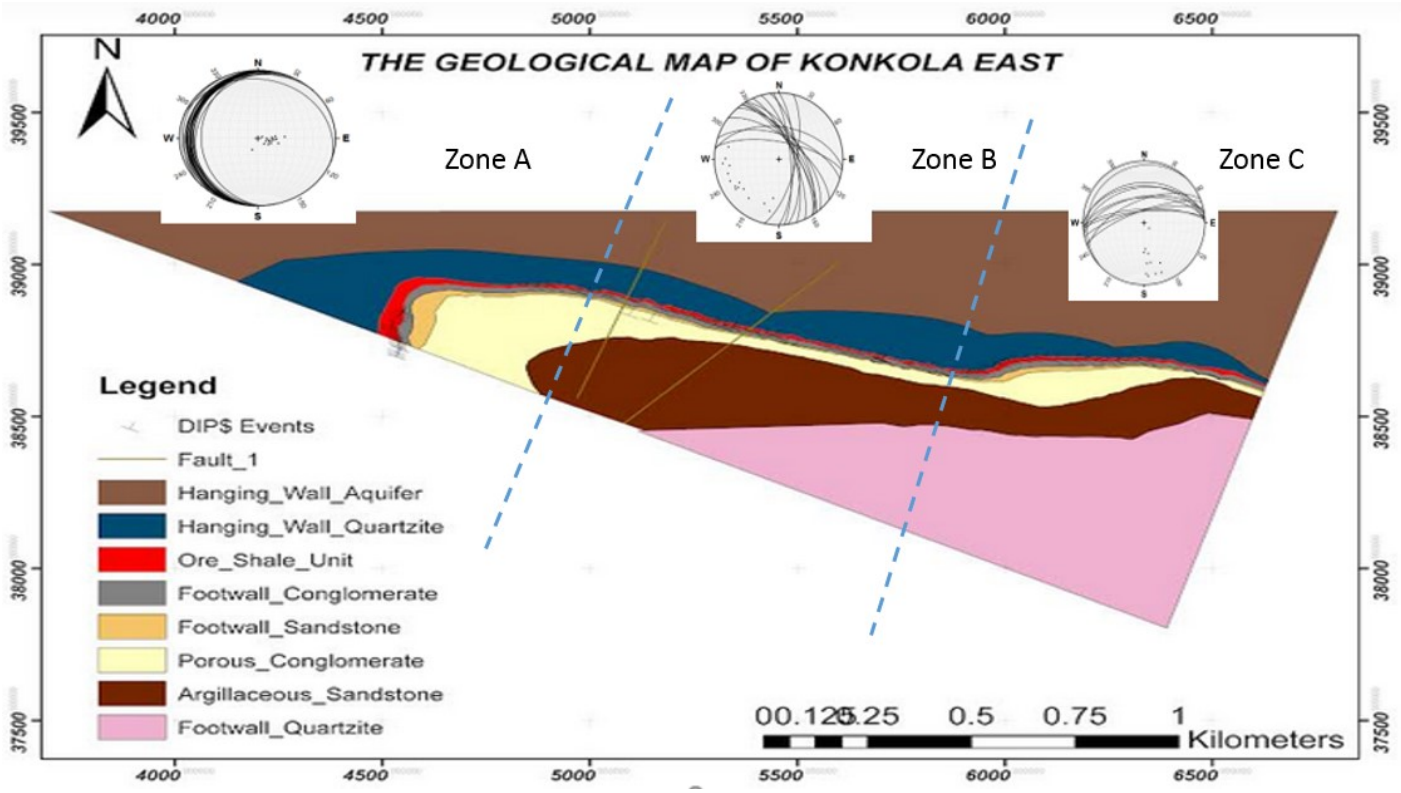


Figure 4-1: Geological map of Konkola East showing the major lithologies and structural features of Konkola east. The area was subdivided into 3 zones, Zone A, Zone B and Zone C based on the average dip and strike of the bedding of the Ore Shale Unit (red).

4.1 Footwall Quartzite

The Footwall Quartzite is the oldest exposed lithology at Konkola east (Figure 2-6). This is exposed mainly in the access cross cuts and ramps where it was mapped. The Footwall Quartzite (FWQ) is light and dark grey (Figure 4-2). It has a fine to medium grained texture. It contains meta-arenites and gritty arkose with red feldspars with occasional conglomerate layers. It is highly jointed and very wet in parts (Figure 4-2).



Figure 4-2: Underground picture showing massive and jointed Footwall Quartzite.

4.2 Argillaceous Sandstone.

The Argillaceous Sandstone (AGSST) overlies the Footwall Quartzite. The contact between the footwall quartzite and the argillaceous sandstone is very distinct in parts, consisting of an abrupt change to a thinly to medium-bedded sandstone, partly kaolinized jointed sandstone. In other areas the contact is observed to be transitional. The Argillaceous Sandstone consists of interbeds of argillite bands and sandstone formation as shown in Figure 4-3.

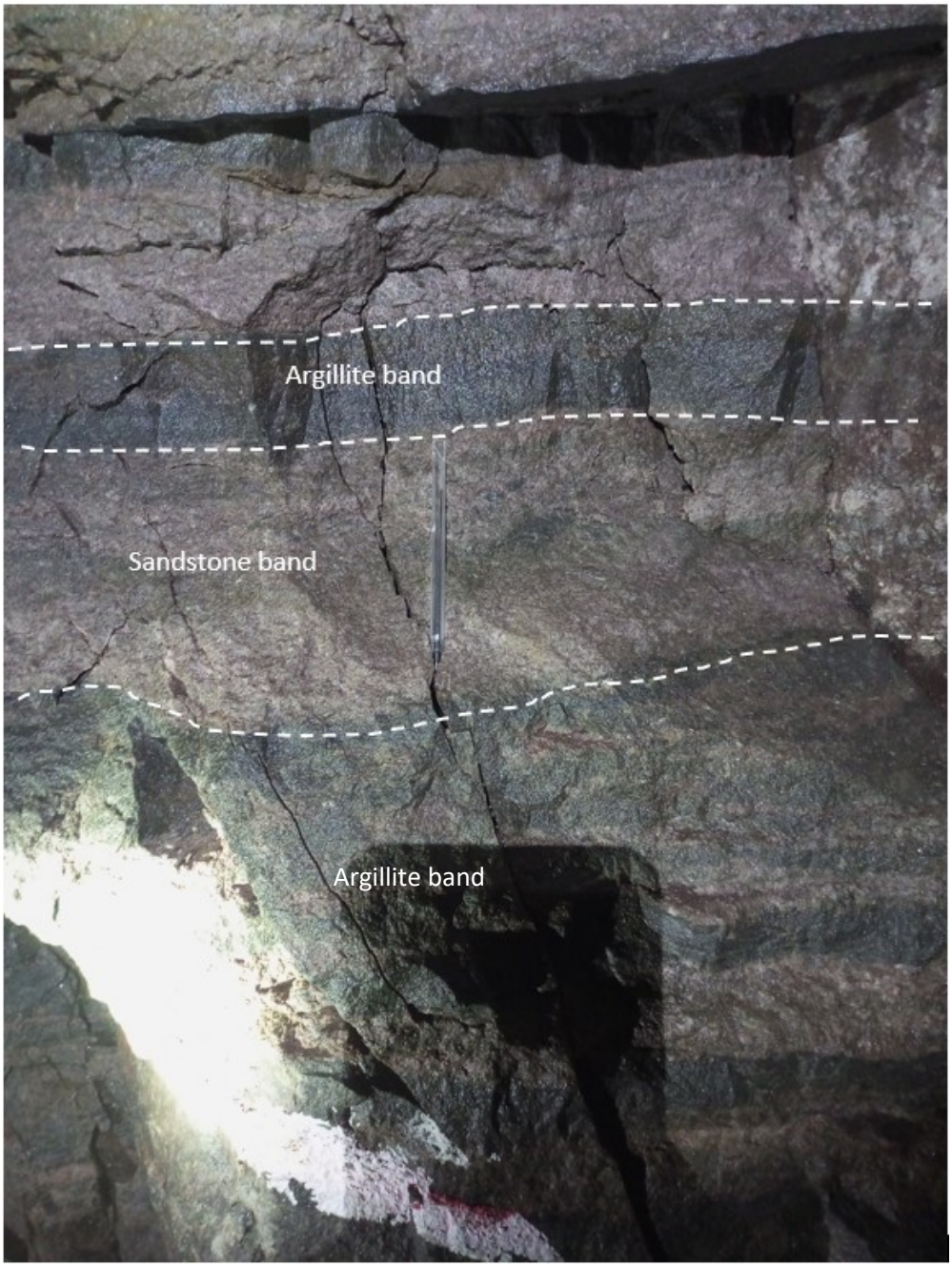


Figure 4-3: Underground picture of Argillaceous Sandstone exposure showing argillite bands interbedded with sandstone. The picture was taken from 760mL, 2400mW (Figure 1-3) crosscut facing north.

4.3 Porous Conglomerate

The Porous Conglomerate (PC) consists of a poorly to moderately well-sorted mixture of well-rounded, cobble and pebble sized clasts. It also has a matrix of coarse-grained to fine-grained sandstone that constitutes approximately 15% of the rock volume. Maximum clast size is about 55 cm and no clast-to-clast contact was observed here. The cobbles are predominantly made up of pink, coarse-grained granite, which consists of quartz, feldspars and micas. Fine-grained quartzite cobbles are also present. This conglomerate unit is very thickly interbedded with pebbly beds having well-rounded quartz and

feldspathic pebbles up to 2 cm in diameter, set in a fine sand size matrix of quartz, feldspar and clay minerals. Occasional well-rounded coarse- grained granite cobbles also occur in these pebbly beds (Figure 4-4). The pebbly beds do not occur at regular intervals but rather randomly at spaces not less than 3 m in the unit and their average thickness is 1 m.

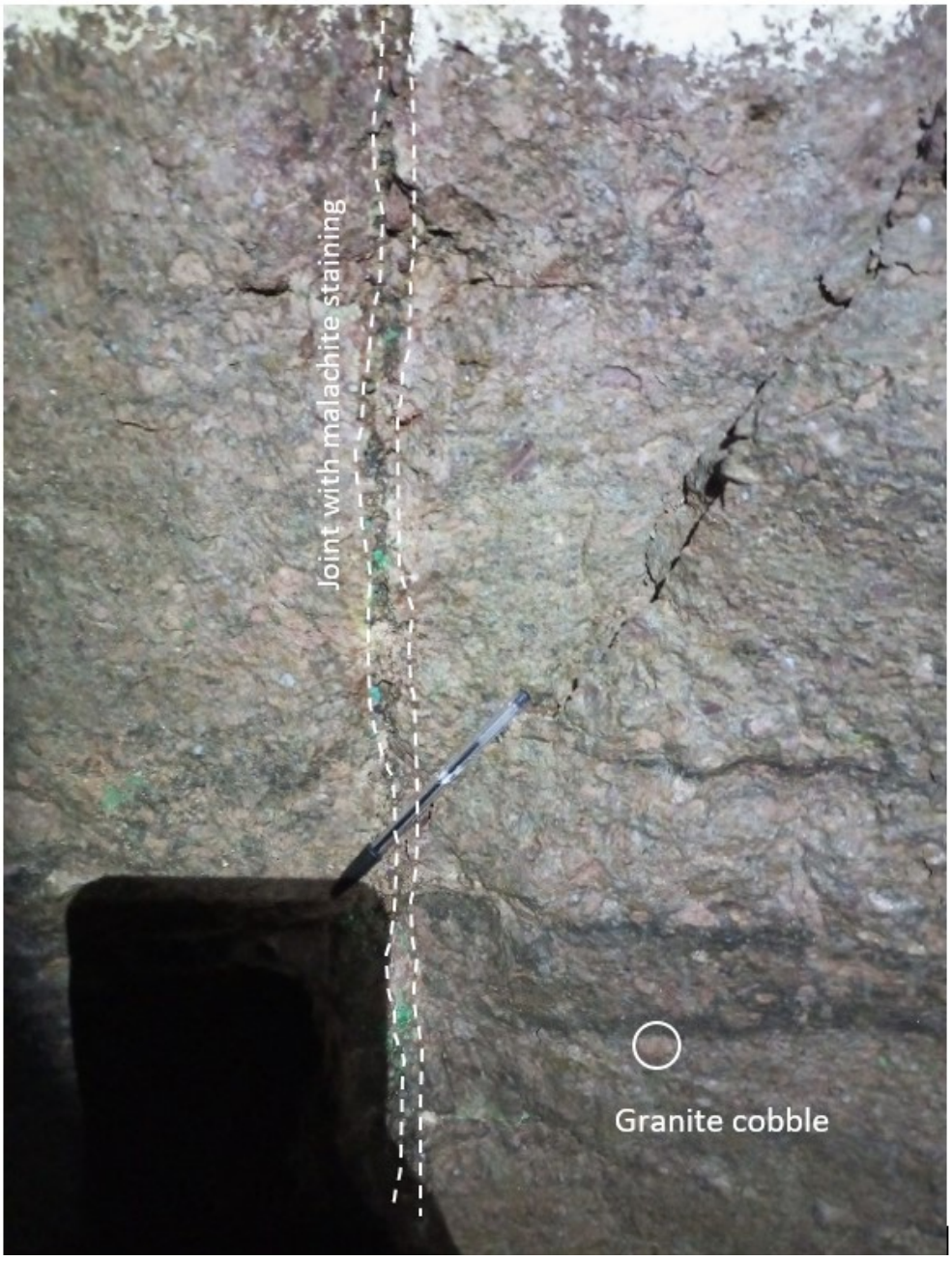


Figure 4-4: Underground picture taken from 2400mW crosscut facing east showing the Porous Conglomerate with malachite staining along the joints.

4.4 Footwall Sandstone

The Footwall Sandstone (FWS) is just above the Porous Conglomerate. The contact with the Porous Conglomerate is sharp (Figure 4-5). This formation is dark to light grey in color. It is of medium to coarse grained texture with occasional bands of shale (Figure 4-5). It is strongly silicified, massive, pitted and vuggy. Occasional malachite tints are observed especially along joints.

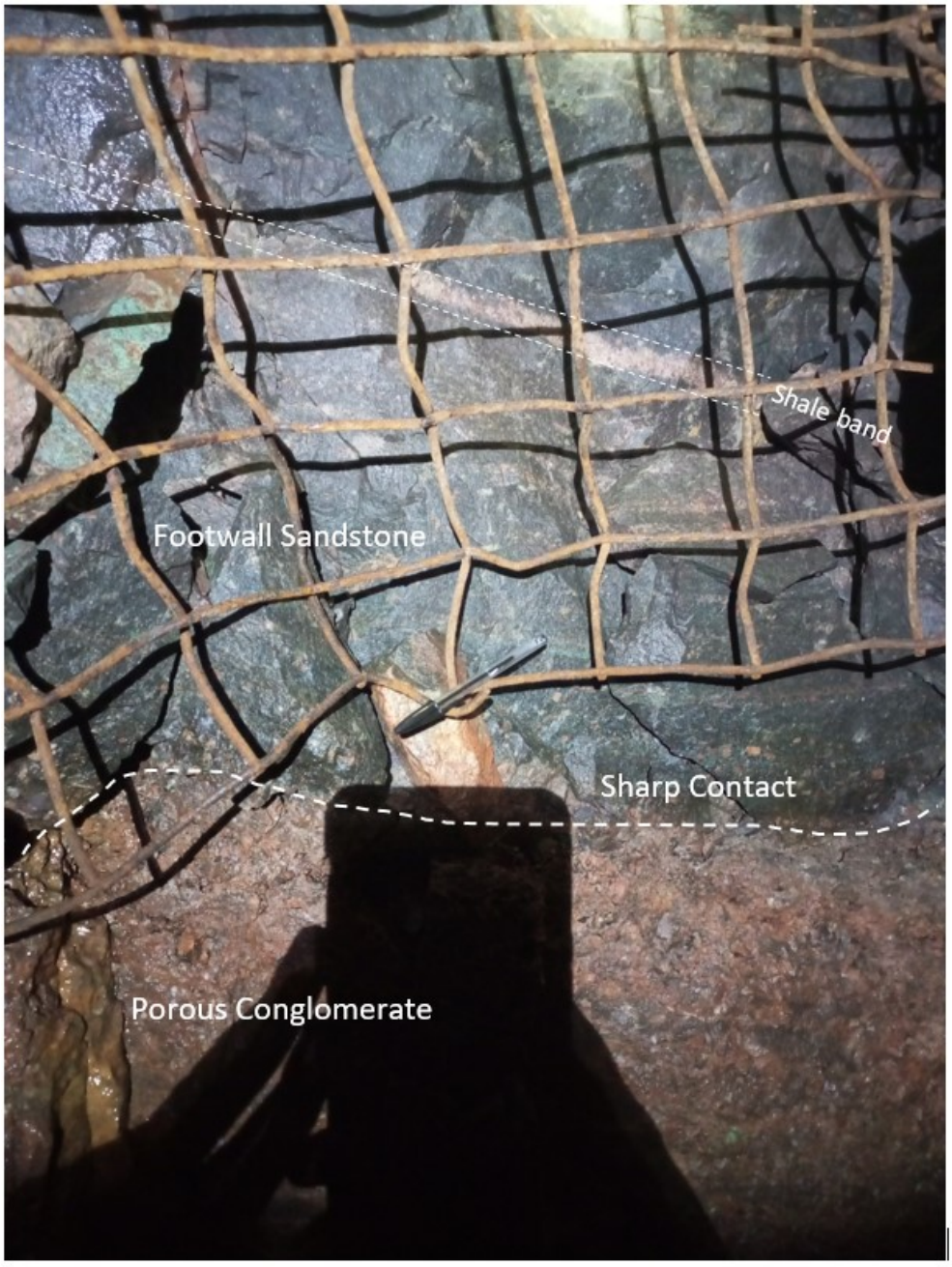


Figure 4-5: Underground picture showing the contact between the Porous Conglomerate and the Footwall Sandstone. Note pen for scale. Picture taken on 780 mL, 2400 MW crosscut (Figure 1-3).

4.5 Footwall Conglomerate

The Footwall Conglomerate (FWC) is pink in color. The Footwall Conglomerate contact with Footwall Sandstone which it overlies is sharp. This conglomerate is generally matrix-rich and is mostly interbedded with sandstone.

The lower unit is greyish pink and approximately 2 m thick. It is poorly sorted, matrix-supported and thinly bedded. This unit consists of sub angular to sub rounded pebbles of quartz and feldspar up to 3 cm in diameter. Its matrix is fine sand to silt size and is made up of quartz, feldspar, and clay minerals.

The middle Unit is characterized by vague bedding with poorly defined bedding planes. The pink layers consist of sub angular to sub rounded pebbles of quartz and feldspar in a siltstone matrix made up of chlorite, kaolinite, malachite, cuprite and chalcopyrite in addition to quartz and feldspar. The grey layers are comprised of silt size particles consisting of clay minerals.

The top unit is approximately 1.5 m thick. It consists of alternating pink and grey lamination (Figure 4-6). It is poorly sorted and has minor sub rounded granitic cobbles up to 15 cm in diameter. The granite cobbles are brown to pink in color and of medium-grained texture. The minerals observed in the granite cobbles are quartz, feldspar, micas and chlorite. The unit also consists of a mixture of sub-rounded and elongate pebbles of feldspar and quartz. The cobbles and pebbles are set in a fine sand size matrix of mainly quartz, feldspar and clay minerals. This unit was also observed to contain copper mineralization.

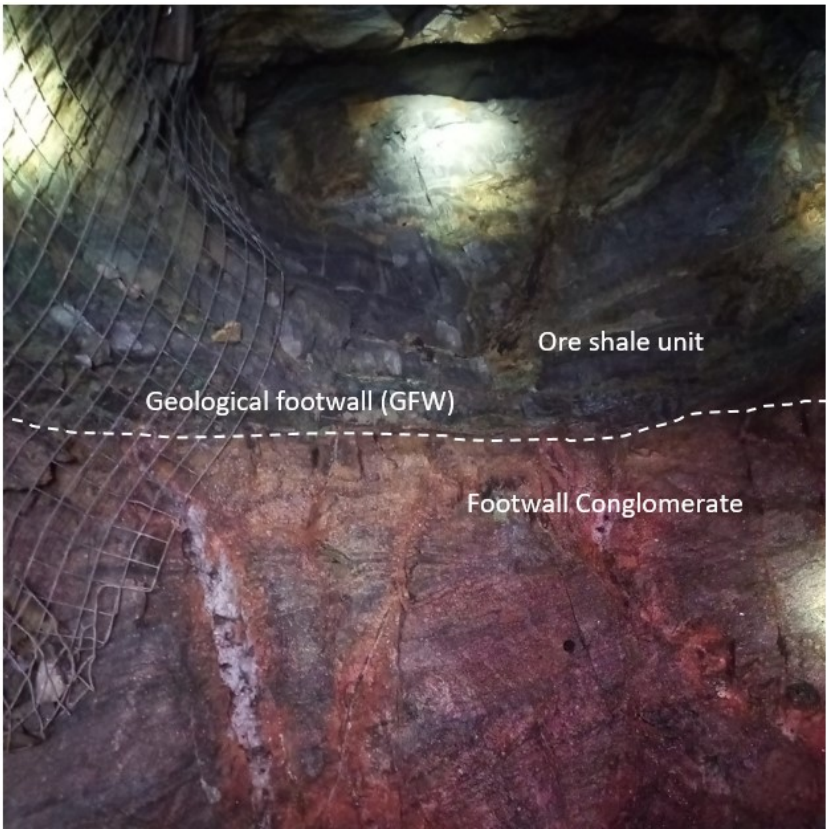


Figure 4-6: Underground face mapping. 760mL 2400mW access to orebody showing the top part of the Footwall Conglomerate where it makes contact with the Ore Shale unit. This contact is also called the Geological Footwall (GFW).

4.6 Ore Shale Unit

The Ore Shale Unit (OSU) overlies the Footwall Conglomerate (Figure 4-6). The contact between the Footwall Conglomerate and the Ore Shale Unit which is also referred to as the geological footwall (GFW) is abrupt (Figure 4-6). The Oreshale Unit at Konkola east is observed to consists of a sequence of fine grained laminated calcareous siltstones. It also contains shale grading into siltstone with interbeds of feldspathic arenite with dolomitic bands. Distinct bedding is observed in the Ore Shale Unit (Figure 4-7). It ranges from fine siltstone laminations of about 5 milimeters to massive units of about 0.5 meters.



Figure 4-7: Underground picture from 2400mW showing distinct bedding in the Ore shale Unit.

The Ore Shale Unit is made up of fine grains of quartz, biotite, muscovite, k-feldspar,and plagioclase supported by a matrix that is mainly clay and carbonate minerals. It also has layer parallel quartz veins as observed in hand specimen (Figure 4-8).



Figure 4-8: Hand specimen of the Ore Shale Unit showing bornite mineralization occurring in layer parallel veins

5 Petrographic Analysis

Microscopic descriptions of the Footwall Conglomerate and the Ore Shale Unit are given below. The samples in Figure 5-1 show where the samples described were prepared from.

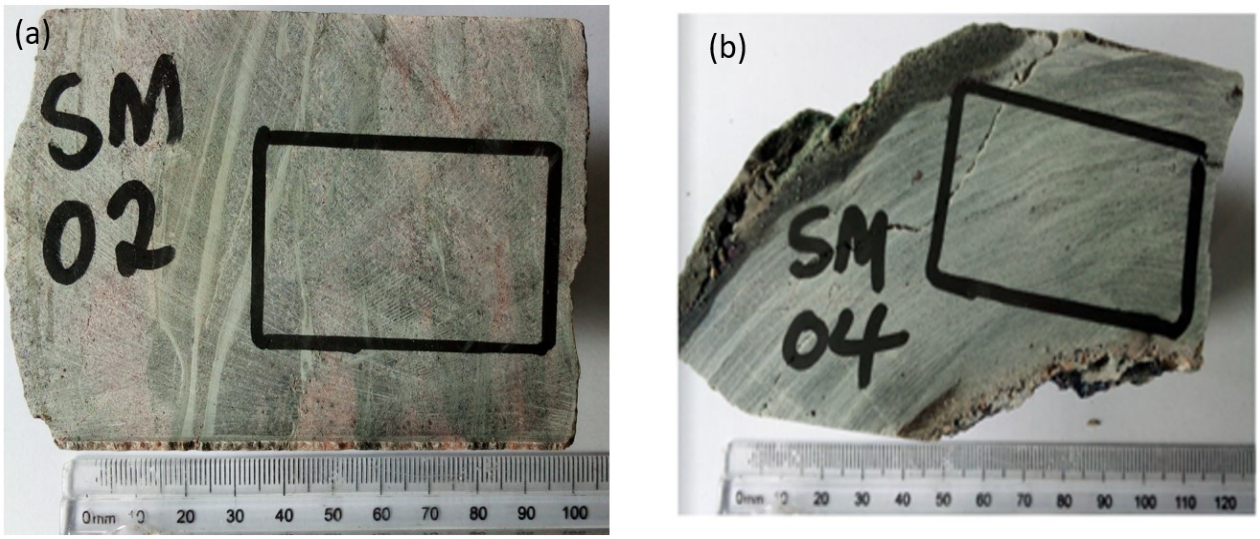


Figure 5-1: Core samples showing where the photomicrographs discussed in this chapter were prepared from. (a) SM 02 sample of footwall conglomerate from borehole BPN 881 (b) SM 04 sample of the Ore Shale Unit.

5.1 Description of the Footwall Conglomerate Under cross polarized and under plane polarized light.

When viewed under cross polarized light and plane polarized light, the Footwall Conglomerate is observed to be composed of quartz, microcline, orthoclase, muscovite and sericite (Figure 5-2). Quartz is the major mineral present making up to 40% of the total composition. The other minerals are microcline (35%), orthoclase (5%), muscovite (10%) and clay minerals (10%).

The quartz grains are sub-angular to sub-rounded, with some muscovite and sericite in their interstices. The quartz grains are observed to also contain sub grains. The quartz grains and the feldspars are elongated in what appears to be a preferred orientation. On rotation, the quartz crystals appear to be exhibiting an undulose extinction. The micas exhibit a sinusoidal shape suggesting that they were present during a component of shear deformation.

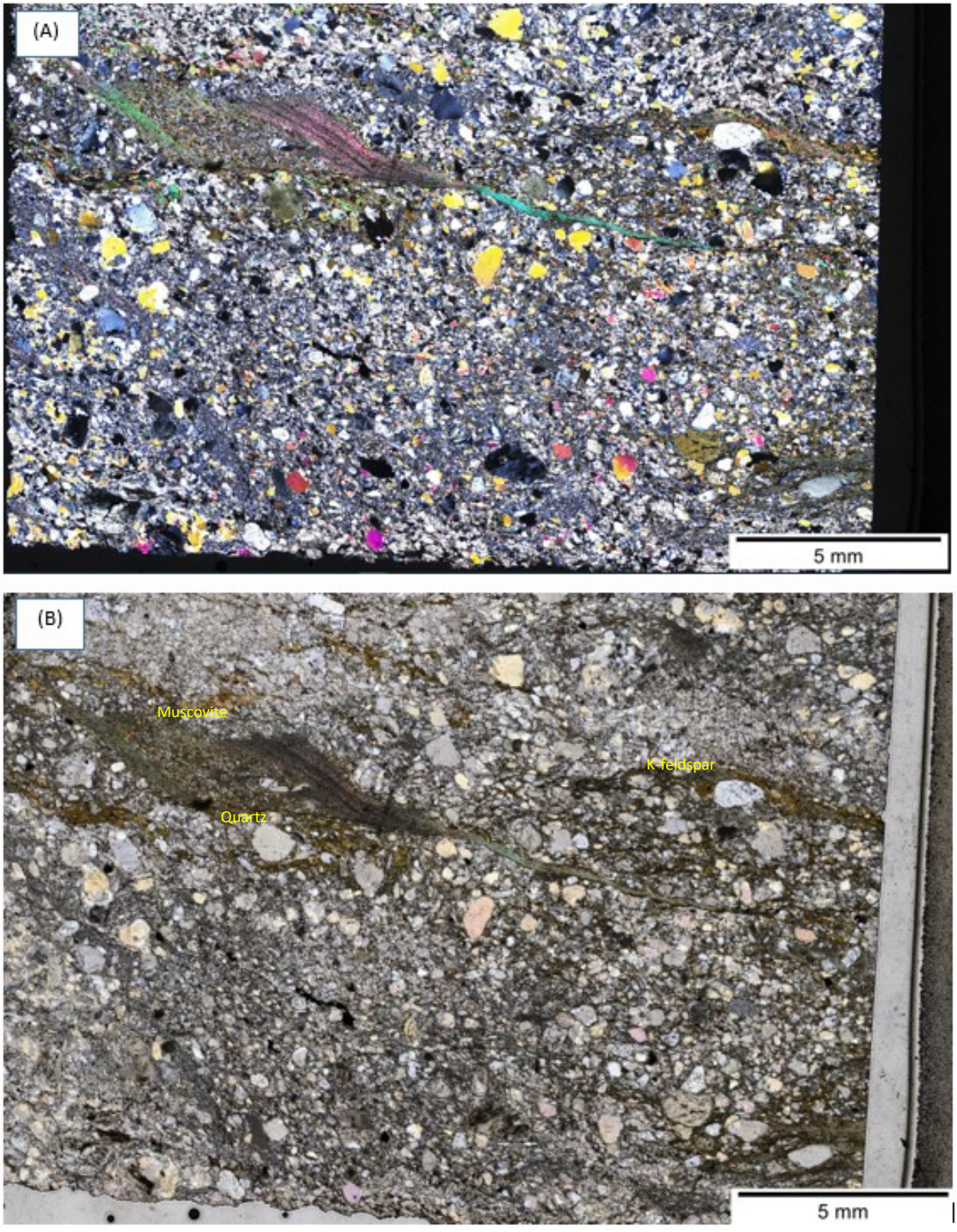


Figure 5-2: Photomicrographs of the footwall Conglomerate, SM02 showing sinusoidal mica. (A) Viewed under cross polarized light. (B) Viewed under plane polarized light.

5.2 Description of the Footwall Conglomerate under reflected light Microscopy

When observed under reflected light, the Footwall Conglomerate is observed to be coarse grained. The footwall conglomerate is further observed to contain chalcocite (CC). Minor malachite (MLT) is observed to be replacing the chalcocite along the grain boundaries. (Figure 5-3)

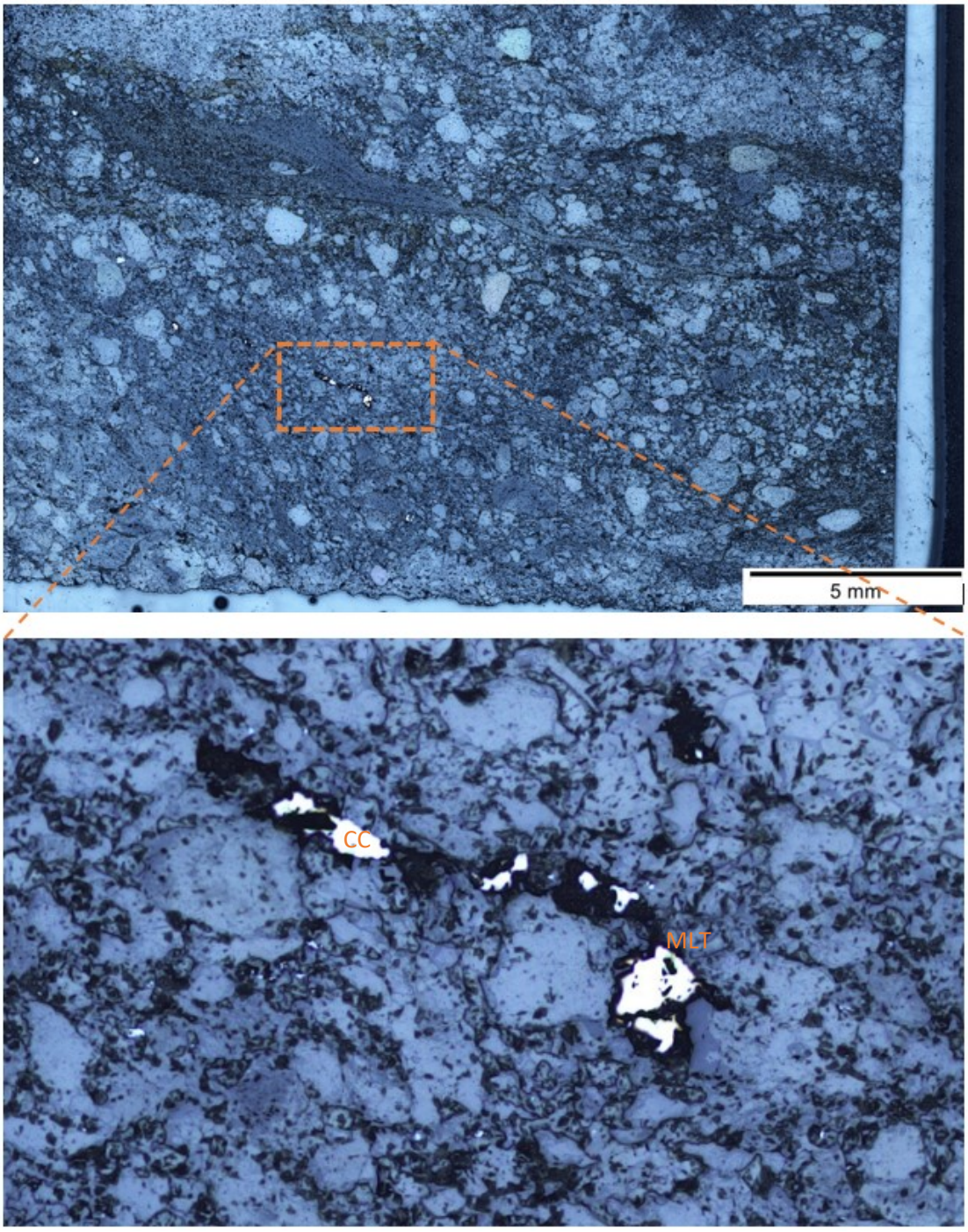


Figure 5-3: Photomicrograph of SM 02 (Footwall conglomerate) viewed under reflected light showing chalcocite (whitish grey) being replaced by malachite (green) along the grain boundaries.

5.3 Description of Ore Shale Under Cross polarized and transmitted light Microscopy.

When observed under cross polarized light, the ore shale unit is observed to contain fine-grained quartz, biotite, muscovite, chlorite and calcite in a calcareous clay matrix defining laminations that alternate with medium-grained laminations of dolomite, calcite and quartz (Figure 5-4). Quartz grains are fine-grained, anhedral and oriented parallel to foliation. Biotite and muscovite are anhedral to subhendral. Carbonate veins are finely disseminated in the ground mass and are also anhedral to subhendral.

Ore minerals are observed to be dark, finer and highly concentrated in lamination planes.

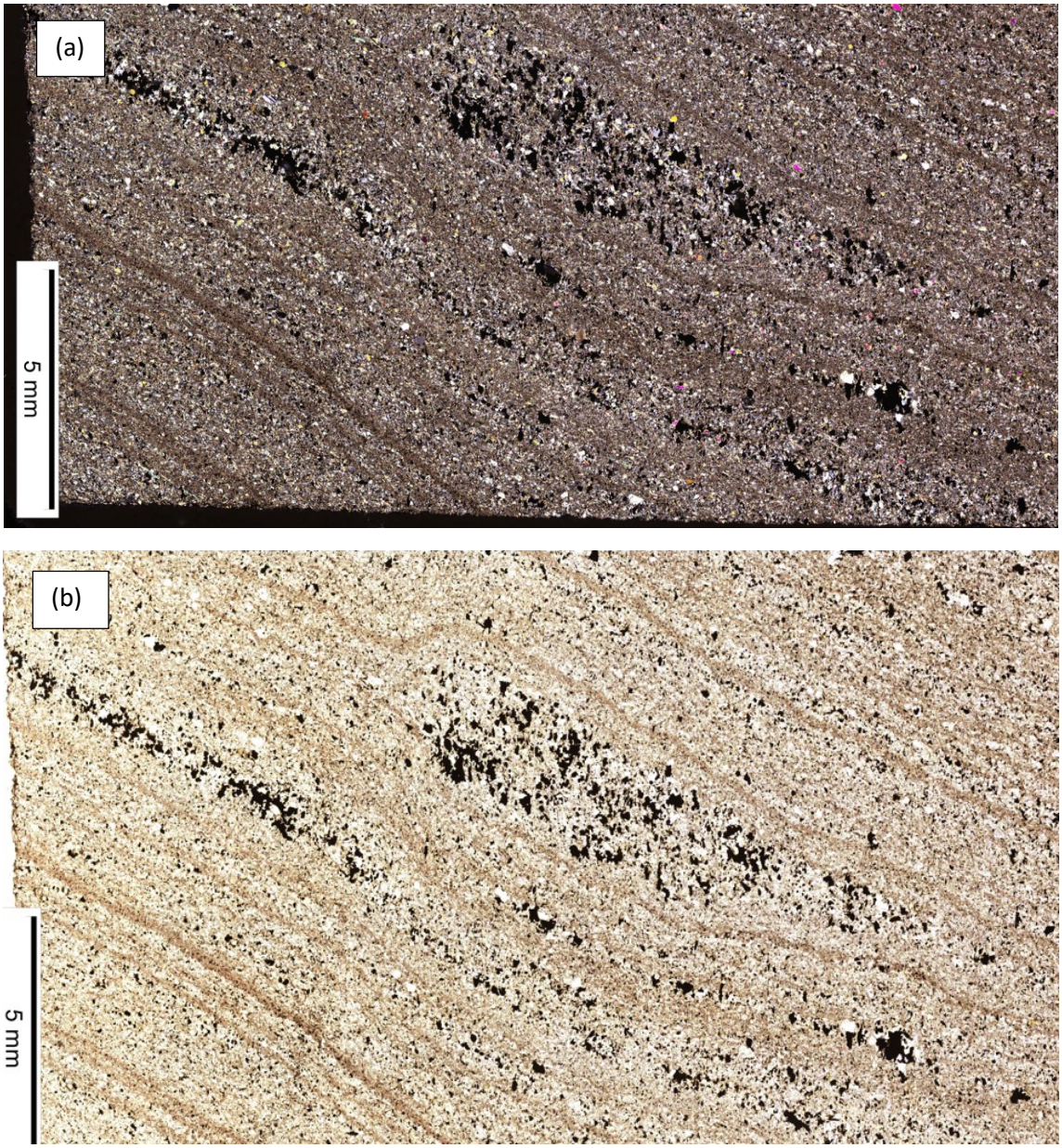


Figure 5-4: Photomicrograph of SM 04 as observed under (a) cross polarized light and (b) plane polarized light. Ore minerals appear dark in both cross polarized light and plane polarized light and occur mainly along layers.

5.4 Description Ore Shale Unit Under reflected light microscopy

The Ore Shale Unit observed at konkola east when viewed under reflected light contains the ore minerals bornite (BN), chalcocite (cc) and chalcopyrite (CP)(Figure 5-5).

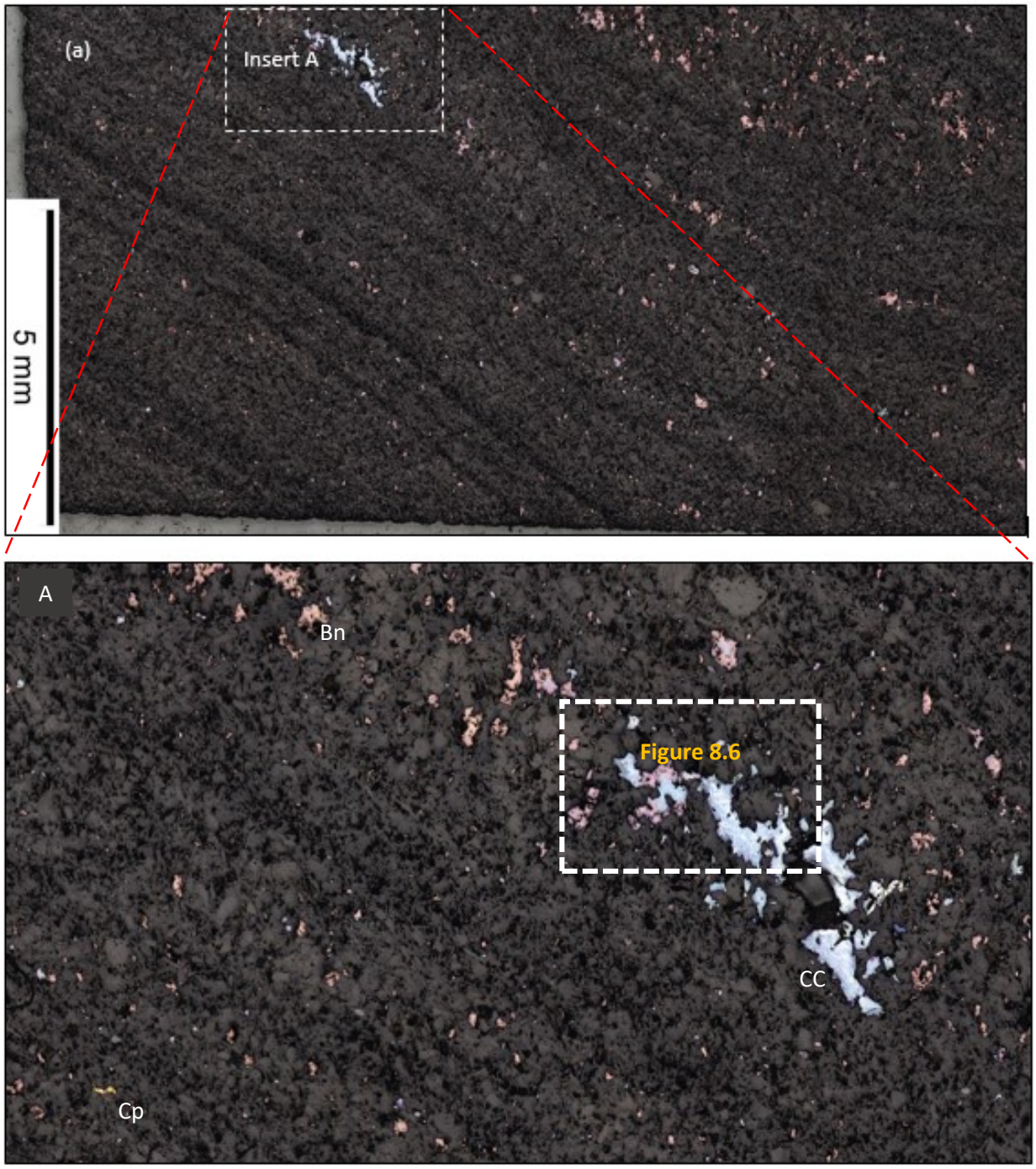


Figure 5-5: Photomicrograph of SM 04 viewed under Reflected light showing the major ore minerals being bornite (pinkish brown), chalcocite (whitish grey) and chalcopyrite (yellow). In insert A in the bottom, chalcocite is observed to be replacing the relic bornite grains.

The ore minerals occur predominantly along lamination planes. The main ore mineral observed is bornite which is pinkish-brown in colour and exists as discrete finely disseminated grains. The bornite grains seem to be coarser along the lamination plans. A few bornite grains are observed to be intergrown with chalcocite grains. Some pre-existing grains of bornite are being replaced by chalcocite (Figure 5-5). Grains of chalcopyrite are few and finely disseminated.

Chalcocite also occurs as free grains but mostly it is observed to be replacing bornite. It is also coarser along the lamination planes. Along the rims of the grains, minor malachite (green) is observed to be replacing chalcocite (Figure 5-6).

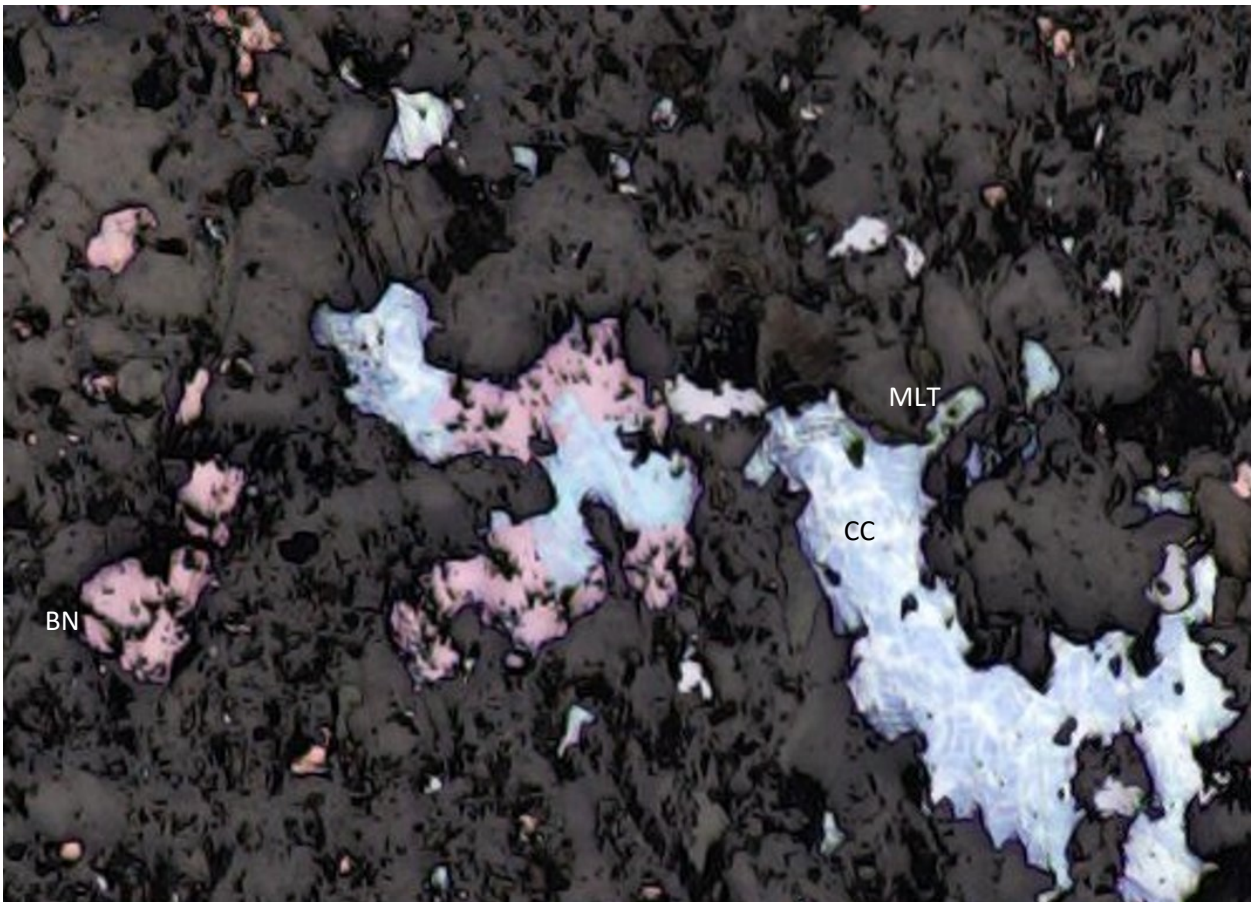


Figure 5-6 : Part of the photomicrograph (SM04), an extract from figure 8.3 showing textural relationship between bornite (BN), chalcocite (CC) and malachite (MLT)

6 Structural Elements of Konkola East.

A structural analysis was conducted for Konkola east in order to understand the orientation of the major geological structures that may influence mining and also that can be used in the creation of a short term geological model. The analysis was done by studying various mining excavations in the study area. Sidewall mapping across the strike of the ore body allowed for a close analysis of the nature of contacts, joint orientation, bedding plane orientation and other meso-scale geological structures. Figure 6-1 shows 2400 mW crosscut, an example of one such sidewall mapping that was conducted during the study.

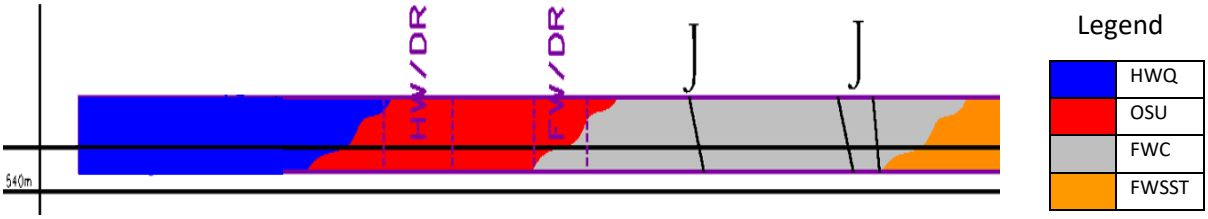


Figure 6-1: Eastern Sidewall mapping of 2400mW showing the lithologies and joints observed in the cross cut. Two drives, hanging wall drive (HW/DR) and foot wall drive (FW/DR) are shown by the dotted lines.

The mapping exercise included the observation of lithological variation and the orientation of major structures that included faults, folds and orientation of major joints. The data was recorded following the standard Konkola mine geological mapping template (See Appendix A).

A geological map shown in Figure 6-2 was produced from this exercise

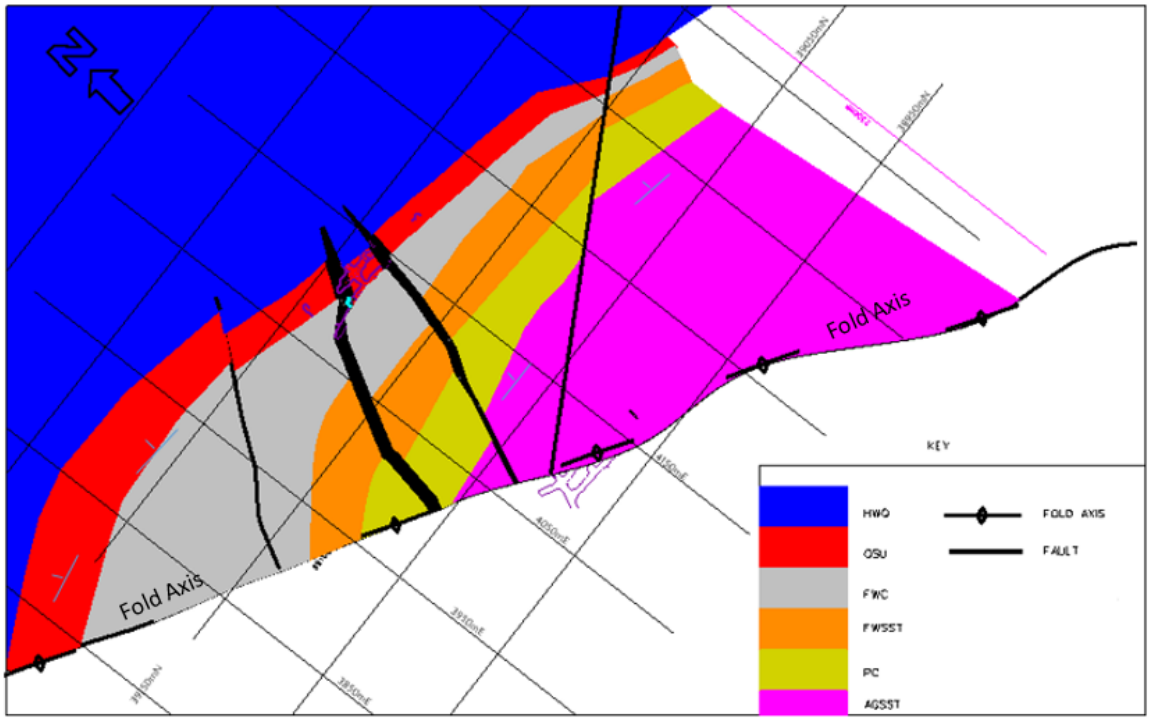


Figure 6-2: Geological map of 780 ml produced after mapping the mining excavations.

The mining block under study is situated on the northern limb of the major Kirilabombwe anticline. The fold axis (Figure 6-2) was inferred in mapping at the point where the dip direction changed to the opposite direction when mapping along the access cross cuts that are mined across strike. Digitized mapping from upper levels was also used to project the approximate location and orientation of the fold axis.

6.1 Bedding and Foliation

The ore bearing rock, the Ore shale Unit (OSU) also known as the Copperbelt Ore Member (COM) at Konkola has a strongly developed, bedding parallel shaly cleavage, S_1 (Figure 6-3). The orientation of S_1 varies along the general strike. In the western part, S_1 is generally oriented northeast- southwest and generally dipping shallowly to the North West. In the eastern part, S1 trends east-west and generally dipping to the north with a relatively steep dip averaging 45 °.

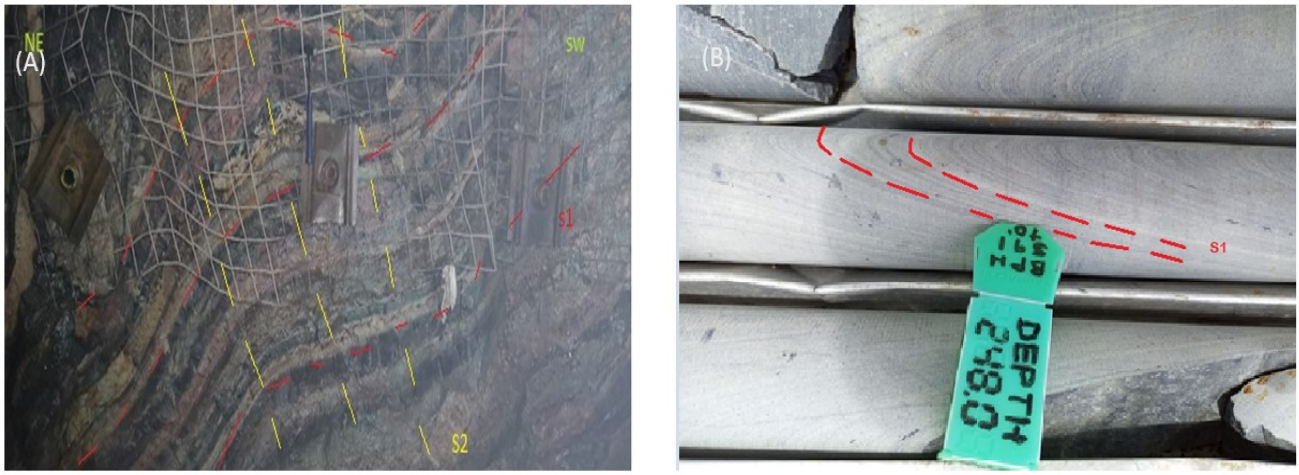


Figure 6-3: (A) 780mL 2400mw pillar cross cut 6 showing the S_1 fabric strongly developed in the ore shale and the fairly to poorly developed S_2 fabric. (B) Strongly developed S_1 fabric in ore shale as observed in core.

Opening of cracks oriented sub-perpendicular to the S_1 fabric represents the S_2 fabric. S_2 is also marked by the elongation of minerals perpendicular to the S_1 fabric. In the immediate footwall formation which is a conglomerate, this cleavage is poorly developed but can be inferred from the occasional bands of sandstone. In the immediate hanging wall which is a quartzite with argillite bands, the S_1 cleavage is moderately developed (Figure 6-4).

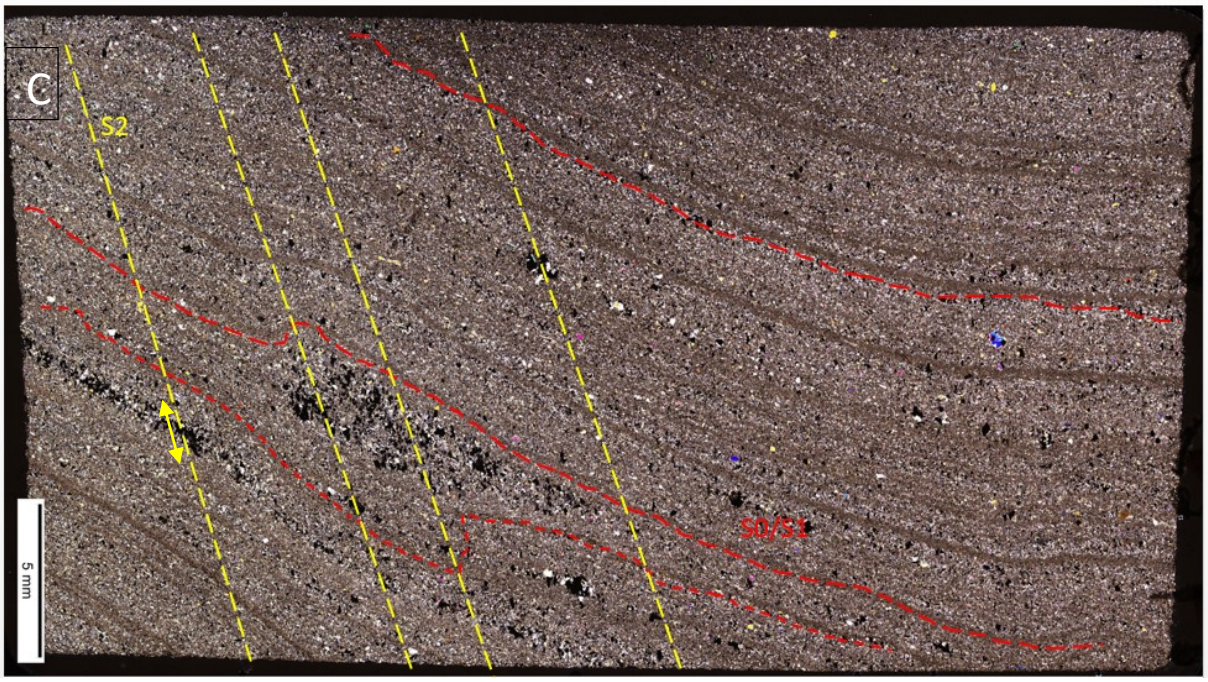


Figure 6-4 : Cross polarized light thin section of SM 04 showing S_0/S_1 fabric and S_2 fabric shown by the elongation of sulphide minerals appearing black. The yellow line represents S_2 and the yellow arrows shows the elongation direction.

Based on the dip and dip direction, three zones, A, B and C from west to east have been identified (Figure 6-5). The average dip gradually increases from 13° in Zone A to around 45° in zone C.

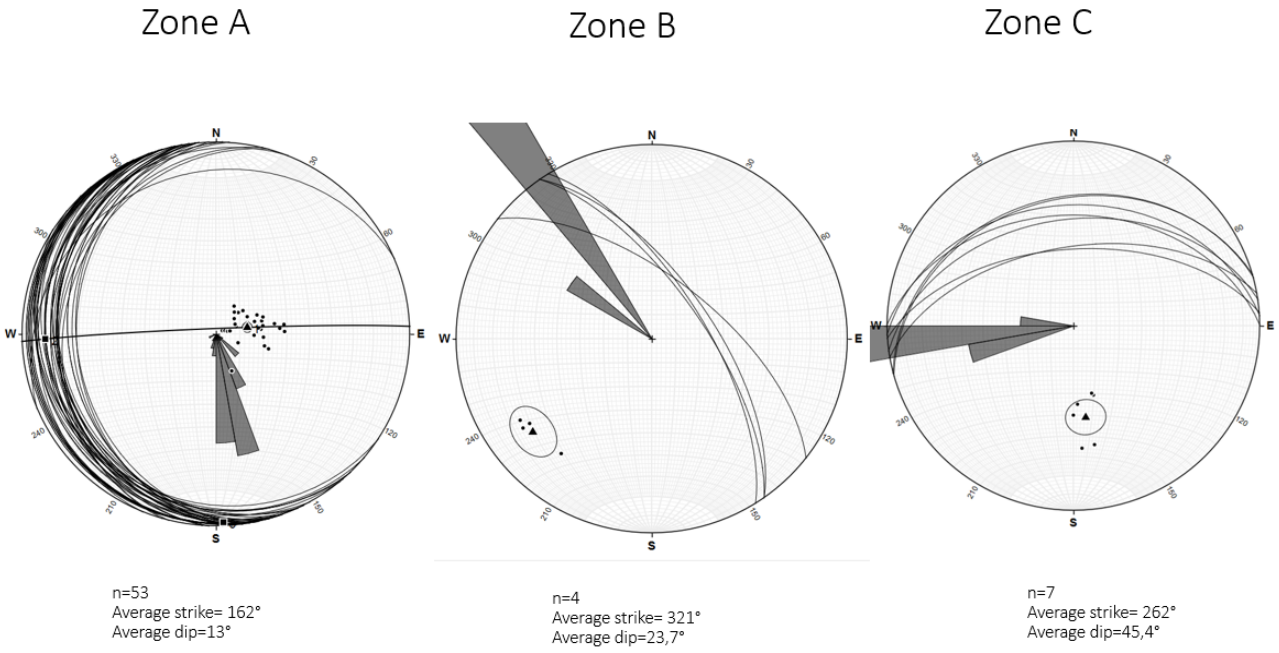


Figure 6-5: Lower hemisphere Stereo plots of S_1 on the 3 zones identified as shown in Figure 4-1

In the footwall conglomerate, another set of two planar structures (S-C fabric) are observed at a microscopic scale (Figure 6-6). The porphyroclast of mica in photomicrograph is lenticular forming a mica fish structure. The tail of the mica fish is parallel to the C-fabric.

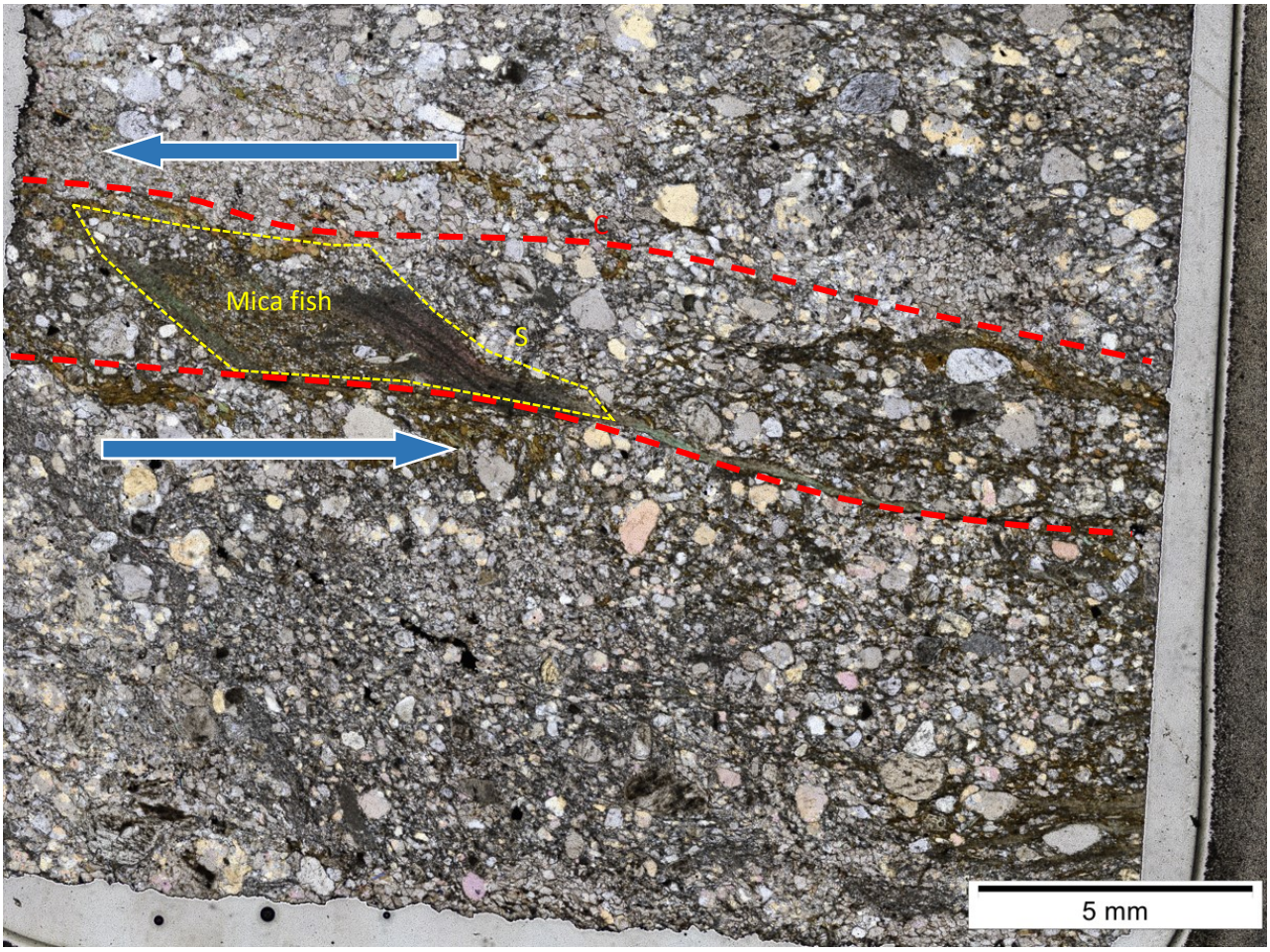


Figure 6-6: Photomicrograph SM 02, of the footwall conglomerate viewed under plane polarized showing mica fish developed and interpreted as a shear sense indicator of a left lateral shear.

6.2 Folds

Konkola East is situated on the northern limb of a major fold, the Kirilabombwe anticline. The anticline has a plunge of 10° to 15° to the northwest. The fold axis has a strike of N75°W. It is a tight and upright anticline with a sub vertical axial plane and an interlimb angle of 35° to 45°(Torremans et al., 2012). The Kirilabombwe anticline defines the first order folding. In Konkola East, parasitic folds are observed along the first order fold (Figure 6-7).

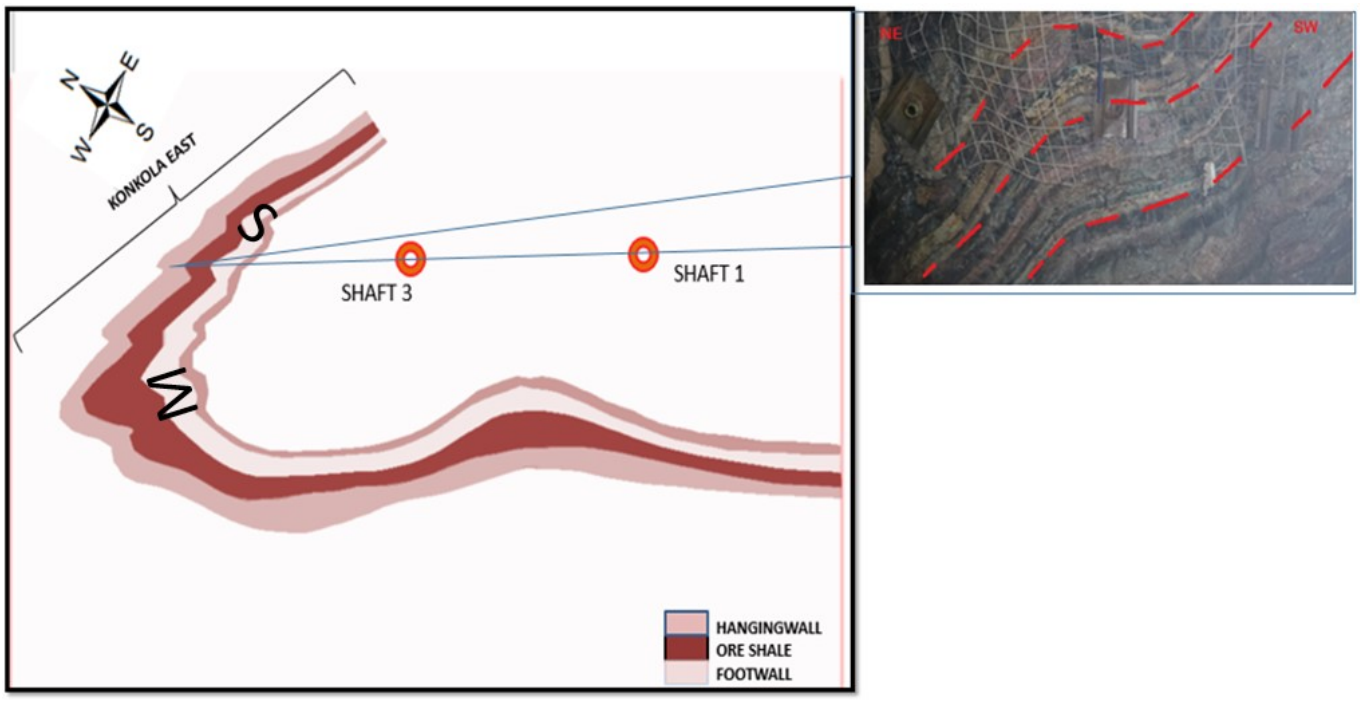


Figure 6-7: Schematic map of the Kirilabombwe anticline (not to scale) showing the location of Konkola east and the parasitic fold along the main fold.

The parasitic folds observed are m-folds in the western part close to the nose of the main fold and s-folds in the northern limb. The parasitic folds range from centimeter scale to meter scale. They are mainly symmetrical to slightly asymmetrical. The interlimb angle is approximately 110 degrees making most of them relatively open folds (Figure 6-8).

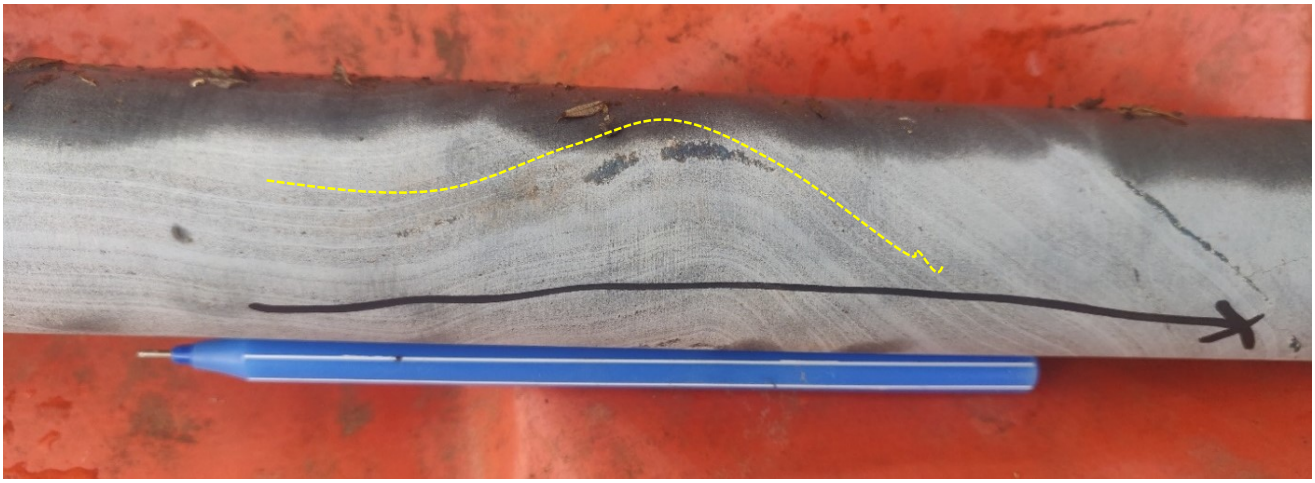


Figure 6-8: A relatively open fold observed from borehole BPN 881.

However, analysis of some core samples through logging showed that other parasitic folds are much tighter with a smaller inter-limb angle of less than 90 ° (Figure 6-9).



Figure 6-9: Folds observed in core logged. (a) Ore shale with well moderately open parasitic fold. Two generations of folds are observed here. F1 fold is refolded in folding event F2. (b) Folding observed in ore Hangingwall quartzite. (c) Folds in highly weathered ore shale unit with malachite mineralization (d) moderately open to tight folds developed in ore shale unit with chalcocite mineralization.

6.3 Faults

In Konkola East, four major faults were observed through mapping. These are steep with dips ranging from 55^0 to 80^0. They are oriented in NE- SW direction with displacement of approximately 15 m (Figure 6-2). There are also reverse faults which trend generally in the east to west direction but are generally observed to be of minor displacement ranging from centimeter scale to a few meters (commonly less than 5 m)(Figure 6-11). Close inspection of well-exposed fault surfaces in underground crosscuts suggested that stratigraphic displacement could be both dip-slip direction (Figure 6-11) and also lateral slip (Figure 6-15).

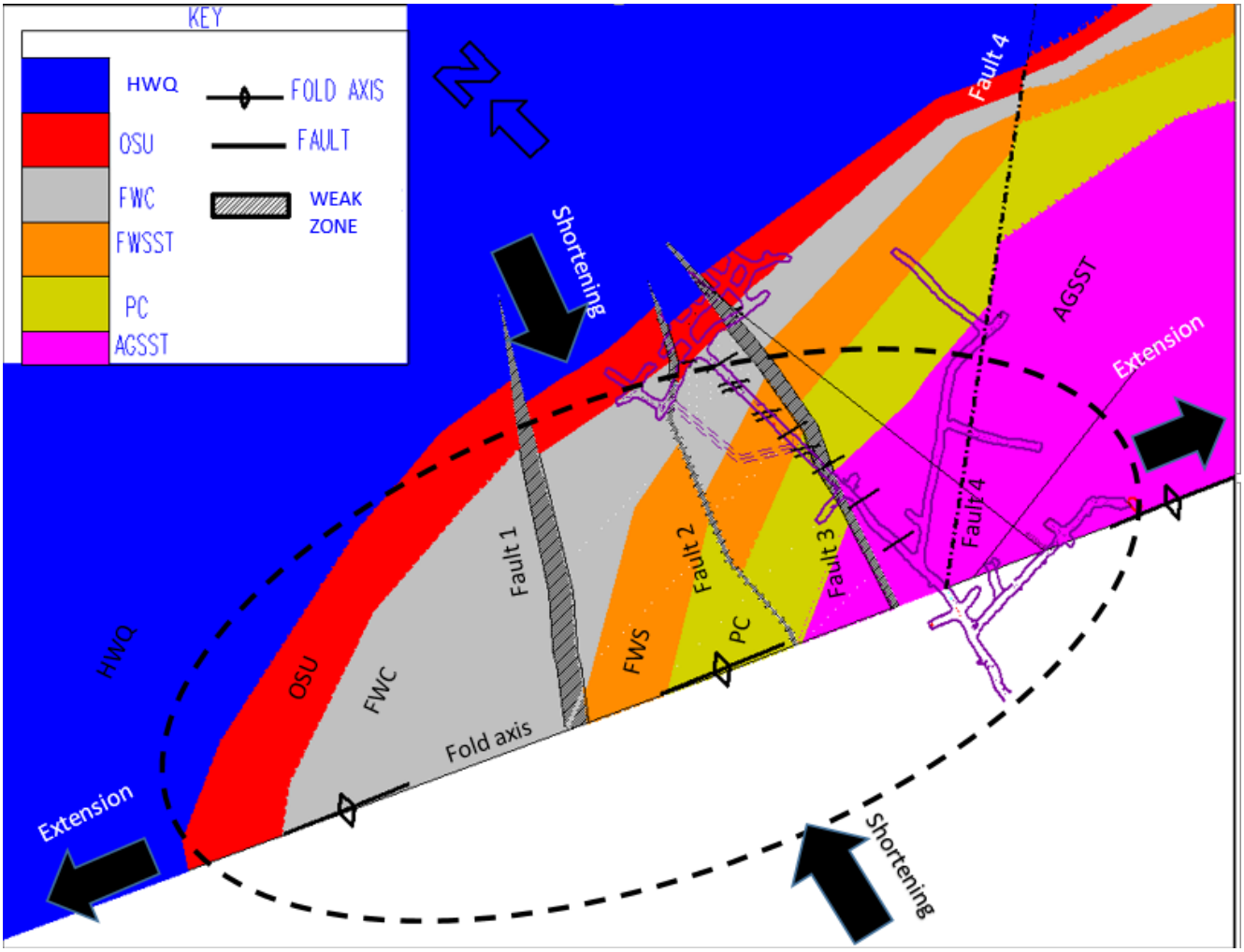


Figure 6-10: 780mL geological map showing the major structures and the ellipse demonstrating zones of extension and zones of compression

The faulting surfaces observed are not always straight but may be curved as shown in Figure 6-11. Two quartz veins are observed in Figure 6-11(a). The first one is layer parallel and attenuates at the fault plane and is significantly displaced upwards. The second quartz vein is observed to be oriented parallel to the strike of the observed fault plane Figure 6-11 (a). The fault trace at the point at which the second quartz vein forms is observed to be making a bend. This could mean this is a releasing bend and accommodation

was created that allowed accumulation of hydrothermal fluids that later crystalized to form the second quartz vein.

In Figure 6-11 (b), the fault trace is also observed to be curved. The hangingwall to this fault is observed to have significant malachite mineralization with most of it concentrated along the fault trace and at the fault bend. No quartz veins were observed on the fault bend. The concentration of the malachite mineralization is observed to be more in the up-dip direction of the fault bend and less down dip. These observations could mean that this is a retraining bend. The weathering observed along the fault trace could further mean that the fault acted as a conduit of water up until the retraining bend.

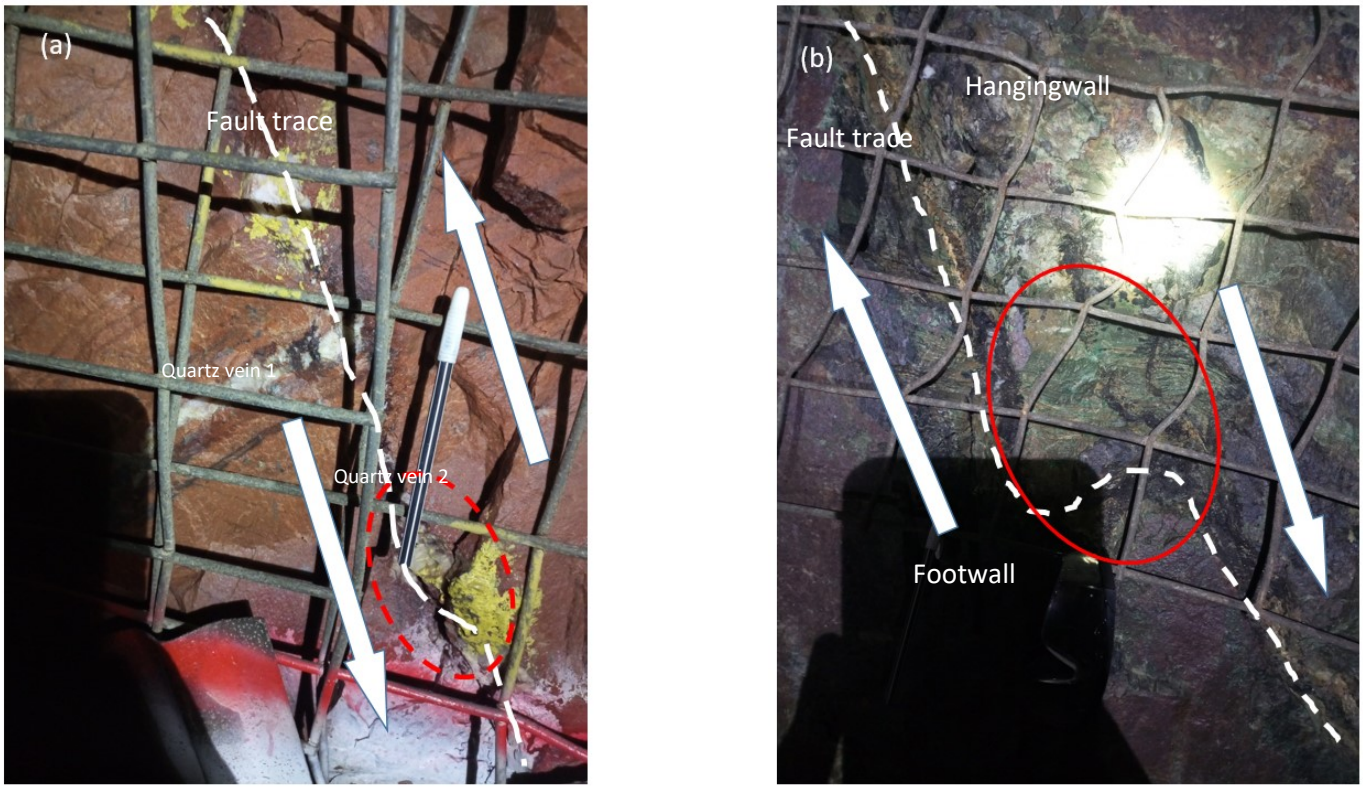


Figure 6-11: High angle faults observed in Konkola east. (a) Steep reverse fault with a releasing bend (circled in red) observed facing east. (b) A normal fault with a restraining bend (circled in red) as observed on the 2400mW pillar cross cut 3 facing northwest.

Mapping in the area and detailed analysis of the core also revealed the existence of a number of fault zones. The fault zones are of varying orientation and also of varying scales from centimeter scale to a few meters thick. The shear sense indication is mainly dip-slip in both a normal and reverse direction (Figure 6-12). The fault zones range from brecciated to highly weathered unconsolidated material. These fault zones when intersected in drill core tend to have very poor recovery and very low rock quality designation (RQD). When encountered underground, they are often wet, loosely consolidated and tend to develop sudden inflows of mud.

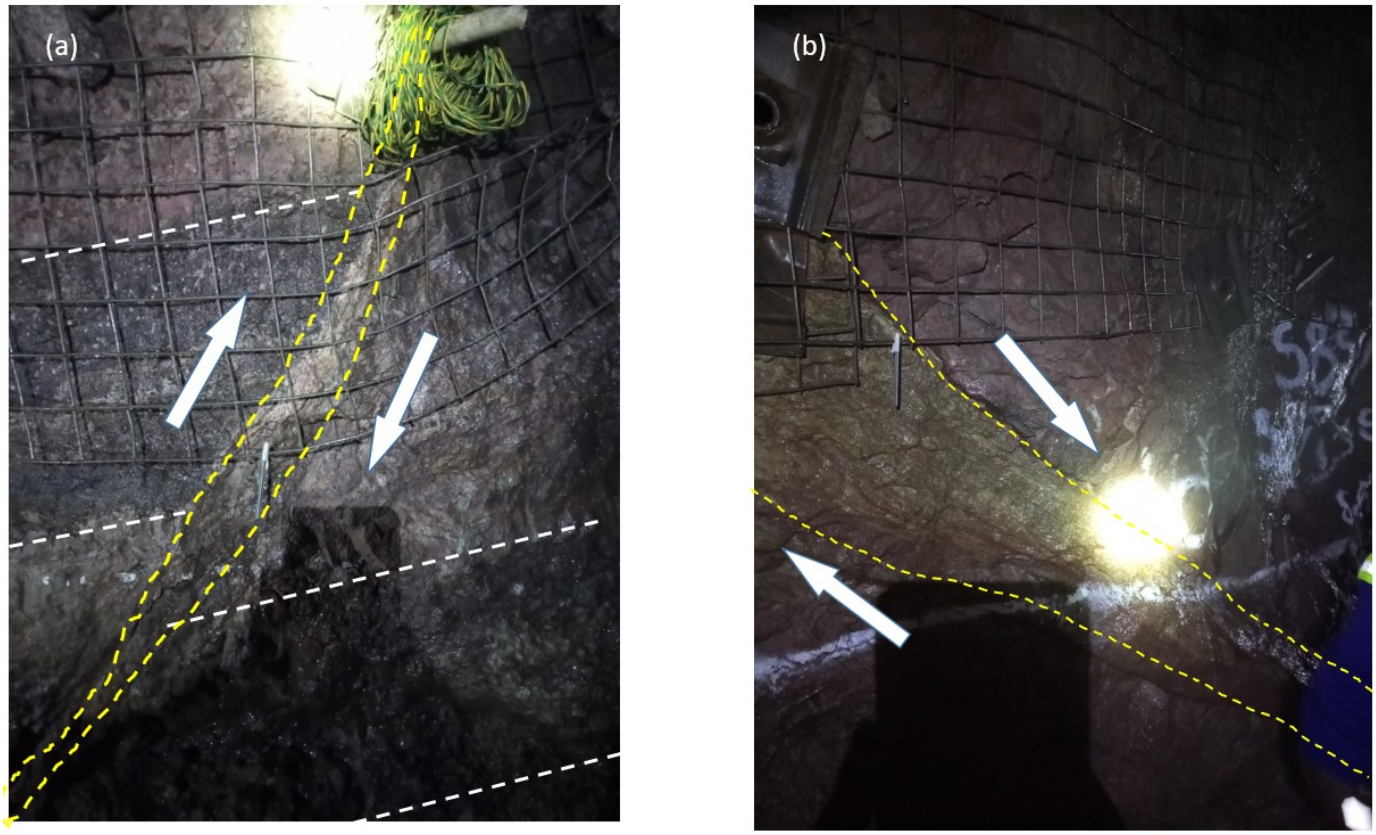


Figure 6-12 Mapped fault zones from underground. (a) Minor fault zone with a reverse shear sense and minor displacement. (b) Medium sized fault zone with a normal shear sense and displacement above 5 meters.

The fault zones are generally observed to contain an aggregate of highly fractured rock fragments with a matrix of some other finer grains. Most of the fragments observed around the fault zones are sharp and angular. The grains are generally poorly sorted and in some parts the general grain size is reduced compared to the rest of the rock on either side of the fault zone. This could have been formed through cataclasis. The intensity of cataclasis observed in the fault zones was both relatively low as shown in Figure 6-13 and also relatively high as shown in Figure 6-14.

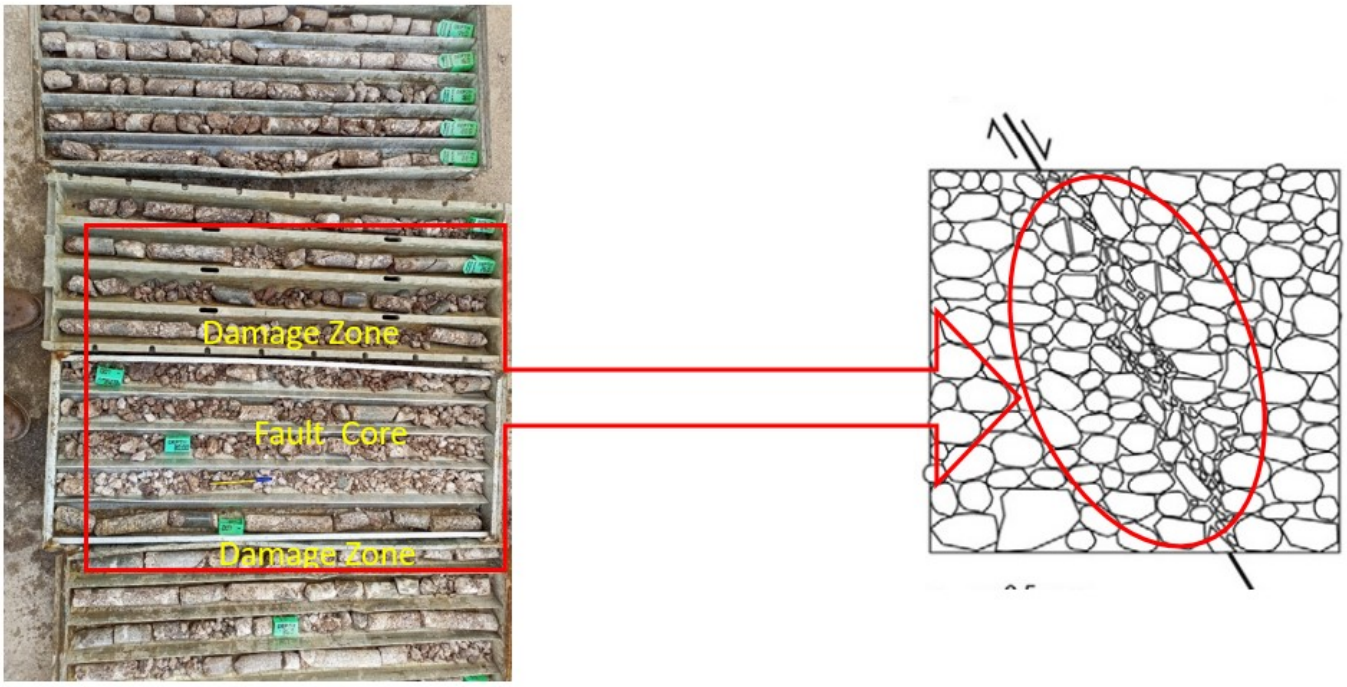


Figure 6-13: Observed brecciated Fault zone in DVN 1592 with relatively low intensity of cataclasis.

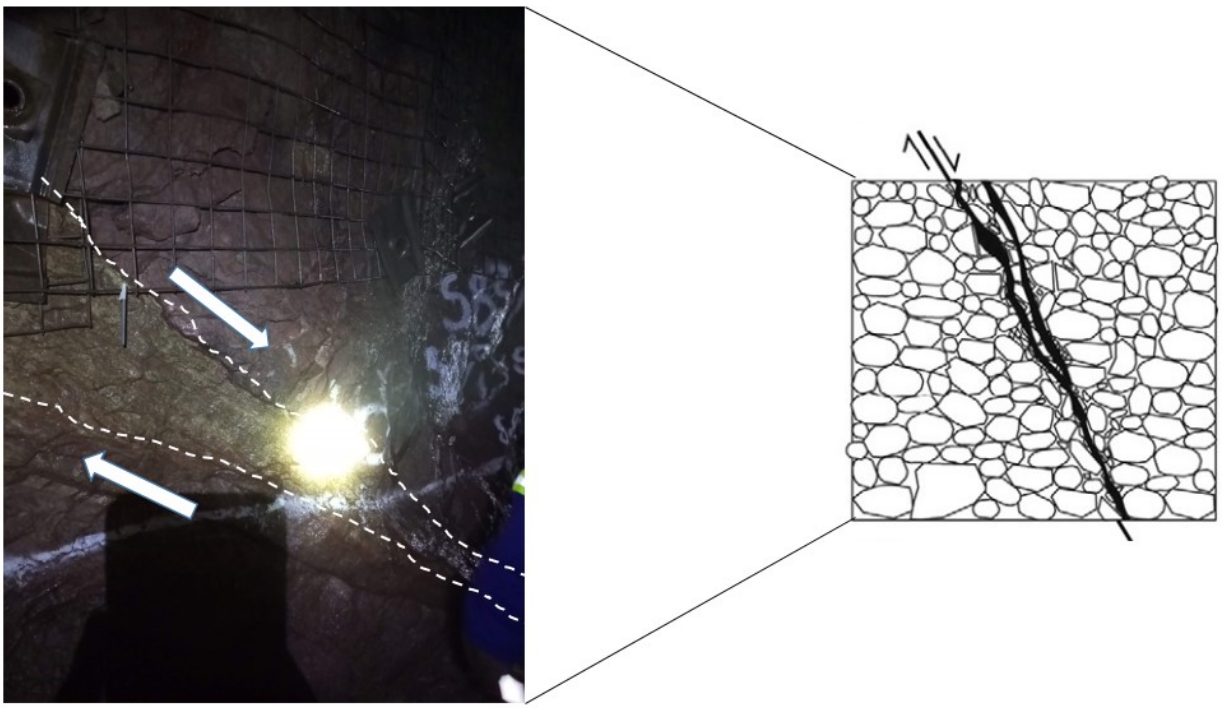


Figure 6-14: Underground photo from 2400mW Konkola east showing a normal fault with relatively high intensity of cataclasis.

There are also minor normal faults that show a much smaller displacement (less than 1 m). These are numerous and are observed both in underground cross cuts and also in some boreholes drilled in Konkola East (Figure 6-15).



Figure 6-15: Minor fault structures observed at Konkola East. (a) Minor strike slip fault observed in BPN 893. (b) Slickensides observed in a quartz filled faulting surface. Kinematic analysis on this site based on the smoothening direction indicated the fault to be a low angle reverse fault . (c) Slickensides observed along bedding planes in BPN 883. This confirmed the existence of bedding concordant faults that contributed to creation of saddles. (d) A fault indicated by a sharp contact between the oreshale Unit and the footwall sandstone. In this borehole and at this site the footwall conglomerate is missing indicating a stratigraphic gap caused by faulting. (e) Minor normal fault observed from BPN 876.

6.4 Joints

Konkola east is cross-cut by a network of joints, and three main joint sets are observed based on the data collected through this study and a correlation with historical data from levels above (Figure 6-16).

Joint set, J_1 trends northwest to southeast and dips to the northeast. This strike is sub parrallel to the general strike of Konkola east and also subparallel to the axial plane of the main Kirilabombwe fold. J2 trends from northwest to the southeast and dips to the southwest. J_3 is northeast – southwest trending and dips to the southeast (Figure 6-17).

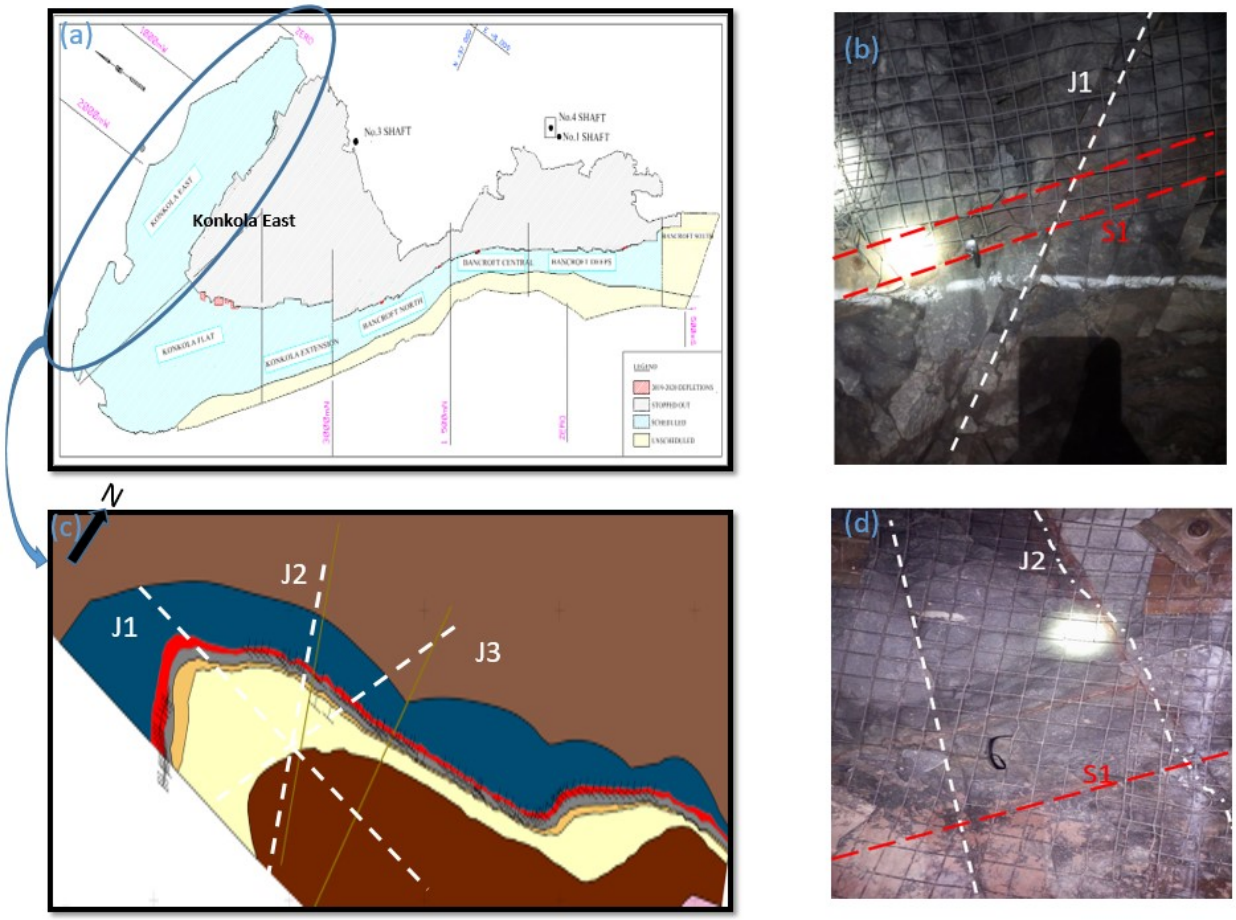


Figure 6-16 Jointing pattern in Konkola East. (a) General map showing the location of Konkola east. (b) Underground photo showing the relationship between S1 and J1. (c) Geological map of Konkola East showing the general trend of the identified major joint sets, J1, J2 and J3. (d) Underground picture showing the Orientation of J3 and J2 in relation to the bedding parallel S1.

Joint set 1, J_1, is observed to have rough surfaces. It is moderately wet and has no visible infilling mineral. The joint apperture is mostly less than 1 mm. The J1 discontinuities have an average spacing of 20 cm and they are persistant over an average length of 3 meters. Joint set J2 is smooth, with iron oxide infill. It is relatively wide spaced ranging from 60 cm to 200 cm. The joint apperture is approximately 1 mm and it is consistent over length of 3 meters to 10 meters. The third joint set J3, is smooth and has iron oxide infill. It has a discontinuity spacing of 20 cm to 60 cm and joint apperture of 1 mm to 1.5 mm. J3 is consistent over lengths of 3 meters to 10 meters.

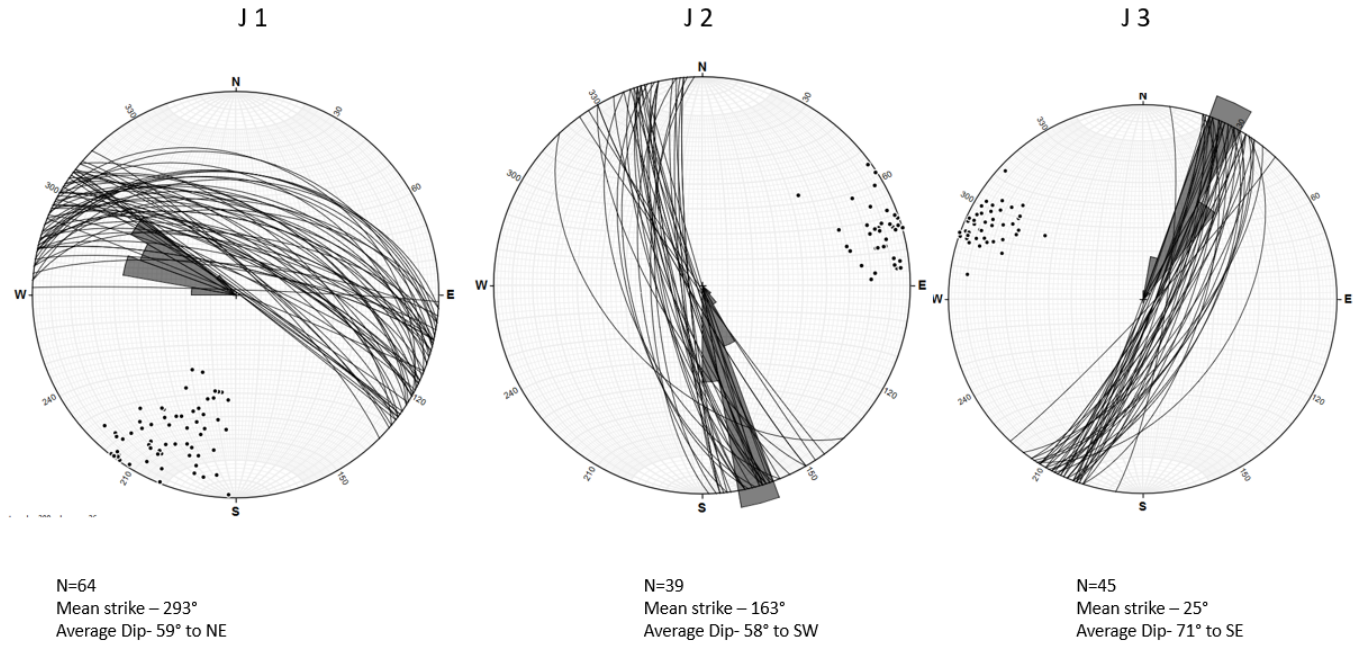


Figure 6-17: Lower hemisphere plot of the orientation of the established joint sets.

The intensity of jointing varies from rock type to rock type as shown in Table 3. Joint spacing ranges from 5 mm to over 2000 mm. The Ore Shale Unit is observed to have the most closely spaced jointing pattern (5 mm-20 mm to 20-500 mm) while the joint spacing in the Footwall Quartzite is wide and often observed to be over 2000 mm.

Table 3: Range of joint spacing per lithology in Konkola East

Lithology	Range of discontinuity spacing (mm)	Description
Footwall Quarzite	500-2000 to >2000	Widely spaced
Argillaceous Sand stone	60-200 to 200-500	Moderately to closely spaced
Porous Conglomerate	200-500 to 500-2000	Moderately to widely spaced
Footwall Sandstone	60-200 to200-500	Moderately to closely spaced
Footwall Conglomerate	200-500	Moderately spaced
Ore shale Unit	5-20 to 20-500	Closely spaced to medium spaced

J1 is oriented sub-parallel to the fold axis and could have developed as cracks as the elasticity limit was reached during the main folding event. Joint sets J2 and J3 are oriented north to south and cut across the fold axis.

6.5 Structure and Mineralization

The structures observed in this study were compared to mineralization. The goal was to establish if there was a relationship between the observed geological structures and mineralization.

Hinge zones of folded structures tend to have enhanced grades (Figure 6-18). The fold hinges acting as dilatational zones offered accommodation through flexural slip. Folding and faulting that is concordant to bedding is observed to have led to dilation of some hinge zones by forming simple saddles providing sites for later mineralization (Figure 6-18). Through flexural slip, the bedding planes are separated on a local scale to create accommodation in which mineralizing fluids can flow.

Bedding concordant faults are observed as planes parallel to the bedding planes and appear to be propagating through the hinge zone and causing general displacement of strata beyond the hinge zone (Figure 6-19). In this situation, faults that started initially as bedding concordant faults ends up being discordant on the other side of the hinge zones.

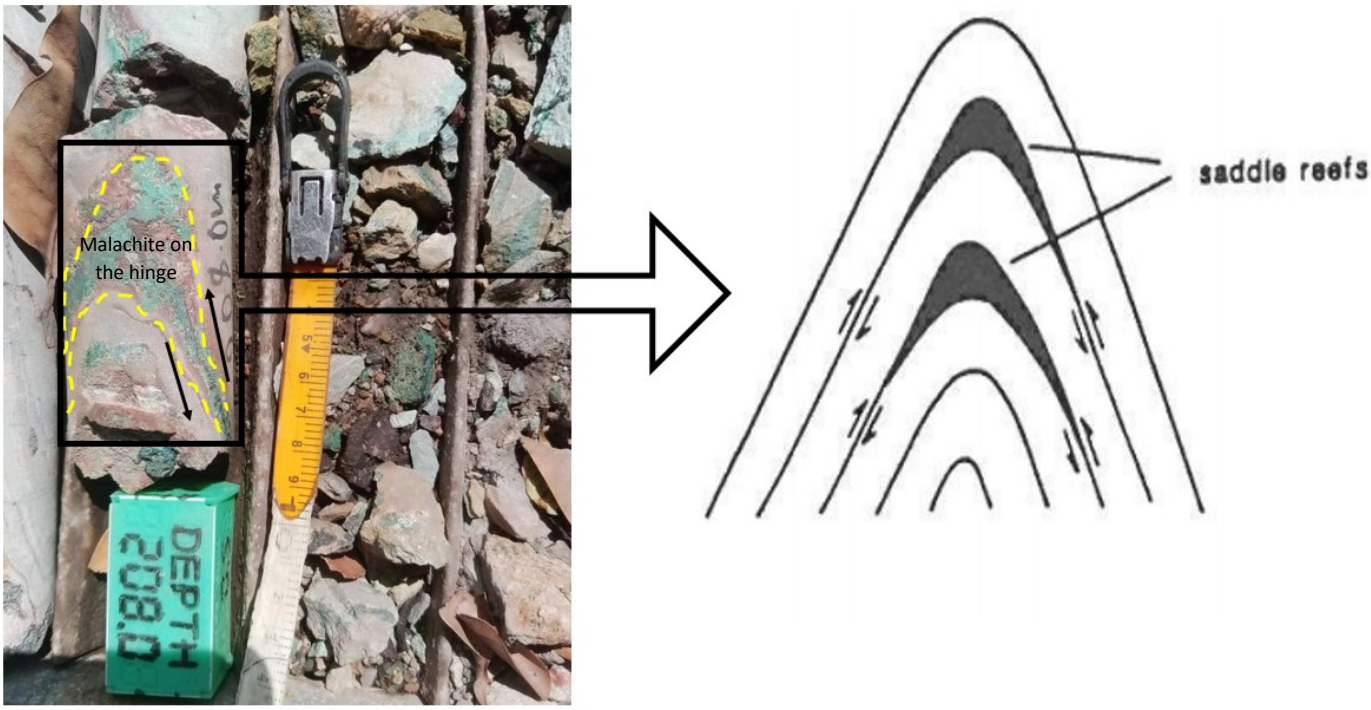


Figure 6-18: Photo from BPN 891 showing crescentic saddles created through flexural slip and hinge dilation through the folding process. Malachite mineralization is observed to be concentrated on the fold hinge. Schematic illustration done after(Cox et al., 1991)



Figure 6-19: Core photo from BPN 881 showing bedding discordant fault resulting from flexural slip on one limb that goes through and breaks across the fold hinge. Schematic illustration done after (Cox et al., 1991)

The four major faults that were mapped were plotted against the 2016 Konkola resource model (Figure 6-20). While there is a zone of high grade between Fault 2 and Fault 3, only a few high grade blocks are observed around Fault 1 and Fault 4 has no high grade blocks in its vicinity.

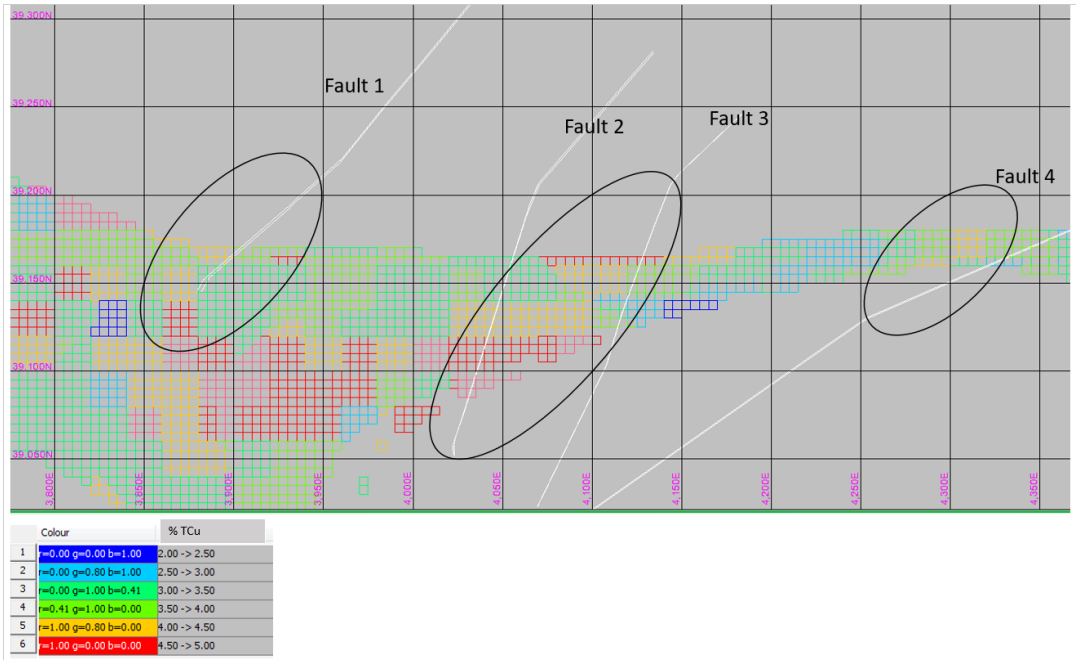


Figure 6-20: Grade maps showing grade in relation to the four major faults modelled on 609m level elevation. The circled areas show range associated with the faults.

7 Geological Modelling of Konkola East

A short term geological model was created from the geological structures that were collected in this study and this chapter explains how this was achieved. A brief history of geological modelling at Konkola mine is first provided. The available data for modelling and the validation procedure are explained. The modelling process used is also described. Finally, the model results and the validation of those results are given in this chapter.

7.1 Available Data

The short term geological model in this study was created using both historical information and also data that was collected during the course of this study. The data included historical boreholes drilled from surface (8) and recent boreholes (21). Mapping from old upper levels was also scanned (Figure 3-3) and digitized then used in the modelling process. Part of the historical data was available in Excel format. This mainly included the orientation of joint sets (dip and dip direction) and bedding planes (see Appendix A).

Table 4 below summarizes the available data that was used for geological modelling exercise in this study.

Table 4 : Available data that was used in the creation of the short-term geological model.

SN	Data	Description	Amount of data used
1	KLB drill holes	Historical surface holes	8 boreholes.
2	BPN drill holes	Underground exploration holes	18 holes.
3	DVN drill holes	Underground Infill drilling (stope delineation) holes	3 holes.
4	Scanned plans	Scanned and digitized historical mapping from old mine working levels	3 level plans.
6	Current mapping	Mapping done in this study was used in the modelling process	12 cross cuts.

7.2 Data Validation

The borehole data in the three tables, collar table (Appendix B), survey table (Appendix C) was subjected to a validation process before it could be used in the modelling process. The main errors identified in the validation process were inconsistences in naming in the various tables. For example, while in the collar table the borehole id would be referred to as “BPN 870”, in the survey and other tables, the same drill hole would be named “BPN870” without spacing. This was easily resolved by ensuring consistency in all fields. It was also noticed that 2 boreholes had no indicated depth “EOH”. This was resolved by referring back to the geological log sheets.

The other common error that was noticed was differing borehole depths in various tables. Some boreholes would be captured in the collar table to be of a depth shorter than the logged meters in the geology table (see Appendix E). This was observed in borehole number BPN 873, BPN 877 and BPN 888. These drill holes were rejected in all other tables. This was resolved by referring back to the log sheets and reconciling with the drilling reports. This was made possible by the availability of the log sheets.

In the geology table, the main error that was noted in the validation process was over lapping samples in the geology field (see Appendix E). This was also resolved by referring back to the log sheets.

7.3 Modelling Process

The geological model was created using Surpac 6.6 software following the work flow shown in Figure 7-1. The process started by first validating the data available in Table 4 to ensure errors were eliminated. The digitized historical data was then combined with current mapping data in microstation software and then imported into surpac software.

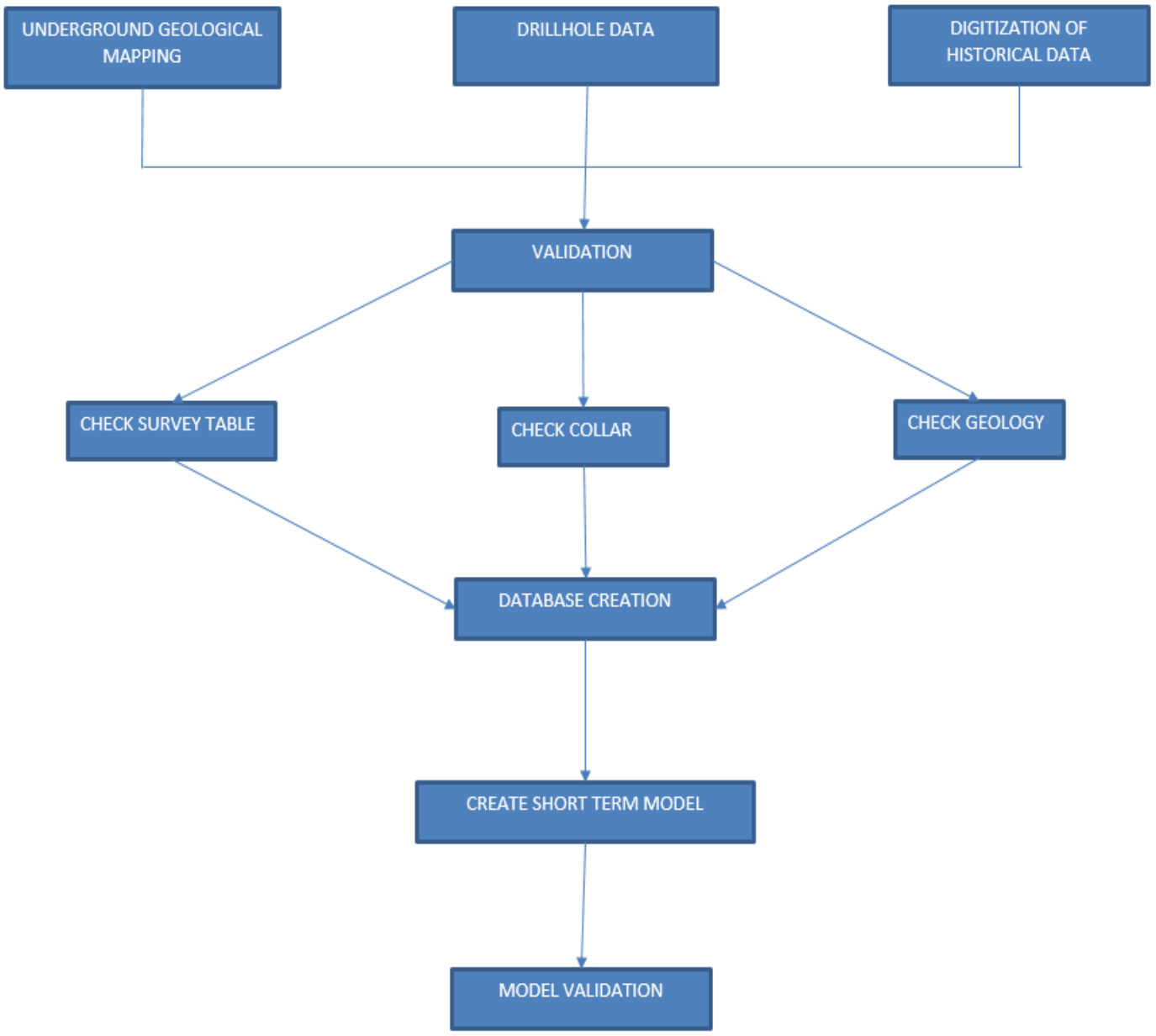


Figure 7-1: Workflow followed in generating the short term geological model.

The model was created with extents such that one level was included both above and below the current working areas (760 m and 780 m levels). The levels included were 800 m below and 740 m above. This meant the vertical extent of the created short term geological model was 60 m. The horizontal extents were based on the extent of the 2520 m West retreat which stretches from 2800 m West to 2400 m West

giving a strike length of approximately 400 m. Fault 4 was taken to be the eastern limit and the western limit was the 2800 m West orientation line.

On the basis of the major faults identified in the structural analysis, the 2520 m West block was further subdivided into four blocks for ease of modelling. The blocks were subdivided according to the faults and the faults formed the boundaries between the blocks (Figure 7-2). Vertical sections were created in each block at a 15 m spacing in block 1, 10 m spacing in blocks 2 and 3 and at 15 m spacing in block 4. This spacing was based on the availability of data such that the increased data allowed higher confidence in the modelling process.

The sections were then manually snapped to both the mapping data and the boreholes. A solid was created for the ore shale by triangulation of these sections in each block. The ore shale lithology was defined by the contact between footwall conglomerate (FWC) and ore shale in the footwall side, also called geological footwall (GFW) and Hangingwall quartzite (HWQ) the contact between ore shale unit, also called the geological Hangingwall (GHW).

For the other footwall formations, only surfaces were created in this exercise. These surfaces defined the bottom (footwall contact) of each formation. The footwall formations that were exposed and modelled as surfaces were the Footwall Conglomerate (FWC), Footwall Sandstone (FWS) and the Porous Conglomerate (PC).

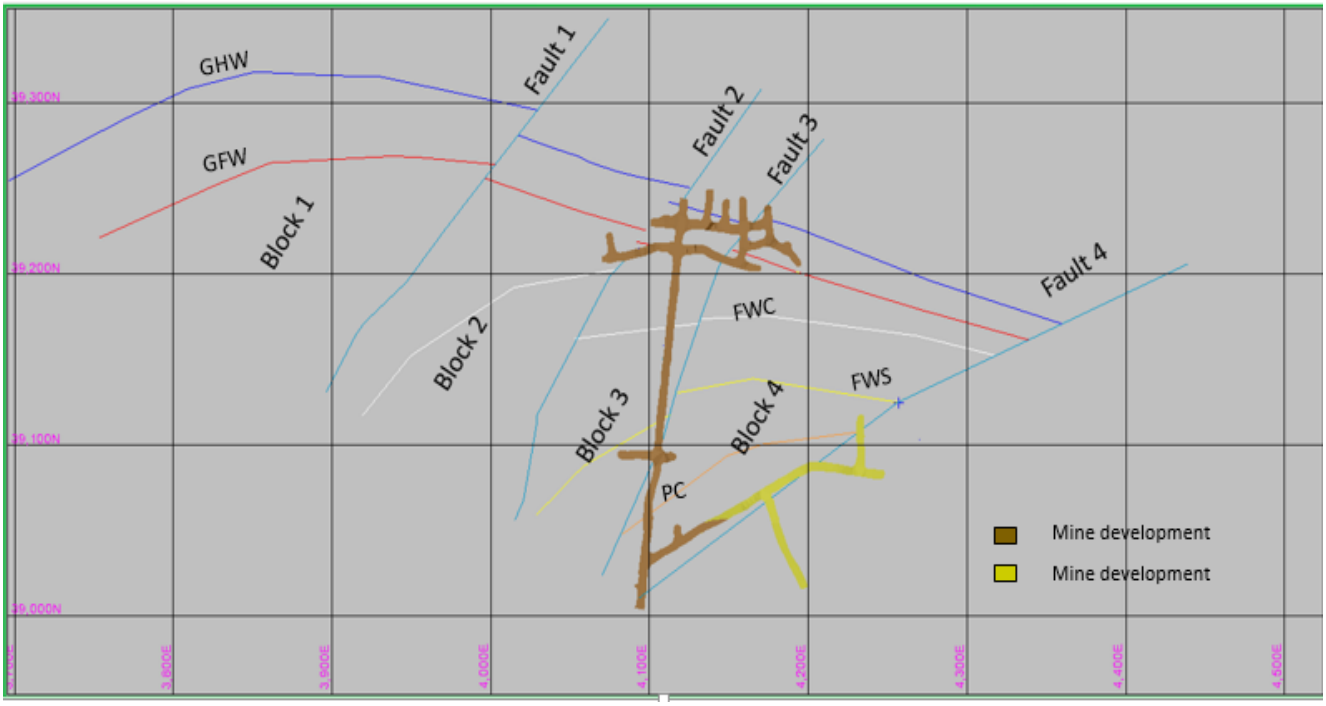


Figure 7-2: Surpac plan view of 780 m level showing the 4 blocks and the 4 major faults. The lines indicate lithological contacts.

7.4 Model Results

The geological model was successfully created and from the plan view (Figure 7-3), a section A-A' (Figure 7-4) was generated. When viewed in isometric view (Figure 7-5), the modelled faults are observed to be steep, sub-parallel to each other and cutting across the general strike of the ore shale unit.

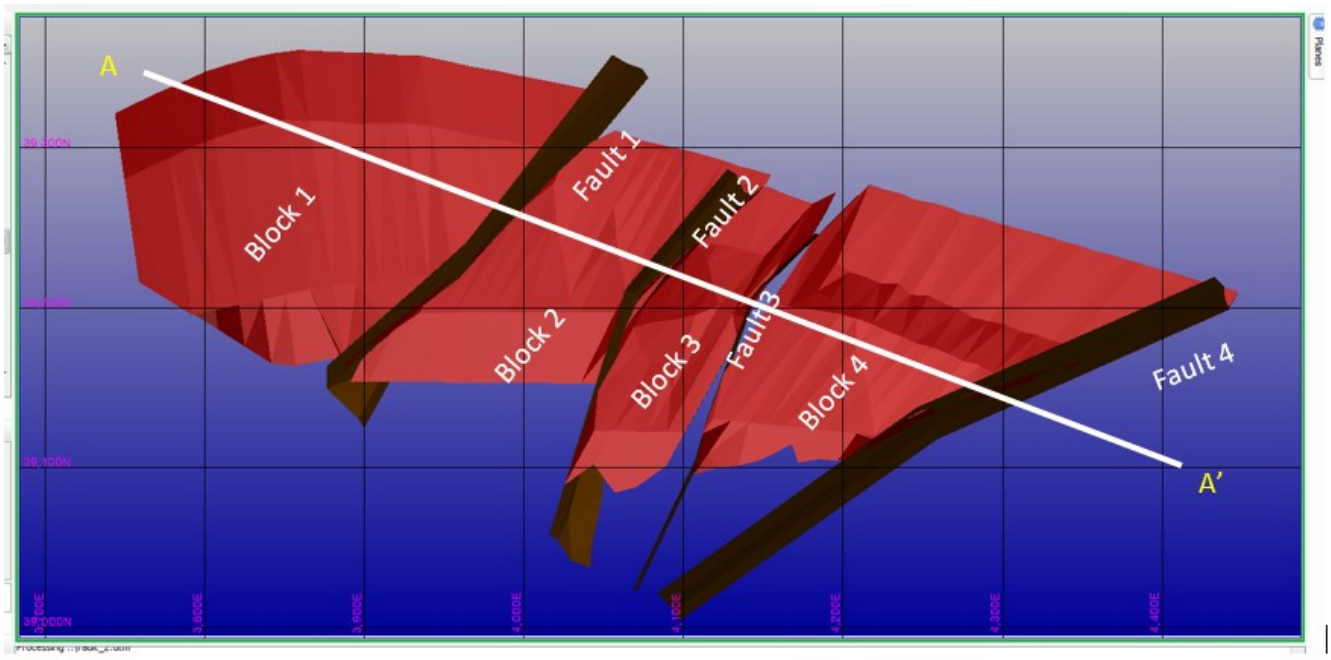


Figure 7-3: Plan view of the created geological model showing the four faults and the 4 blocks.

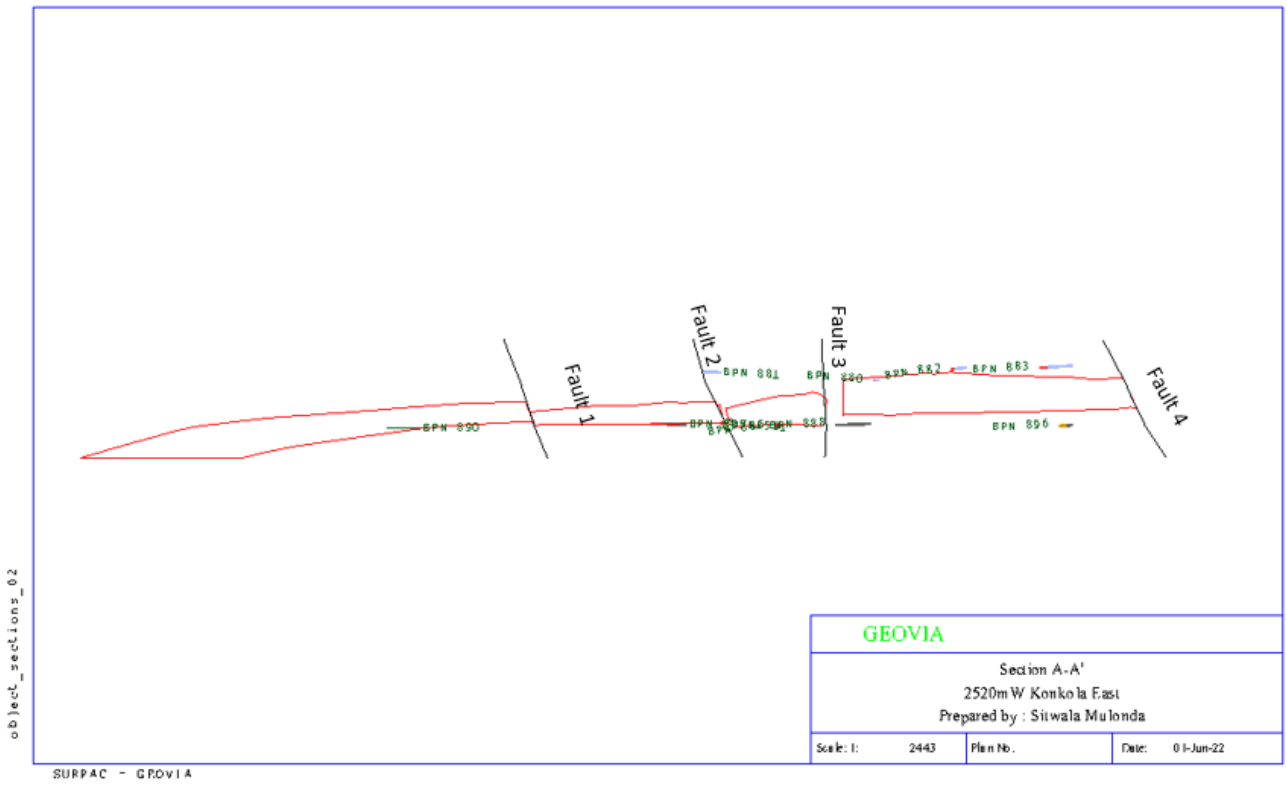


Figure 7-4: Section along A-A' showing the four major faults identified in the study and the ore shale lithology

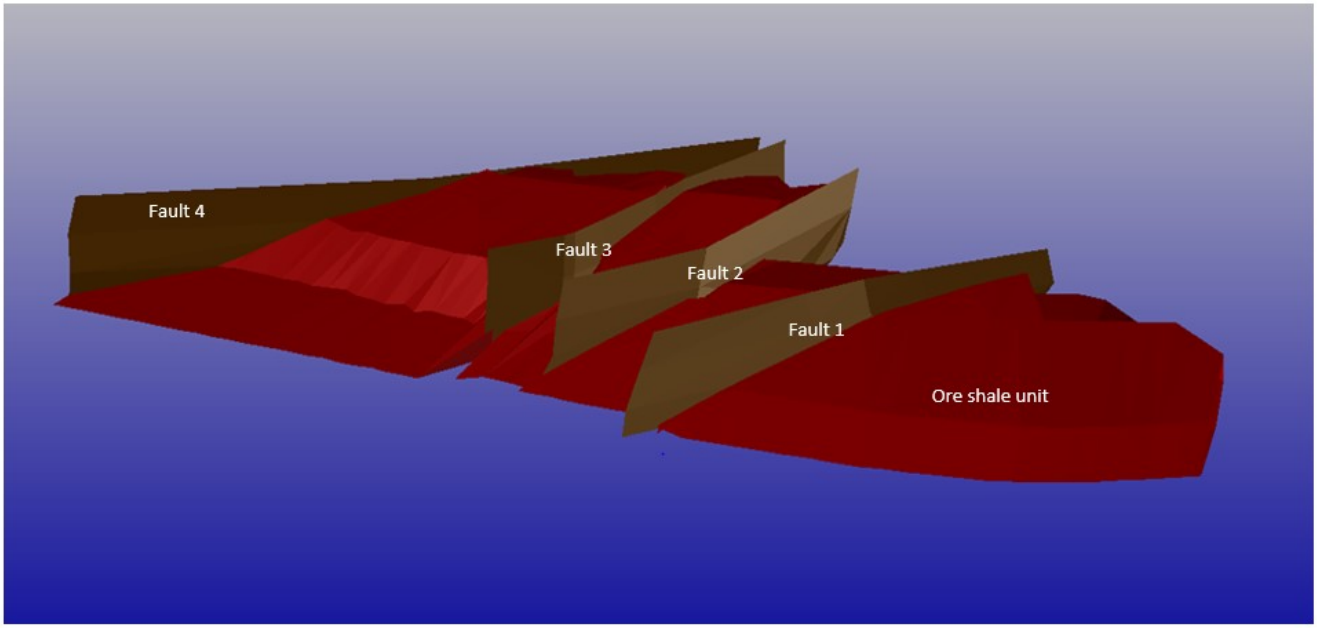


Figure 7-5: Isometric view of the created model facing south-west the four main faults identified (in brown) and the ore shale unit lithology in red.

Solids for the ore shale lithology were created for all the four blocks (Figure 7-3). The geological model gave volumes of 464569m^3, 149984m^3, 124460m^3 and 293186m^3 in block1, block 2, block 3 and block 4

respectively (see Appendix F). The total volume for the ore shale lithology as modelled was found to be 1,032,199m^3.

7.5 Model validation

The model was validated by creating random cross sections and long sections (Figure 7-6). This was meant to check that the model thickness was as expected. It was also meant to check if the created model was reflective of the primary data used for modelling such as mapping data and drill holes. Most sections randomly checked were found to be of the expected thickness.

The solid once created was also validated to check for open and disconnected objects. This validation was done using surpac software and a report was generated (see Appendix G). The report as shown indicated that some edges were invalid. This was corrected by manually re-triangulating the affected edges.

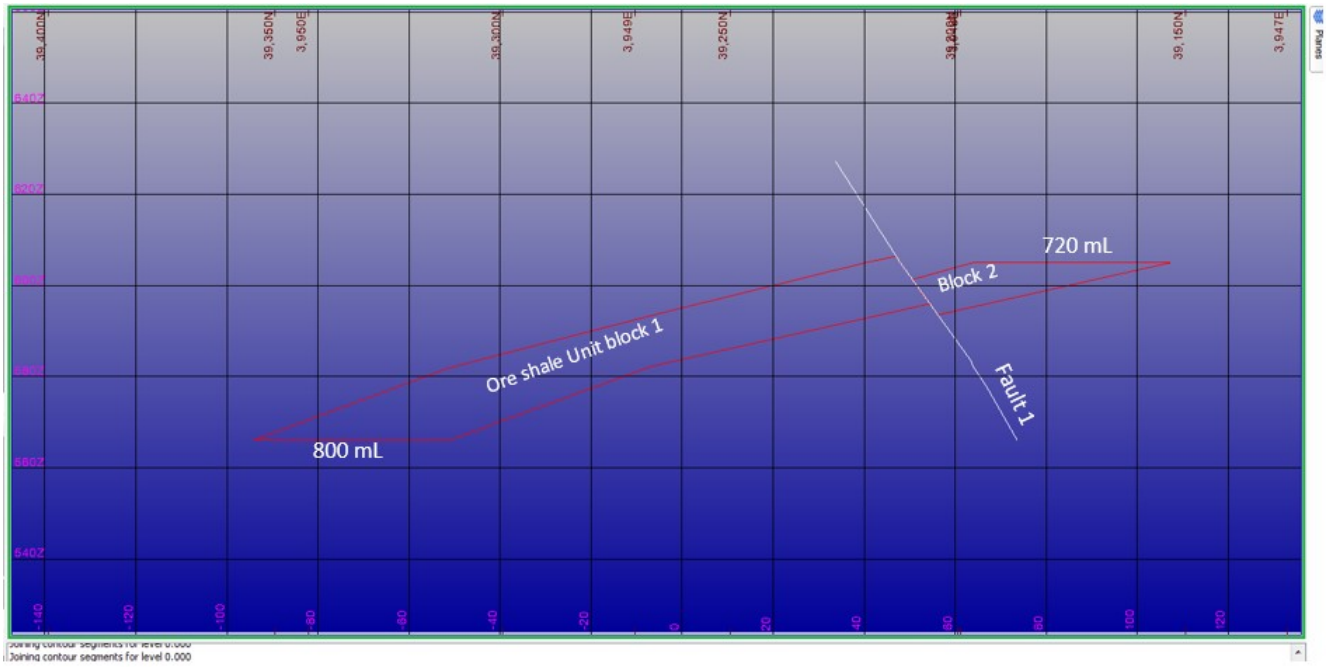


Figure 7-6 : Random section of the created model used for validation purposes showing the ore shale lithology displaced in a normal way along fault 1.

8 Discussion

Major and minor geological structures have been identified and mapped in Konkola East. These geological structures include major normal faults striking north-south and low angle reverse faults striking east-west and sub- parallel to the regional fold axis. Parasitic folds were also identified. Further, a network of three joint sets was also mapped.

From the structures mapped in this exercise, Konkola east could be part of a dextral strike slip fault structural pattern as shown in Figure 8-1. All the four normal faults strike north to south and are steeply dipping. The reverse faults (Figure 8-1) trend west to east and dip to the south. The fold axis is inferred to be oriented east to west.

The fold axis and the reverse faults at Konkola east just like in Figure 6-2 are developed parallel to the direction of maximum extension. On the other hand, the normal faults are developed perpendicular to this direction and parallel to the direction of maximum shortening. J1 is oriented sub-parallel to the fold axis and could have developed as cracks as the elasticity limit was reached during the main folding event. Joint sets J2 and J3 are oriented north to south and cut across the fold axis.

The orientation of the mapped structures largely conform to the expected pattern of a dextral strike slip fault (Figure 8-1).

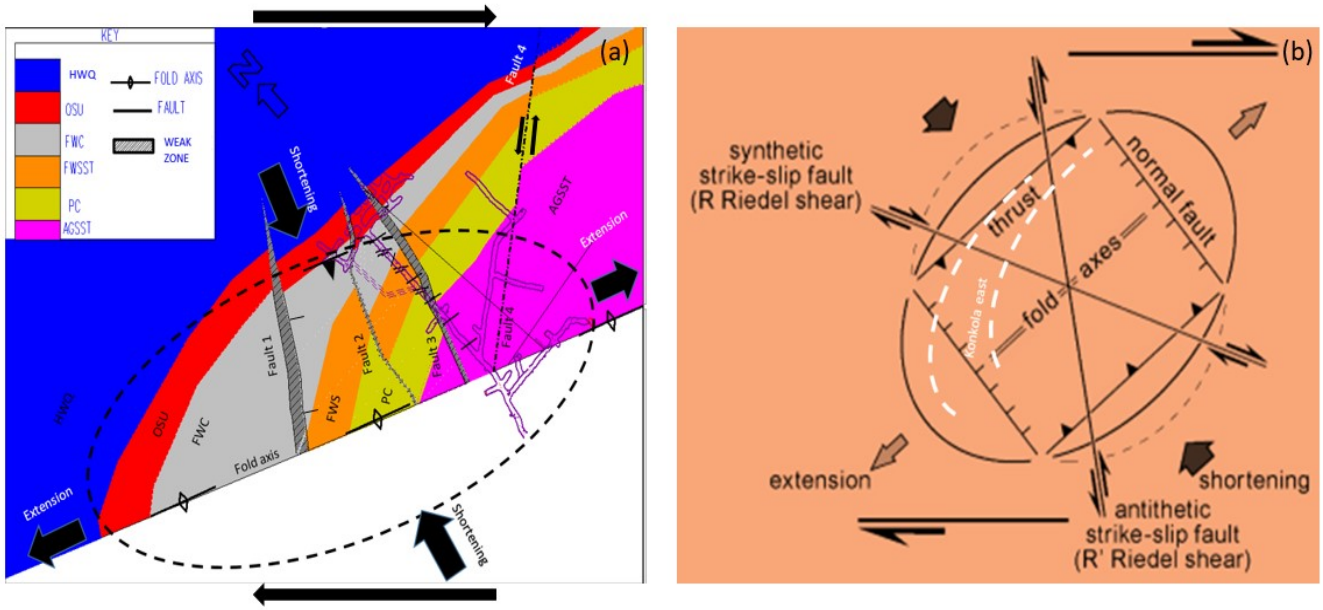


Figure 8-1: Structural pattern of Konkola East compared to the expected structural pattern of a typical dextral strike slip fault. (a) structural pattern observed and mapped at Konkola east in this study. (b) Structural pattern of a typical dextral strike slip fault (Eggers, 2016)

Although fault 4 is mapped as a normal fault, it registers a significant lateral displacement and it could be interpreted as an antithetic strike –slip fault (Figure 8-1).These strike slip faults were interpreted as being induced by the collision of the Kalahari craton and Congo craton which led to the clockwise rotation of the blocks of the Lufilian belt (Porada and Berhorst, 2000)

Most of these structures are observed to be influencing mineralization in some way. The hinge zones of folds are observed to contain significant volumes of ore. Grade maps for the study area (Figure 6-20) however indicate that the highest grade blocks are not in the vicinity of the mapped and modelled faults.

The trend observed in this study is fairly consistent with the observations by Torremans et al.,(2012) who concluded that these structures were pivotal in the mobilization, remobilization and eventual enrichment of ore. These structures offered permeability that allowed for movement of supergene fluids, and the concentration and leaching of metal.

According to (Sixtus, 1991), fracture zones and faults are the major flow channels for ground water at Konkola. In this study, the structural analysis of Konkola east and subsequent geological modeling revealed the existence of major faults, shear and 3 joint sets. These structures act as conduits for water flow from aquifers in to areas that are otherwise considered relatively dry making them extremely wet (Konkola Copper Mines, 2020a). In Konkola east, this is almost always true for joint set J_2 which is relatively open and observed to be wet. Faults and shear zones however on the other hand can either increase or decrease permeability(Bense et al., 2013).

8.1 Deformation history

In this study, three deformation phases are recognized. The first deformation phase is regarded as a result of deep burial and led to the formation of the bedding parallel foliation as observed in Figure 6-4.

Inversion of tectonics from extension to compression led to the formation of the main folds and among them the Kirilabombwe anticline where Konkola east is located (Brems et al., 2009) . In this study, it is proposed that the earliest indication of inversion in Konkola east is the formation of the layer parallel veins (Figure 4-8).

Similar to the Nkana deposit, supralithostatic fluid pressure is required for fluids to attain a vertical opening against burial pressure (Muchez et al., 2010). This can however be made easier to achieve with compressive pressure which could have been provided by the onset of the compression during the Lufilian orogeny (Brems et al., 2009). The formation of F2 folds (Figure 6-9) and the small offset reverse faults could have probably also happened late in this deformation phase.

The third deformation phase is inferred from the existence of faults of varying scale and orientation. This together with joints cross cut the folds at an angle to their axial surfaces. This has also been observed at other deposits in the Lufilian arc and has been estimated to occur at the end of the Lufilian orogeny or possibly postdating the Lufilian orogeny (Haest et al., 2007). The compression introduced by the Lufilian orogeny could have re-activated the syn-rift faults at Konkola in a near dextral manner leading to the formation of Kirilabombwe anticline and the other related structures.

These three deformation phases observed at Konkola east in this study correlates fairly well with earlier work done on a regional scale as shown in Table 5.

Table 5: Table showing major deformation events noted in Konkola east and correlated to other previous work done on a regional scale. Modified after (Kampunzu and Cailteux, 1999)

INTERNATIONAL LITHOSTRAGRAPHIC SUBDIVISIONS	According to Francois (1974, 1987, 1993) and Cahen ct al. (1984)				According to Kampunzu and Cailteux (1999)			This Study (Konkola East)		Stress Regime
	Organic cyc	EVENT	AGE	Main effect in the region	EVENT	AGE	Main effect in the region	EVENT	EFFECT	
PALEOZOIC 540Ma	LUFILIAN OROGENY	Transverse folding (phase v)	503Ma	Transverse undulations to the main trend of the lufilian arc	chilatembo (D3)	>460Ma <540Ma	Late transversal folding. Post date ks-3.	D3	Development of brittle structures . High angle normal faults , low angle reverse faults , shear zones and the three joint sets mapped	COMPRESSIONAL REGIME
		Monwezian (phase IV)	>602Ma	E-W Faulting (e.g Monwezi fa	Monwezian (D2)	>540Ma less than 690 Ma	Strike slip and escape block tectonics. Lateral extrusion with cumulative displacent >130km. Clockwise rotation of crustal blocks and related development of comvex structure of the Lufilian arc.			
		Kundelungu ian (phase III)	?<656 M	Folds with axial planes vertical or dipping **N** in the external folds of the lufilian arc. Post-date ks-3						
NEO PROTOROZOIC		Epeiro genesis (phase II)		Uplift and near the kunde lungu plateau. Post-date ks-2.2.	Kolwezian (D1)	>690ma Climax 790-750 Ma < 850 Ma	Northward fold - and thrust tectonics (Present orientation of the Lufilian arc: ± E-W trend in the western part and NW- SE in the Eastern part). Major vergence to the N back folding to South. Post-date Ks-2.2.	D2	Development of bedding parrallel veins and formation of the Kirilabombwe anticline in its current orientation. Saddles and hinge zones were developed late in this deformation period	
		Kolwezian (phase I)	656 Ma	Folds with axial dipping S. Napes displaced several tens of km from S to N in Katanga . End of the movement ± Ks-2.1						
	LUSAKAN FOLDING		± 850 M	Deep burial of lower Roan? (metamorphic veins at Luanshya). Post-date Ki Supper group.	KATANGAN RIFTING	< 900Ma	Extensional tectonics 9 from continental up to proto-oceanic rifts). Emplacement of mafic + minor felsic igeneous rocks. Deposition of the Roan supper group (detrital minerals from ca 900ma granites occur in the lower part of the Roan supper roup).	D1	Continous development of S1 (bedding parallel foliation) due to deep burial	EXTENSIONAL REGIME
±1000 Ma	LOMAMIAN OROGENY		± 950 M	Recument folds in lower Roan at Chingola and Luanshya. Recumbent folds at Mwinilunga and Solwezi. Post-date Roan super group.				Katangan Rifting	Development of the Lubengele fault and the fitwaula Synrift faults bounding the Konkola deposits and onset of the deposition of the Roan super group	

8.2 Geotechnical Implications

A good understanding of the spatial distribution of geological contacts and the associated discontinuities is a major geological factor in stability of both underground mine and open pit mine excavation (Xavier et al., 2022).The major structures controlling stability in the study area faults, folds, joints and bedding planes. These structures determine the stress regime and the ground condition and therefore induce both stress and structural related failure mechanisms.

The mapped faults show distinct orientations with respect to the ore body trending from sub-parallel or longitudinal to transverse or orthogonal and dipping in different directions. The dip/dip direction, magnitude of displacement, condition of the fault, water, aperture size and rock mass condition around the fault will determine the failure mechanism, amount of disturbance/damage and challenges when excavating through them. In addition to locked up energy, blasting also introduces some energy changes and mechanism that induce slip/ground movement more fracturing/spalling and seismicity in brittle rock, sloughing/crumbling in very weak, and runaways in fissured materials (Konkola Copper Mines, 2020a).

The major faults mapped have an average displacement of 20 m with sheared and weathered surfaces. Their apertures range from tight (< 1 cm) filled with soft or hard materials, to very open (>10 m) filled with weathered breccia and fines (fissured). Some portions are very wet with gushing water while other are relatively dry. A water spectrum of dry, wet, dripping, flowing and gushing exist at different faults and locations (Konkola Copper Mines, 2020a). Water reduces cohesion between sliding surfaces and has potential to cause mud rush in fissured zones. Therefore, the conditions of the faults range from extremely poor to poor and always pose geotechnical challenges.

The major joints that affect stability are orthogonal to the bedding planes (Figure 8-2). These cross joints become sub-parallel when mining crosscuts. Like faults, the orientation of the planes, condition (weathering, type of fill, roughness), apertures and water determine their strength and hence stability.

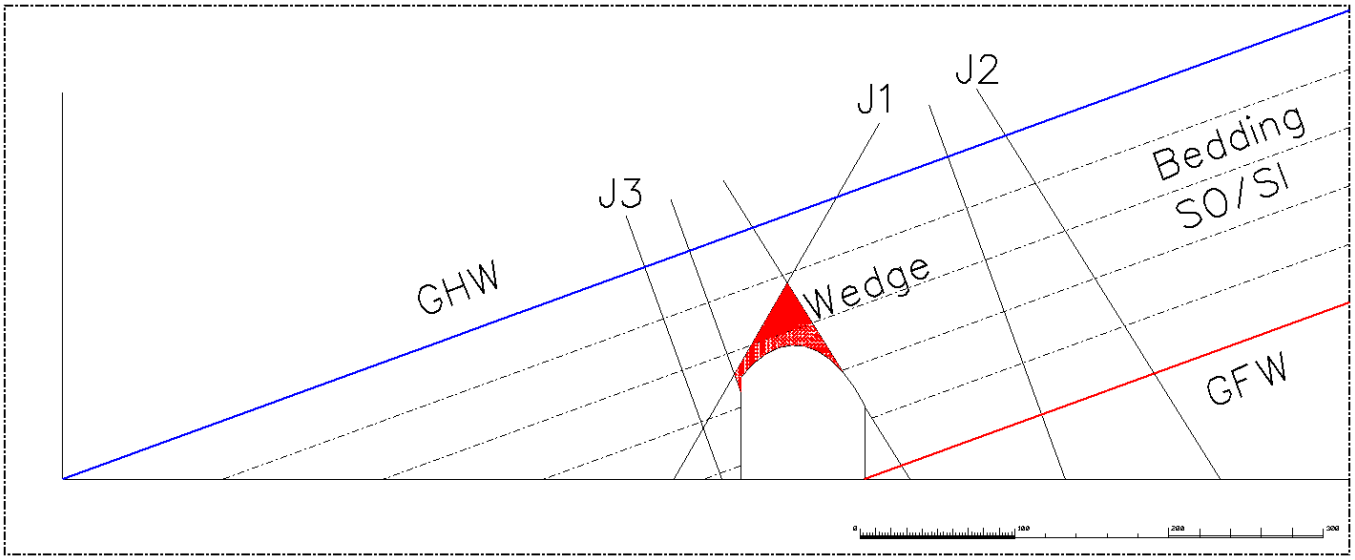


Figure 8-2: Cross section view (facing east) illustrating formation of wedge failure as a result of the interaction of the bedding planes and the joint orientation.

Most of joints picked are of low quality and strength due to orientation with respect to excavation, weathering, cohesion and water. The predominant failure mechanism on joints is spalling and wedge failure where huge rocks just dislodge from the roof of the mined excavations (Figure 8-3).



Figure 8-3: Picture of rock dislodged due to wedge failure on 760mL 2400mW access to the ore body.

The flat dipping bedding plane with weathered planes in some portions are predominant for slabbing and beam failures. Buckling and crushing are the major failures caused by stresses and geological structures.

Bedding planes are very pronounced in the ore body and therefore the various planes makes the ore body susceptible to geotechnical failure.

The presence of geological structures in this area has created disturbed/damaged zones and dynamic loading that pose serious geotechnical challenges making the area very sensitive to mine due to high risks of falls of ground that can lead to loss of both expensive mining equipment (Figure 8-4) and also loss of life.



Figure 8-4: Picture of an underground mine accident that involved fall of ground (rock fall) in weak zones attributed to geological structures.

9 Conclusion

A geological model was successfully created with solids for the ore bearing lithology, the Ore Shale Unit. The model included four major faults. The total volume for the ore shale lithology solid was found to be 1,032,199m3. The steps taken to create this model were documented into a work flow procedure that can be replicated to other parts of the mine.

This study established that Konkola east, which is part of the Konkola deposit of the domes region of the Zambian Copperbelt lies on the northern limb of a major fold, the Kirilabombwe anticline. This study reveals that Konkola east could be part of a major dextral strike-slip fault system related to the Lufilian orogeny that introduced a north to south compression regime and an east to west oriented extensional regime.

This structural configuration supports the orientation of the mapped structural elements of the four normal faults striking north to south, an inferred fold axis oriented east to west and low angle reverse faults oriented east to west. Parasitic folds were also observed in this study. It was also established through this study that Konkola east has 3 main joint sets (J1, J2 and J3).

Three deformation phases are identified through this study with the first being the development of a bedding parallel foliation due to deep burial. The second deformation at the start of convergence is marked by the development of layer parallel veins that could have required high fluid pressure to achieve. This compression also led to the formation of the main folded structure and the observed parasitic folds. The third and final deformation phase is related to the brittle structures like the 4 normal faults modelled and the three joints sets and the low angle reverse faults.

These structures have a major implication on short term mine planning. The major one is on geotechnical stability. The interaction of the bedding planes with joints and the faults creates wedges and other rock failure mechanisms. The understanding of these patterns are therefore crucial in attaining safe mining. The other major implication is in the hydrogeological environment. This study identified that the geological structures in Konkola east act as conduits connecting the major aquifers that are at Konkola. This leads to introduction of water into mine working areas and contributes significantly to mining costs through water pumping costs. Therefore, geological structures have a major influence on the short term mine plan.

10 Recommendations

Further work is still required to fully understand the structural configuration of Konkola east. This study did not cover any provenance studies or geochronological studies to give the timing of events and the deformation phases were based on field observations and crosscutting relationship. Therefore, provenance studies and/or paleo current analysis would give a much more conclusive structural configuration and deformation history.

The modelling process was done explicitly using surpac software. This was a lot more time consuming as surfaces were manually triangulated to create 3 dimensional models. Some triangles could not be created or manipulated to fit the exact observations underground. Further, incorporating structural measurements in to the geological model proved to be a challenge. Against this background, it is recommended that another model should be created implicitly that will allow easy import of structural measurements and can be done rapidly. This will also allow for multiple simulations using available data and can be done much faster.

11 Bibliography

Batumike, M.J., Cailteux, J.L.H. and Kampunzu, A.B. 2007. Lithostratigraphy, basin development, base metal deposits, and regional correlations of the Neoproterozoic Nguba and Kundelungu rock successions, central African Copperbelt. Gondwana Research, 11, 432–447.

Bense, V.F., Gleeson, T., Loveless, S.E., Bour, O. and Scibek, J. 2013. Fault zone hydrogeology. Earth-Science Reviews, 127, 171–192.

Brems, D., Muchez, P., Sikazwe, O. and Mukumba, W. 2009. Metallogenesis of the Nkana copper-cobalt South Orebody, Zambia. Journal of African Earth Sciences, 55, 185–196.

Bull, S., Selley, D., Broughton, D., Hitzman, M., Cailteux, J., Large, R. and McGoldrick, P. 2011. Sequence and carbon isotopic stratigraphy of the Neoproterozoic Roan Group strata of the Zambian copperbelt. Precambrian Research, 190, 70–89.

Cailteux, J.L.H., Kampunzu, A.B. and Lerouge, C. 2007. The Neoproterozoic Mwashya-Kansuki sedimentary rock succession in the central African Copperbelt, its Cu-Co mineralisation, and regional correlations. Gondwana Research, 11, 414–431.

Cailteux, J.L.H., Kampunzu, A.B., Lerouge, C., Kaputo, A.K. and Milesi, J.P. 2005. Genesis of sediment-hosted stratiform copper - Cobalt deposits, central African Copperbelt. Journal of African Earth Sciences, 42, 134–158.

Cox, S.F., Wall, V.J., Etheridge, M.A. and Potter, T.F. 1991. Deformational and metamorphic processes in the formation of mesothermal vein-hosted gold deposits - examples from the Lachlan Fold Belt in central Victoria, Australia. Ore Geology Reviews, 6, 391–423.

Eggers, M. 2016. Engineering geological modelling for pit slope design in the porphyry copper-gold deposits of Southeast Asia. Perth, Australian Centre for Geomechanics, 49–82pp.

Greyling, L.N. 2009. Fluid evolution and characterisation of mineralising solutions in the Central African Copperbelt. Phd thesis, University Of Witswatersrand, 278pp.

Haest, M., El Desouky, H., Muchez, P. and Dewaele, S. 2007. Contributions from structural analysis and remote sensing to the timing of mineralization in the Lufilian arc and its foreland. Digging Deeper, 2, 217–220.

Hitzman, M.W., Broughton, D.W., Selley, D., Woodhead, J. and Bull, S. 2012. The Central African Copperbelt: Diverse Stratigraphic, Structural, and Temporal Settings in the World's Largest Sedimentary Copper Distric. Economic Geology, 487–514.

Jackson, M.P.A., Warin, O.N., Woad, G.M. and Hudec, M.R. 2003. Neoproterozoic allochthonous salt tectonics during the Lufilian orogeny in the Katangan Copperbelt, central Africa. Bulletin of the Geological Society of America, 115, 314–330.

Kampunzu, A.B. and Cailteux, J. 1999. Tectonic Evolution of the Lufilian Arc (Central Africa Copper Belt) during Neoproterozoic Pan African Orogenesis. Gondwana Research, 2, 401–421.

Koegelenberg, C., Basson, I.J., Sinkala, H., Lupapulo, H. and Hornsby, P. 2019. Pan-African structural evolution of Paleoproterozoic basement gneiss and Cu-Co mineralized shear zones in the Domes Region of the Lufilian Belt, Mwombezhi Dome, Zambia. Journal of Structural Geology, 127, 103869.

Konkola Copper Mines 2013. Unpublished Report., 1–15pp.

Konkola Copper Mines 2020a. Konkola Mine Hydrogeology Training Manual.

Konkola Copper Mines 2020b. Review of the Update of the Geological and Resource model for Konkola.

Master, S. 2021. Stratabound, Sediment-Hosted Cu-Co Deposits (with special reference to the Central African Copperbelt). Encyclopedia of Geology, 5, 899–913.

Master, S., Rainaud, C., Armstrong, R.A., Phillips, D. and Robb, L.J. 2005. Provenance ages of the Neoproterozoic Katanga Supergroup (Central African Copperbelt), with implications for basin evolution. Journal of African Earth Sciences, 42, 41–60.

McGowan, R.R., Roberts, S. and Boyce, A.J. 2006. Origin of the Nchanga copper-cobalt deposits of the Zambian Copperbelt. Mineralium Deposita, 40, 617–638.

Muchez, P., André-Mayer, A.S., El Desouky, H.A. and Reisberg, L. 2015. Diagenetic origin of the stratiform Cu–Co deposit at Kamoto in the Central African Copperbelt. Mineralium Deposita, 50, 437–447.

Muchez, P., Brems, D., Clara, E., De Cleyn, A., Lammens, L., Boyce, A., De Muynck, D., Mukumba, W. and Sikazwe, O. 2010. Evolution of Cu-Co mineralizing fluids at Nkana Mine, Central African Copperbelt, Zambia. Journal of African Earth Sciences, 58, 457–474.

Porada, H. and Berhorst, V. 2000. Towards a new understanding of the Neoproterozoic-Early Palaeozoic Lufilian and northern Zambezi Belts in Zambia and the Democratic Republic of Congo. Journal of African Earth Sciences, 30, 727–771.

Selley, D., Broughton, D., Scott, R., Hitzman, M., Bull, S., Large, R., McGoldrick, P., Croaker, M., Pollington, N. and Barra, F. 2005. A New Look at the Geology of the Zambian Copperbelt., 965–1000pp.

Selley, D., Scott, R., Emsbo, P., Koziy, L., Hitzman, M.W., Bull, S.W., Duffett, M., Sebagenzi, S., Halpin, J., Broughton, David W.Arribas R., A.M. and Mauk, J.L. 2019. Structural Configuration of the Central African Copperbelt: Roles of Evaporites in Structural Evolution, Basin Hydrology, and Ore Location. Metals, Minerals, and Society, 115–156.

Sillitoe, R.H., Perelló, J., Creaser, R.A., Wilton, J., Wilson, A.J. and Dawborn, T. 2017. Age of the Zambian Copperbelt. Mineralium Deposita, 52, 1245–1268.

Sixtus, M. 1991. Ground Water flow Through Konkola (Bancroft) Copper Mine-Zambia. Phd thesis, University Of London, 30604pp.

Torremans, K., Gauquie, J., Boyce, A.J., Barrie, C.D., Dewaele, S., Sikazwe, O. and Muchez, P. 2013. Remobilisation features and structural control on ore grade distribution at the Konkola stratiform Cu-Co ore deposit, Zambia. Journal of African Earth Sciences, 79, 10–23.

Torremans, K., Muchez, P. and Sintubin, M. 2018. Non-cylindrical parasitic folding and strain partitioning during the Pan-African Lufilian orogeny in the Chambishi-Nkana Basin, Central African Copperbelt. Solid Earth, 9, 1011–1033.

Torremans, K., Muchez, P., Sintubin, M. and Sikazwe, O. 2012. Structural control of the copper-cobalt grade distribution at the Konkola ore deposit , Zambia. Tectonics Studies Group, Annual General Meeting, 1.

Turlin, F., Eglinger, A., Vanderhaeghe, O., André-Mayer, A.S., Poujol, M., Mercadier, J. and Bartlett, R.

2016. Synmetamorphic Cu remobilization during the Pan-African orogeny: Microstructural, petrological and geochronological data on the kyanite-micaschists hosting the Cu(-U) Lumwana deposit in the Western Zambian Copperbelt of the Lufilian belt. Ore Geology Reviews, 75, 52–75.

Twite, F., Broughton, D., Nex, P., Kinnaird, J., Gilchrist, G. and Edwards, D. 2019. Lithostratigraphic and structural controls on sulphide mineralisation at the Kamoa copper deposit, Democratic Republic of Congo. Journal of African Earth Sciences, 151, 212–224.

Xavier, B.C., Egydio-Silva, M., Sadowski, G.R., de Assis Silva, B. and Takara, V.J. 2022. Construction of Structural Geological Model Using Monte Carlo Simulation. Springer International Publishing, 1345–1361pp.

Zientek, M.L., Bliss, J.D., Broughton, D.W., Christie, M., Denning, P.D., Hayes, T.S., Hitzman, M.W., Horton, J.D., Frost-Killian, S., Douglas, J.J., Master, S., Parks, H.L., Taylor, C.D., Wilson, A.B., Wintzer, N.E. and Woodhead, J. 2010. Sediment-hosted stratabound copper assessment of the Neoproterozoic Roan Group, Central African Copperbelt, Katanga basin, Democratic Republic of the Congo and Zambia. 162.

12 Appendices

12.1 Appendix A: Konkola structural Mapping data for Konkola

DIP	DIP_DIRECTION	LEVEL	SCANLINE ID	TAPE DRN	TAPE DIP	DIST.	SET_TYPE	FILL_TYPE	IRS Mpa	SMALL SCALE EXPRESSION	DIP LENGTH	WATER CONDITION
85	98	700mL	S025	80	10	0,3	J	Feo	75	IV	3	DRY
73	84	700mL	S025	80	10	0,9	J	Feo	75	IV	4	DRY
72	86	700mL	S025	80	10	1	J	Feo	75	IV	4	DRY
70	71	700mL	S025	80	10	1,3	J	Feo	75	IV	3	DRY
78	94	700mL	S025	80	10	1,4	J	Feo	75	IV	0,1	DRY
84	114	700mL	S025	80	10	1,7	J	Feo	75	IV	1	DRY
64	74	700mL	S025	80	10	2,3	J	Feo	75	IV	2	DRY
66	120	700mL	S025	80	10	2,4	J	Feo	75	IV	1	DRY
85	138	700mL	S025	80	10	2,65	J	Feo	75	IV	0,05	DRY
75	77	700mL	S025	80	10	3	J	Feo	75	IV	2	DRY
77	75	700mL	S025	80	10	3,2	J	Feo	75	IV	2	DRY
80	291	700mL	S025	80	10	3,7	J	Feo	75	IV	2,5	DRY
67	108	700mL	S025	80	10	3,9	J	Feo	75	IV	2,5	DRY
70	87	700mL	S025	80	10	4	J	Feo	75	IV	2	DRY
90	97	700mL	S025	80	10	4,35	J	Feo	75	IV	0,3	DRY
89	97	700mL	S025	80	10	4,42	J	Feo	75	IV	0,3	DRY
83	118	700mL	S025	80	10	4,6	J	Feo	75	IV	2	DRY
90	94	700mL	S025	80	10	5,3	J	Feo	75	IV	0,8	DRY
90	82	700mL	S025	80	10	5,5	J	Feo	75	IV	1,5	DRY
89	80	700mL	S025	80	10	5,6	J	Feo	75	IV	3	DRY
70	58	700mL	S025	80	10	6,1	J	Feo	75	IV	0,4	DRY
80	271	700mL	S025	80	10	6,6	J	Feo	75	IV	1,5	DRY
85	263	700mL	S025	80	10	6,7	J	Feo	75	IV	3	DRY
78	75	700mL	S025	80	10	6,9	J	Feo	75	IV	0,2	DRY
83	81	700mL	S025	80	10	7,5	J	Feo	75	IV	1	DRY
87	275	700mL	S025	80	10	7,9	J	Feo	75	IV	1	DRY
82	53	700mL	S025	80	10	8,1	J	Feo	75	IV	1	DRY
76	111	700mL	S025	80	10	8,4	J	Feo	75	IV	0,5	DRY
74	110	700mL	S025	80	10	8,6	J	Feo	75	IV	0,2	DRY
75	99	700mL	S025	80	10	9,9	J	Feo	75	IV	1	DRY
28	50	700mL	S025	80	10	10,6	J	Feo	75	IV	1	DRY
70	58	700mL	S025	80	10	11,1	J	Feo	75	IV	2	DRY
75	56	700mL	S025	80	10	11,2	J	Feo	75	IV	2	DRY
73	55	700mL	S025	80	10	11,3	J	Feo	75	IV	2	DRY
80	84	700mL	S025	80	10	11,5	J	Feo	75	IV	0,2	DRY
80	74	700mL	S025	80	10	11,6	J	Feo	75	IV	0,2	DRY
85	85	700mL	S025	80	10	11,7	J	Feo	75	IV	0,2	DRY
87	111	700mL	S025	80	10	11,9	J	Feo	75	IV	2	DRY
75	13	700mL	S025	80	10	12,05	J	Feo	75	IV	0,2	DRY
86	97	700mL	S025	80	10	12,2	J	Feo	75	IV	2	DRY
87	88	700mL	S025	80	10	12,45	J	Feo	75	IV	0,5	DRY
86	90	700mL	S025	80	10	12,48	J	Feo	75	IV	0,5	DRY
88	87	700mL	S025	80	10	12,5	J	Feo	75	IV	0,5	DRY

85	97	720mL	S025	80	10	12,54	J	Feo	75	IV	0,5	DRY
88	95	720mL	S025	80	10	12,6	J	Feo	75	IV	0,5	DRY
87	96	720mL	S025	80	10	12,7	J	Feo	75	IV	0,5	DRY
80	256	720mL	S025	80	10	12,85	J	Feo	75	IV	0,5	DRY
90	98	720mL	S025	80	10	13,05	J	Feo	75	IV	2	DRY
90	95	720mL	S025	80	10	13,1	J	Feo	75	IV	0,5	DRY
89	93	720mL	S025	80	10	13,15	J	Feo	75	IV	0,5	DRY
90	254	720mL	S025	80	10	13,35	J	Feo	75	IV	0,5	DRY
89	251	720mL	S025	80	10	13,45	J	Feo	75	IV	1,5	DRY
90	138	720mL	S025	80	10	13,55	J	Feo	75	IV	0,5	DRY
85	77	720mL	S025	80	10	13,65	J	Feo	75	IV	2	DRY
87	85	720mL	S025	80	10	14,1	J	Feo	75	IV	0,5	DRY
82	23	720mL	S025	80	10	14,2	J	Feo	75	IV	0,2	DRY
83	265	720mL	S025	80	10	14,9	J	Feo	75	IV	2	DRY
82	264	720mL	S025	80	10	15,05	J	Feo	75	IV	2	DRY
85	265	720mL	S025	80	10	15,15	J	Feo	75	IV	2	DRY
88	272	720mL	S025	80	10	15,8	J	Feo	75	IV	3	DRY
84	71	720mL	S025	80	10	16,15	J	Feo	75	IV	3	DRY
85	115	720mL	S025	80	10	17,2	J	Feo	75	IV	1	DRY
81	88	720mL	S025	80	10	17,4	J	Feo	75	IV	3	DRY
84	95	720mL	S025	80	10	17,45	J	Feo	75	IV	1	DRY
88	292	720mL	S025	80	10	17,5	J	N	75	IV	3	DRY
89	109	720mL	S025	80	10	18	J	MAL	75	IV	0,5	DRY
84	104	720mL	S025	80	10	18,3	J	N	75	IV	3	DRY
75	100	720mL	S025	80	10	18,85	J	N	75	IV	1,5	DRY
83	98	720mL	S025	80	10	19,5	J	Feo	75	IV	0,5	DRY
88	275	720mL	S025	80	10	19,55	J	Feo	75	IV	2,5	DRY
85	253	720mL	S025	80	10	19,85	J	Feo	75	IV	1	DRY
72	30	720mL	S025	80	10	20,05	J	Feo	75	IV	1,5	DRY
60	105	720mL	S025	80	10	20,65	J	N	75	IV	2,5	DRY
65	95	720mL	S025	80	10	21,25	J	N	75	IV	1	DRY
89	237	720mL	S025	80	10	21,55	J	Feo	75	IV	0,3	DRY
82	72	720mL	S025	80	10	21,93	J	N	75	IV	1,5	DRY
90	88	720mL	S025	80	10	22,1	J	MAL	75	IV	2	DRY
78	98	720mL	S025	80	10	26,4	J	N	75	IV	0,2	DRY
86	104	720mL	S025	80	10	26,65	J	MAL	75	IV	0,2	DRY
56	91	720mL	S025	80	10	26,9	J	N	75	IV	0,2	DRY
55	105	720mL	S025	80	10	27,1	J	N	75	IV	0,2	DRY
84	58	720mL	S025	80	10	27,3	J	N	75	IV	0,2	DRY
57	274	720mL	S025	80	10	27,55	J	MAL	75	IV	0,2	DRY
7	132	720mL	S025	80	10	27,65	J	CA	75	IV	0	DRY
63	277	720mL	S025	80	10	27,8	J	Feo	75	IV	0,3	DRY
90	79	720mL	S025	80	10	28,3	J	MAL	75	IV	3	DRY
73	253	740mL	S026	63	0	0	J	Feo	70	IV	0,5	DRY
74	258	740mL	S026	63	0	0,3	J	Feo	70	IV	2	DRY
76	252	740mL	S026	63	0	0,4	J	Feo	70	IV	2,5	DRY
85	248	740mL	S026	63	0	0,8	J	Feo	70	IV	0,5	DRY
80	251	740mL	S026	63	0	1	J	Feo	70	IV	4	DRY

43	28	740mL	S026	63	0	1,3	J	Feo	70	IV	0,3	DRY
89	38	740mL	S026	63	0	1,35	J	Feo	70	IV	0,2	DRY
43	4	740mL	S026	63	0	1,4	J	Feo	70	IV	0,3	DRY
86	93	740mL	S026	63	0	1,5	J	Feo	70	IV	0,2	DRY
72	266	740mL	S026	63	0	1,7	J	Feo	70	IV	0,3	DRY
53	227	740mL	S026	63	0	1,9	J	Feo	70	IV	0,1	DRY
60	61	740mL	S026	63	0	2,1	J	Feo	70	IV	4	DRY
67	37	740mL	S026	63	0	2,3	J	Feo	70	IV	0,1	DRY
75	200	740mL	S026	63	0	2,4	J	Feo	70	IV	3	DRY
62	257	740mL	S026	63	0	2,6	J	Feo	70	IV	0,2	DRY
82	72	740mL	S026	63	0	3	J	Feo	70	IV	4	DRY
76	70	740mL	S026	63	0	3,2	J	Feo	70	IV	2	DRY
70	76	740mL	S026	63	0	3,4	J	Feo	70	IV	0,3	DRY
78	62	740mL	S026	63	0	3,6	J	Feo	70	IV	2	DRY
79	258	740mL	S026	63	0	4	J	Feo	70	IV	0,5	DRY
70	65	740mL	S026	63	0	4,2	J	Feo	70	IV	4	DRY
89	35	740mL	S026	63	0	4,45	J	Feo	70	IV	0,1	DRY
84	60	740mL	S026	63	0	4,6	J	Feo	70	IV	0,2	DRY
81	75	740mL	S026	63	0	4,95	J	Feo	70	IV	0,1	DRY
82	354	740mL	S026	63	0	5	J	Feo	70	IV	0,5	DRY
69	56	740mL	S026	63	0	5,4	J	Feo	70	IV	4	DRY
84	72	740mL	S026	63	0	6	J	Feo	70	IV	0,1	DRY
70	74	740mL	S026	63	0	6,1	J	Feo	70	IV	0,2	DRY
81	72	740mL	S026	63	0	6,3	J	Feo	70	IV	1,5	DRY
89	203	740mL	S026	63	0	6,65	J	Feo	70	IV	0,2	DRY
89	203	740mL	S026	63	0	6,7	J	Feo	70	IV	0,2	DRY
84	252	740mL	S026	63	0	6,8	J	Feo	70	IV	0,1	DRY
80	190	740mL	S026	63	0	6,9	J	Feo	70	IV	0,1	DRY
73	250	740mL	S026	63	0	7,3	J	Feo	70	IV	4	DRY
66	60	740mL	S026	63	0	7,7	J	Feo	70	IV	0,2	DRY
89	22	740mL	S026	63	0	8,1	J	Feo	70	IV	0,3	DRY
86	37	740mL	S026	63	0	8,3	J	Feo	70	IV	0,2	DRY
56	32	740mL	S026	63	0	8,75	J	Feo	70	IV	5	DRY
84	252	740mL	S026	63	0	9,1	J	Feo	70	IV	4	DRY
60	145	740mL	S026	63	0	9,6	J	Feo	70	IV	0,1	DRY
80	147	740mL	S026	63	0	9,9	J	Feo	70	IV	0,2	DRY
75	122	740mL	S026	63	0	10	J	Feo	70	IV	0,3	DRY
88	253	740mL	S026	63	0	10,1	J	Feo	70	IV	0,4	DRY
88	234	740mL	S026	63	0	10,3	J	Feo	70	IV	0,4	DRY
75	258	740mL	S026	63	0	10,4	J	Feo	70	IV	5	DRY
40	110	740mL	S026	63	0	10,4	B	Feo	70	IV	0,1	DRY
90	88	740mL	S026	63	0	10,6	J	Feo	70	IV	0,2	DRY
78	258	740mL	S026	63	0	10,75	J	Feo	70	IV	2	DRY
86	72	740mL	S026	63	0	10,9	J	Feo	70	IV	3	DRY
86	72	740mL	S026	63	0	11	J	Feo	70	IV	0,2	DRY
86	72	740mL	S026	63	0	11,1	J	Feo	70	IV	0,1	DRY
86	72	740mL	S026	63	0	11,2	J	Feo	70	IV	5	DRY
86	72	740mL	S026	63	0	11,22	J	Feo	70	IV	5	DRY

85	111	740mL	S026	63	0	11,05	J	Feo	70	IV	0,2	DRY
61	255	740mL	S026	63	0	11,5	J	Feo	70	IV	0,1	DRY
88	70	740mL	S026	63	0	11,6	J	Feo	70	IV	1,5	DRY
85	72	740mL	S026	63	0	11,95	J	Feo	70	IV	5	DRY
89	68	740mL	S026	63	0	12,5	J	Feo	70	IV	5	DRY
89	74	740mL	S026	63	0	12,95	J	Feo	70	IV	5	DRY
89	72	740mL	S026	63	0	13	J	Feo	70	IV	0,15	DRY
71	306	740mL	S026	63	0	13,1	J	Feo	70	IV	0,3	DRY
86	254	740mL	S026	63	0	13,7	J	Feo	70	IV	0,4	DRY
78	245	740mL	S026	63	0	14	J	Feo	70	IV	5	DRY
15	252	740mL	S026	63	0	14,3	J	Feo	70	IV	0,3	DRY
72	240	740mL	S026	63	0	14,3	J	Feo	70	IV	0,1	DRY
70	59	740mL	S026	63	0	14,35	J	Feo	70	IV	0,4	DRY
50	51	740mL	S026	63	0	14,4	J	Feo	70	IV	0,5	DRY
75	25	740mL	S026	63	0	14,8	J	Feo	70	IV	0,3	DRY
85	65	740mL	S026	63	0	14,81	J	Feo	70	IV	2	DRY
90	74	740mL	S026	63	0	15,5	J	Feo	70	IV	5	DRY
70	268	740mL	S026	63	0	16,1	J	Feo	70	IV	0,4	DRY
78	6	740mL	S026	63	0	16,2	J	Feo	70	IV	0,3	DRY
90	69	740mL	S026	63	0	16,9	J	Feo	70	IV	5	DRY
85	240	740mL	S026	63	0	17,95	J	Feo	70	IV	0,2	DRY
85	240	740mL	S026	63	0	17,97	J	Feo	70	IV	0,2	DRY
82	262	740mL	S026	63	0	18	J	Feo	70	IV	0,3	DRY
84	82	740mL	S026	63	0	18,02	J	Feo	70	IV	0,2	DRY
88	78	740mL	S026	63	0	18,55	J	Feo	70	IV	4	DRY
90	107	740mL	S026	63	0	19,4	J	Feo	70	IV	0,4	DRY
88	77	740mL	S026	63	0	19,6	J	Feo	70	IV	5	DRY
66	18	740mL	S026	63	0	19,5	J	Feo	70	IV	0,1	DRY
68	22	740mL	S026	63	0	20	J	Feo	70	IV	2	DRY
85	287	740mL	S026	63	0	20,8	J	Feo	70	IV	3	DRY
60	248	740mL	S026	63	0	21,2	J	Feo	70	IV	3	DRY
78	253	740mL	S026	63	0	21,8	J	Feo	70	IV	0,3	DRY
75	60	740mL	S026	63	0	22,2	J	Feo	70	IV	0,3	DRY
78	75	740mL	S026	63	0	22,48	J	Feo	70	IV	3	DRY
82	77	740mL	S026	63	0	22,65	J	Feo	70	IV	1,5	DRY
85	80	740mL	S026	63	0	22,9	J	Feo	70	IV	3	DRY
66	263	740mL	S026	63	0	23,35	J	Feo	70	IV	0,2	DRY
88	2	740mL	S026	63	0	23,6	J	Feo	70	IV	1,5	DRY
88	250	740mL	S026	63	0	23,78	J	Feo	70	IV	5	DRY
79	13	740mL	S026	63	0	24,2	J	Feo	70	IV	1	DRY
79	13	740mL	S026	63	0	24,1	J	Feo	70	IV	1	DRY
85	245	740mL	S026	63	0	24,4	J	Feo	70	IV	5	DRY
88	36	740mL	S026	63	0	24,55	J	Feo	70	IV	0,4	DRY
60	270	760mL	S026	63	0	25,3	J	Feo	70	IV	0,5	DRY
70	250	760mL	S026	63	0	25,6	J	Feo	70	IV	0,2	DRY
69	236	760mL	S026	63	0	25,65	J	Feo	70	IV	0,1	DRY
56	4	760mL	S026	63	0	25,7	J	Feo	70	IV	0,5	DRY
45	352	760mL	S026	63	0	25,85	J	Feo	70	IV	0,1	DRY

45	352	760mL	S026	63	0	26,1	J	Feo	70	IV	0,1	DRY
82	72	760mL	S026	63	0	26,15	J	Feo	70	IV	4	DRY
88	32	760mL	S026	63	0	26,7	J	Feo	70	IV	2,5	DRY
80	10	760mL	S026	63	0	26,8	J	Feo	70	IV	0,2	DRY
77	97	760mL	S026	63	0	26,8	J	Feo	70	IV	2	DRY
89	37	760mL	S026	63	0	27,3	J	Feo	70	IV	0,3	DRY
74	30	760mL	S026	63	0	27,32	J	Feo	70	IV	1,5	DRY
84	173	760mL	S026	63	0	27,7	J	Feo	70	IV	0,2	DRY
74	30	760mL	S026	63	0	27,98	J	Feo	70	IV	0,1	DRY
70	13	760mL	S026	63	0	28,1	J	Feo	70	IV	0,5	DRY
74	26	760mL	S026	63	0	28,2	J	Feo	70	IV	0,5	DRY
60	326	760mL	S026	63	0	28,3	J	Feo	70	IV	0,3	DRY
89	66	760mL	S026	63	0	28,7	J	Feo	70	IV	1,5	DRY
80	336	760mL	S026	63	0	28,9	J	Feo	70	IV	0,4	DRY
88	340	760mL	S026	63	0	29,1	J	Feo	70	IV	0,2	DRY
78	52	760mL	S026	63	0	29,75	J	Feo	70	IV	3	DRY
74	37	760mL	S026	63	0	29,9	J	Feo	70	IV	2	DRY
62	40	760mL	S026	63	0	30,1	J	Feo	70	IV	2,5	DRY
80	70	760mL	S026	63	0	30,4	J	Feo	70	IV	4	DRY
85	73	760mL	S027	82	0	0	J	Feo	70	IV	4	DRY
80	72	760mL	S027	82	0	0,2	J	Feo	70	IV	4	DRY
71	62	760mL	S027	82	0	0,5	J	Feo	70	IV	4	DRY
84	66	760mL	S027	82	0	0,7	J	N	70	IV	3	DRY
82	240	760mL	S027	82	0	0,8	J	N	70	IV	2	DRY
83	242	760mL	S027	82	0	0,9	J	N	70	IV	2	DRY
88	114	760mL	S027	82	0	1,2	J	N	70	IV	1	DRY
90	110	760mL	S027	82	0	1,27	J	N	70	IV	0,5	DRY
60	68	760mL	S027	82	0	1,3	J	N	70	IV	2	DRY
86	102	760mL	S027	82	0	1,55	J	N	70	IV	2	DRY
75	247	760mL	S027	82	0	1,8	J	Feo	70	IV	1	DRY
85	109	760mL	S027	82	0	2,1	J	Feo	70	IV	3	DRY
84	254	760mL	S027	82	0	2,5	J	Feo	70	IV	1	DRY
86	256	760mL	S027	82	0	2,75	J	CA	70	IV	2	DRY
90	75	760mL	S027	82	0	2,85	J	Feo	70	IV	0,1	DRY
90	92	760mL	S027	82	0	3,45	J	Feo	70	IV	2	DRY
86	82	760mL	S027	82	0	3,6	J	Feo	70	IV	1	DRY
87	88	760mL	S027	82	0	3,85	J	Feo	70	IV	2	DRY
71	65	760mL	S027	82	0	4,55	J	Feo	70	IV	0,1	DRY
74	66	760mL	S027	82	0	4,59	J	Feo	70	IV	0,1	DRY
87	67	760mL	S027	82	0	4,7	J	Feo	70	IV	1	DRY
85	64	760mL	S027	82	0	4,75	J	Feo	70	IV	0,3	DRY
90	70	760mL	S027	82	0	4,85	J	Feo	70	IV	0,5	DRY
90	69	760mL	S027	82	0	4,98	J	Feo	70	IV	3	DRY
85	115	760mL	S027	82	0	5,2	J	Feo	70	IV	1	DRY
84	60	760mL	S027	82	0	5,75	J	Feo	70	IV	0,5	DRY
50	160	760mL	S027	82	0	6	J	Feo	70	IV	3	DRY
89	79	760mL	S027	82	0	6,15	J	Feo	70	IV	3	DRY
85	252	760mL	S027	82	0	6,2	J	Feo	70	IV	0,5	DRY

88	70	760mL	S027	82	0	6,3	J	Feo	70	IV	3,5	DRY
69	35	760mL	S027	82	0	6,35	J	Feo	70	IV	4	DRY
85	72	760mL	S027	82	0	6,7	J	Feo	70	IV	2	DRY
79	116	760mL	S027	82	0	6,95	J	QTZ	70	IV	1	DRY
65	123	760mL	S027	82	0	7	J	QTZ	70	IV	1	DRY
71	125	760mL	S027	82	0	7,15	J	N	70	IV	0,3	DRY
69	74	760mL	S027	82	0	7,35	J	N	70	IV	4	DRY
72	77	760mL	S027	82	0	7,85	J	QTZ	70	IV	4	DRY
85	78	760mL	S027	82	0	8,15	J	N	70	IV	2,5	DRY
89	79	760mL	S027	82	0	8,4	J	QTZ	70	IV	2	DRY
87	60	760mL	S027	82	0	8,65	J	QTZ	70	IV	0,4	DRY
84	69	760mL	S027	82	0	8,75	J	N	70	IV	2	DRY
83	75	760mL	S027	82	0	9	J	N	70	IV	1,5	DRY
88	70	760mL	S027	82	0	9,1	J	N	70	IV	2,5	DRY
70	78	760mL	S027	82	0	9,35	J	Feo	70	IV	3	DRY
68	124	760mL	S027	82	0	9,7	J	N	70	IV	0,4	DRY
84	281	760mL	S027	82	0	9,9	J	N	70	IV	0,2	DRY
86	115	760mL	S027	82	0	9,95	J	N	70	IV	0,2	DRY
83	297	760mL	S027	82	0	10,1	J	N	70	IV	1,5	DRY
69	318	760mL	S027	82	0	10	J	N	70	IV	0,1	DRY
90	95	760mL	S027	82	0	10,3	J	N	70	IV	0,5	DRY
90	96	760mL	S027	82	0	10,34	J	N	70	IV	0,2	DRY
86	305	760mL	S027	82	0	10,75	J	N	70	IV	0,2	DRY
90	280	760mL	S027	82	0	10,87	J	N	70	IV	2,5	DRY
90	75	760mL	S027	82	0	11	J	N	70	IV	3	DRY
66	342	760mL	S027	82	0	11,1	J	N	70	IV	0,1	DRY
25	335	760mL	S027	82	0	11,25	J	N	70	IV	0,1	DRY
64	346	760mL	S027	82	0	11,4	J	N	70	IV	0,6	DRY
83	67	760mL	S027	82	0	11,95	J	Feo/QTZ	70	IV	3	DRY
88	71	760mL	S027	82	0	12,35	J	N	70	IV	2	DRY
90	264	760mL	S027	82	0	12,45	J	N	70	IV	2	DRY
74	90	760mL	S027	82	0	12,65	J	QTZ	70	IV	0,2	DRY
80	70	760mL	S027	82	0	12,85	J	N	70	IV	3,2	DRY
75	29	760mL	S027	82	0	13,25	J	N	70	IV	2,5	DRY
77	72	760mL	S027	82	0	13,6	J	CA/FEO	70	IV	2,5	DRY
79	90	760mL	S027	82	0	13,8	J	N	70	IV	0,5	DRY
76	74	760mL	S027	82	0	14	J	QTZ	70	IV	3,5	DRY
80	83	760mL	S027	82	0	14,3	J	N	70	IV	3,5	DRY
73	336	760mL	S027	82	0	14,75	J	Feo	70	IV	0,05	DRY
74	90	760mL	S027	82	0	14,9	J	N	70	IV	3	DRY
84	115	760mL	S027	82	0	15,05	J	N	70	IV	2,5	DRY
80	313	760mL	S027	82	0	15,45	J	QTZ	70	IV	0,2	DRY
75	318	760mL	S027	82	0	15,75	J	N	70	IV	0,3	DRY
73	315	760mL	S027	82	0	15,8	J	N	70	IV	0,3	DRY
80	143	760mL	S027	82	0	16,1	J	N	70	IV	2	DRY
80	70	760mL	S027	82	0	16,9	J	CA	70	IV	2	DRY
80	163	760mL	S027	82	0	17,3	J	N	70	IV	1,5	DRY
70	251	760mL	S027	82	0	18,25	J	N	70	IV	2	DRY

69	64	760mL	S027	82	0	19,3	J	N	70	IV	2	DRY
56	58	760mL	S027	82	0	19,75	J	N	70	IV	1	DRY
80	65	760mL	S027	82	0	20,55	J	Feo	70	IV	2,5	DRY
90	85	760mL	S027	82	0	20,95	J	Feo	70	IV	3	DRY
85	66	760mL	S027	82	0	21,65	J	Feo	70	IV	3	DRY
87	86	760mL	S027	82	0	22,05	J	Feo	70	IV	3	DRY
87	87	760mL	S027	82	0	22,3	J	Feo	70	IV	1,5	DRY
86	64	760mL	S027	82	0	22,45	J	Feo	70	IV	2,5	DRY
90	54	760mL	S027	82	0	22,7	J	Feo	70	IV	2,5	DRY
85	67	760mL	S027	82	0	22,9	J	Feo	70	IV	2,5	DRY
90	260	760mL	S027	82	0	23,2	J	Feo	70	IV	2,5	DRY
90	68	760mL	S027	82	0	23,7	J	Feo	70	IV	3	DRY
70	242	760mL	S027	82	0	24,23	J	Feo	70	IV	3	DRY
85	208	760mL	S027	82	0	24,78	J	Feo	70	IV	3	DRY
65	68	760mL	S027	82	0	25,25	J	Feo	70	IV	2	DRY
75	265	760mL	S027	82	0	25,25	J	Feo	70	IV	2	DRY
70	72	760mL	S027	82	0	25,45	J	Feo	70	IV	2	DRY
90	284	760mL	S027	82	0	25,55	J	Feo	70	IV	2	DRY
65	76	760mL	S027	82	0	26,35	J	Feo	70	IV	4	DRY
84	72	760mL	S027	82	0	26,51	J	Feo	70	IV	1	DRY
90	69	760mL	S027	82	0	26,58	J	Feo	70	IV	0,3	DRY
87	266	760mL	S027	82	0	26,7	J	Feo	70	IV	1,5	DRY
85	85	760mL	S027	82	0	27	J	Feo	70	IV	3	DRY
85	249	760mL	S028	78	0	0	J	N	65	IV	3	DRY
10	315	760mL	S028	78	0	0,7	B	N	65	VII	0	DRY
63	73	760mL	S028	78	0	0,9	J	N	65	IV	3	DRY
75	70	760mL	S028	78	0	1,4	J	N	65	IV	3	DRY
80	87	760mL	S028	78	0	1,6	J	N	65	IV	2,5	DRY
90	74	760mL	S028	78	0	2,7	J	N	65	IV	3	DRY
75	64	760mL	S028	78	0	3,15	J	N	65	IV	1	DRY
86	83	760mL	S028	78	0	3,7	J	N	65	IV	1	DRY
87	77	760mL	S028	78	0	3,95	J	N	65	IV	2	DRY
85	284	760mL	S028	78	0	4,65	J	FEO	65	IV	3	DRY
85	102	760mL	S028	78	0	4,78	J	N	65	IV	1,5	DRY
85	297	760mL	S028	78	0	5,05	J	FEO	65	IV	1	DRY
64	144	760mL	S028	78	0	5,6	J	N	65	IV	1	DRY
76	114	760mL	S028	78	0	5,65	J	N	65	IV	0,3	DRY
40	87	760mL	S028	78	0	5,8	J	N	65	IV	0,2	DRY
86	51	760mL	S028	78	0	6,15	J	FEO	65	IV	3	DRY
80	40	760mL	S028	78	0	6,25	J	FEO	65	IV	2	DRY
76	48	760mL	S028	78	0	6,3	J	FEO	65	IV	1,5	DRY
78	66	760mL	S028	78	0	6,4	J	N	65	IV	1,5	DRY
84	87	760mL	S028	78	0	6,9	J	FEO	65	IV	1	DRY
65	248	760mL	S028	78	0	7	J	FEO	65	IV	1	DRY
87	83	760mL	S028	78	0	7,8	J	N	65	IV	1,2	DRY
86	74	760mL	S028	78	0	8,25	J	FEO	65	IV	3,5	DRY
55	340	760mL	S033	165	7	0,2	J	N	70	IV	0,1	MOIST
39	359	760mL	S033	165	7	0,3	J	N	70	IV	0,1	MOIST

84	359	760mL	S033	165	7	0,5	J	N	70	IV	0,1	MOIST
84	359	760mL	S033	165	7	0,55	J	N	70	IV	0,1	MOIST
77	24	760mL	S033	165	7	0,75	J	N	70	IV	0,1	MOIST
52	321	760mL	S033	165	7	1,5	J	N	70	VII	0,1	MOIST
62	119	760mL	S033	165	7	2	J	N	70	IV	0,1	MOIST
62	117	760mL	S033	165	7	2,2	J	N	70	IV	0,1	MOIST
70	118	760mL	S033	165	7	2,55	J	N	70	IV	0,15	MOIST
67	128	760mL	S033	165	7	2,7	J	N	70	IV	0,1	MOIST
50	35	760mL	S033	165	7	2,9	J	FEO	70	IV	1,5	MOIST
77	125	760mL	S033	165	7	3,3	J	N	70	IV	0,1	MOIST
49	26	760mL	S033	165	7	3,5	J	N	70	IV	0,5	MOIST
47	22	760mL	S033	165	7	4,1	J	N	70	IV	1	MOIST
37	353	760mL	S033	165	7	4,95	J	N	70	IV	0,2	MOIST
56	22	760mL	S033	165	7	5,1	J	N	70	IV	0,3	MOIST
81	182	760mL	S033	165	7	5,5	J	N	70	IV	0,1	MOIST
71	111	760mL	S033	165	7	5,8	J	N	70	IV	1	MOIST
51	20	760mL	S033	165	7	5,9	J	N	70	IV	0,1	MOIST
84	122	760mL	S033	165	7	10,05	J	N	70	IV	1	MOIST
72	78	780mL	S034	66	0	0	J	N	80	IV	0,2	DRY
84	78	780mL	S034	66	0	0,5	J	N	80	IV	0,2	DRY
87	95	780mL	S034	66	0	0,3	J	N	80	IV	0,2	DRY
78	91	780mL	S034	66	0	0,6	J	N	80	IV	3	DRY
70	85	780mL	S034	66	0	0,65	J	N	80	IV	3	DRY
75	116	780mL	S034	66	0	1,1	J	N	80	IV	1	DRY
82	115	780mL	S034	66	0	1,23	J	N	80	IV	3	DRY
55	85	780mL	S034	66	0	1,8	J	N	80	IV	4	DRY
73	0	780mL	S034	66	0	2,3	J	N	80	IV	0,2	DRY
75	22	780mL	S034	66	0	2,5	J	N	80	VII	0,1	DRY
77	85	780mL	S034	66	0	2,7	J	N	80	IV	0,5	DRY
82	67	780mL	S034	66	0	3,1	J	N	80	IV	2,5	DRY
76	57	780mL	S034	66	0	3,47	J	N	80	IV	1	DRY
76	56	780mL	S034	66	0	3,55	J	N	80	IV	1	DRY
87	65	780mL	S034	66	0	3,8	J	N	80	IV	0,1	DRY
85	86	780mL	S034	66	0	3,81	J	N	80	IV	0,1	DRY
79	18	780mL	S034	66	0	4,4	J	N	80	IV	2,5	DRY
88	90	780mL	S034	66	0	4,55	J	N	80	IV	0,2	DRY
90	304	780mL	S034	66	0	4,8	J	N	80	IV	0,2	DRY
67	113	780mL	S034	66	0	5	J	N	80	IV	0,3	DRY
77	108	780mL	S034	66	0	5,15	J	N	80	IV	0,2	DRY
72	114	780mL	S034	66	0	5,2	J	N	80	IV	0,2	DRY
56	352	780mL	S034	66	0	5,4	J	N	80	IV	1	DRY
75	1	780mL	S034	66	0	5,3	J	N	80	IV	0,2	DRY
73	76	780mL	S034	66	0	5,5	J	N	80	IV	2	DRY
80	15	780mL	S034	66	0	5,85	J	N	80	IV	0,3	DRY
65	108	780mL	S034	66	0	6,1	J	N	80	IV	0,2	DRY
52	104	780mL	S034	66	0	6,5	J	N	80	IV	0,3	DRY
47	25	780mL	S034	66	0	6,7	J	N	80	IV	0,4	DRY
60	100	780mL	S034	66	0	7,1	J	N	80	IV	1,5	DRY

85	85	780mL	S034	66	0	7,55	J	N	80	IV	1	DRY
88	254	780mL	S034	66	0	7,6	J	N	80	IV	1	DRY
65	95	780mL	S034	66	0	8,5	J	N	80	IV	1	DRY
88	264	780mL	S034	66	0	8,6	J	N	80	IV	2	DRY
76	81	780mL	S034	66	0	9,2	J	N	80	IV	4	DRY
74	80	780mL	S034	66	0	9,4	J	N	80	IV	1	DRY
47	10	780mL	S034	66	0	9,65	J	N	80	IV	0,1	DRY
60	355	780mL	S034	66	0	9,85	J	N	80	IV	0,2	DRY
85	117	780mL	S034	66	0	10	J	N	80	IV	0,3	DRY
77	40	780mL	S034	66	0	10,2	J	N	80	IV	0,3	DRY
80	250	780mL	S034	66	0	10,3	J	N	80	IV	1,7	DRY
85	271	780mL	S034	66	0	10,5	J	N	80	IV	2	DRY
75	32	780mL	S034	66	0	10,6	J	N	80	IV	0,2	DRY
87	82	780mL	S034	66	0	10,95	J	N	80	IV	0,1	DRY
74	93	780mL	S034	66	0	11,1	J	N	80	VII	0,1	DRY
82	270	780mL	S034	66	0	11,4	J	N	80	IV	2	DRY
54	72	780mL	S034	66	0	11,8	J	N	80	IV	0,2	DRY
56	161	780mL	S034	66	0	12,1	J	N	80	IV	0,3	DRY
83	267	780mL	S034	66	0	12,4	J	N	80	IV	2	DRY
85	250	780mL	S035	79	0	0	J	N	65	IV	1	DRY
86	255	780mL	S035	79	0	0,1	J	N	65	IV	1,5	DRY
85	240	780mL	S035	79	0	0,2	J	N	65	IV	0,2	DRY
82	254	780mL	S035	79	0	0,4	J	CA	65	IV	0,3	DRY
89	101	780mL	S035	79	0	0,6	J	N	65	IV	0,4	DRY
75	22	780mL	S035	79	0	0,5	J	N	65	IV	1,6	DRY
67	70	780mL	S035	79	0	1,1	J	N	65	IV	1,2	DRY
65	62	780mL	S035	79	0	1,15	J	N	65	IV	0,3	DRY
77	255	780mL	S035	79	0	1,4	J	FEO	65	IV	4	DRY
72	54	780mL	S035	79	0	1,5	J	FEO	65	IV	3	DRY
90	67	780mL	S035	79	0	2,05	J	N	65	IV	0,5	DRY
82	261	780mL	S035	79	0	2,1	J	N	65	IV	1	DRY
74	72	780mL	S035	79	0	2,27	J	N	65	IV	1,5	DRY
70	72	780mL	S035	79	0	2,4	J	FEO	65	IV	2,5	DRY
80	43	780mL	S035	79	0	2,7	J	N	65	IV	2	DRY
77	27	780mL	S035	79	0	2,8	J	N	65	IV	0,05	DRY
87	250	780mL	S035	79	0	3,5	J	FEO	65	IV	4	DRY
86	228	780mL	S035	79	0	3,67	J	N	65	IV	0,02	DRY
61	69	780mL	S035	79	0	3,8	J	N	65	IV	1,7	DRY
71	252	780mL	S035	79	0	3,9	J	N	65	IV	0,1	DRY
87	312	780mL	S035	79	0	3,85	J	N	65	IV	0,2	DRY
90	67	780mL	S035	79	0	4,2	J	N	65	IV	1	DRY
66	250	780mL	S035	79	0	4,3	J	N	65	IV	0,1	DRY
80	122	780mL	S035	79	0	4,3	J	N	65	IV	0,3	DRY
84	248	780mL	S035	79	0	4,4	J	CA	65	IV	0,5	DRY
84	96	780mL	S035	79	0	4,6	J	N	65	IV	0,1	DRY
45	43	780mL	S035	79	0	4,65	J	N	65	IV	0,01	DRY
55	54	780mL	S035	79	0	4,7	J	N	65	IV	0,2	DRY
82	66	780mL	S035	79	0	4,9	J	CA	65	IV	2,5	DRY

59	88	780mL	S035	79	0	5,5	J	FEO	65	IV	0,3	DRY
86	76	780mL	S035	79	0	5,7	J	FEO	65	IV	2,5	DRY
80	64	780mL	S035	79	0	6	J	FEO	65	IV	5	DRY
85	65	780mL	S035	79	0	6,7	J	N	65	IV	3	DRY
88	242	780mL	S035	79	0	6,75	J	N	65	IV	1,6	DRY
88	256	780mL	S035	79	0	7,1	J	N	65	IV	1,5	DRY
84	74	780mL	S035	79	0	7,4	J	N	65	IV	0,2	DRY
13	78	780mL	S035	79	0	7,5	J	N	65	IV	0,3	DRY
86	68	780mL	S035	79	0	7,7	J	N	65	IV	1,5	DRY
88	66	780mL	S035	79	0	8,3	J	N	65	IV	0,4	DRY
78	60	780mL	S035	79	0	8,45	J	N	65	IV	0,2	DRY
76	73	780mL	S035	79	0	8,6	J	FEO	65	IV	0,6	DRY
72	65	780mL	S035	79	0	8,7	J	N	65	IV	0,3	DRY
75	62	780mL	S035	79	0	8,75	J	N	65	IV	0,3	DRY
82	65	780mL	S035	79	0	8,8	J	FEO	65	IV	0,6	DRY
88	55	780mL	S035	79	0	8,9	J	FEO	65	IV	0,4	DRY
90	51	780mL	S035	79	0	8,95	J	FEO	65	IV	1,5	DRY
86	235	780mL	S035	79	0	9,1	J	FEO	65	IV	0,4	DRY
88	285	780mL	S035	79	0	9,1	J	FEO	65	IV	1,5	DRY
85	62	780mL	S035	79	0	9,1	J	FEO	65	IV	2	DRY
80	72	780mL	S035	79	0	9,35	J	FEO	65	IV	1	DRY
34	25	780mL	S035	79	0	9,8	J	N	65	IV	0,1	DRY
68	282	780mL	S035	79	0	10,05	J	N	65	IV	0,2	DRY
70	74	780mL	S035	79	0	10,4	B	FEO	65	IV	2	DRY
67	80	780mL	S035	79	0	11	J	N	65	IV	1	DRY
69	55	780mL	S035	79	0	11,2	B	N	65	IV	0,1	DRY
83	142	780mL	S035	79	0	11,5	J	N	65	IV	0,2	DRY
70	77	780mL	S035	79	0	11,6	J	FEO	65	IV	3	DRY
80	247	780mL	S035	79	0	11,95	J	N	65	IV	0,5	DRY
80	247	780mL	S035	79	0	1196	J	N	65	IV	0,15	DRY
75	80	780mL	S035	79	0	12	J	N	65	IV	0,3	DRY
74	335	780mL	S035	79	0	12,45	J	N	65	IV	1,5	DRY
86	245	780mL	S035	79	0	12,55	J	N	65	IV	2	DRY
87	66	780mL	S035	79	0	12,6	J	N	65	IV	0,3	DRY
86	246	780mL	S035	79	0	12,75	J	N	65	IV	1,5	DRY
80	245	800mL	S035	79	0	12,9	J	N	65	IV	0,45	DRY
77	245	800mL	S035	79	0	13	J	N	65	IV	0,6	DRY
19	80	800mL	S035	79	0	13,5	J	FEO	65	IV	2	DRY
59	90	800mL	S035	79	0	13,7	J	N	65	IV	0,1	DRY
70	358	800mL	S035	79	0	14,1	J	N	65	IV	0,2	DRY
85	67	800mL	S035	79	0	14,3	J	N	65	IV	2,5	DRY
83	70	800mL	S035	79	0	14,4	J	N	65	IV	1,5	DRY
86	70	800mL	S035	79	0	14,5	J	N	65	IV	1,6	DRY
79	113	800mL	S035	79	0	14,7	J	N	65	IV	2	DRY
80	113	800mL	S035	79	0	15,1	J	N	65	IV	0,5	DRY
79	113	800mL	S035	79	0	15,2	J	N	65	IV	0,5	DRY
90	63	800mL	S035	79	0	15,6	J	N	65	IV	0,3	DRY
90	38	800mL	S035	79	0	15,7	J	N	65	IV	0,4	DRY

83	42	800mL	S035	79	0	15,75	J	FEO	65	IV	0,2	DRY
86	221	800mL	S035	79	0	15,8	J	N	65	IV	0,2	DRY
86	230	800mL	S035	79	0	16	J	N	65	IV	0,5	DRY
90	296	800mL	S035	79	0	16,6	J	N	65	IV	0,1	DRY
90	294	800mL	S035	79	0	16,8	J	N	65	IV	0,1	DRY
73	43	800mL	S035	79	0	17	J	N	65	IV	0,3	DRY
65	62	800mL	S035	79	0	17,3	J	FEO	65	IV	0,1	DRY
87	54	800mL	S035	79	0	17,65	J	N	65	IV	2	DRY
69	10	800mL	S035	79	0	17,9	B	FEO	65	IV	0,4	DRY
88	32	800mL	S035	79	0	17,9	J	FEO	65	IV	2,5	DRY
82	57	800mL	S035	79	0	18	J	FEO	65	IV	2,5	DRY
71	66	800mL	S035	79	0	18,05	B	N	65	IV	0,2	DRY
85	52	800mL	S035	79	0	18,2	J	N	65	IV	0,4	DRY
90	45	800mL	S035	79	0	18,25	J	N	65	IV	0,4	DRY
75	43	800mL	S035	79	0	18,5	J	N	65	IV	0,3	DRY
65	124	800mL	S035	79	0	18,9	J	N	65	IV	0,1	DRY
81	244	800mL	S035	79	0	19	J	N	65	IV	0,2	DRY
60	295	800mL	S035	79	0	19,1	B	N	65	IV	0,2	DRY
79	120	800mL	S035	79	0	19,2	J	N	65	IV	0,2	DRY
77	61	800mL	S035	79	0	19,45	J	FEO	65	IV	0,6	DRY
72	76	800mL	S035	79	0	19,8	J	FEO	65	IV	2,5	DRY
78	65	800mL	S035	79	0	20	J	FEO	65	IV	2,5	DRY
85	71	800mL	S036	152	7	0	J	FEO	65	IV	4	DRY
70	56	800mL	S036	152	7	0,2	J	FEO	65	IV	3	DRY
70	54	800mL	S036	152	7	0,4	J	N	65	IV	0,4	DRY
82	54	800mL	S036	152	7	0,45	J	N	65	IV	0,4	DRY
80	52	800mL	S036	152	7	0,55	J	N	65	IV	2	DRY
75	45	800mL	S036	152	7	0,7	J	N	65	IV	0,1	DRY
85	61	800mL	S036	152	7	0,72	J	N	65	IV	0,2	DRY
68	58	800mL	S036	152	7	0,8	B	N	65	IV	2	DRY
72	40	800mL	S036	152	7	1	J	N	65	IV	5	DRY
75	36	800mL	S036	152	7	1,3	J	N	65	IV	0,4	DRY
75	44	800mL	S036	152	7	1,5	J	N	65	IV	2	DRY
75	63	800mL	S036	152	7	1,7	J	N	65	IV	2	DRY
31	15	800mL	S036	152	7	1,9	J	N	65	IV	0,4	DRY
68	103	800mL	S036	152	7	2,3	B	N	65	IV	0,1	DRY
50	123	800mL	S036	152	7	2,5	J	N	65	IV	0,5	DRY
37	162	800mL	S036	152	7	2,55	J	N	65	IV	0,1	DRY
57	156	800mL	S036	152	7	3,1	J	N	65	IV	0,2	DRY
67	163	800mL	S036	152	7	3,2	B	N	65	IV	0,2	DRY
60	152	800mL	S036	152	7	3,3	B	N	65	IV	0,1	DRY
86	83	800mL	S036	152	7	3,4	J	N	65	IV	0,1	DRY
59	350	800mL	S036	152	7	3,45	J	N	65	IV	0,05	DRY
68	285	800mL	S036	152	7	3,5	B	N	65	IV	0,1	DRY
83	305	800mL	S036	152	7	3,6	J	N	65	IV	0,1	DRY
77	305	800mL	S036	152	7	3,7	J	N	65	IV	0,1	DRY
58	340	800mL	S036	152	7	3,82	J	N	65	IV	0,1	DRY
69	330	800mL	S036	152	7	3,9	J	N	65	IV	0,2	DRY

60	337	800mL	S036	152	7	4,65	B	QTZ	65	IV	0,1	DRY
85	20	800mL	S036	152	7	4,75	J	N	65	VII	1,5	DRY
74	356	800mL	S036	152	7	5,2	J	QTZ	65	IV	0,1	DRY
74	350	800mL	S036	152	7	5,5	J	QTZ	65	IV	0,1	DRY
63	345	800mL	S036	152	7	5,7	J	QTZ	65	IV	0,1	DRY
15	342	800mL	S036	152	7	6	J	QTZ	65	IV	0,1	DRY
65	342	800mL	S036	152	7	6,32	J	N	65	IV	0,1	DRY
74	340	800mL	S036	152	7	6,75	B	QTZ	65	IV	0,1	DRY
81	355	800mL	S036	152	7	7,3	J	QTZ	65	IV	0,4	DRY
89	352	800mL	S036	152	7	7,5	J	QTZ	65	IV	0,2	DRY
89	93	800mL	S036	152	7	7,7	J	N	65	IV	0,1	DRY
63	343	800mL	S036	152	7	7,8	J	N	65	IV	0,2	DRY
74	347	800mL	S036	152	7	7,95	B	N	65	IV	1,5	DRY
61	9	800mL	S036	152	7	8,35	J	N	65	IV	0,05	DRY
88	248	800mL	S038	84	0	2,78	J	FEO	85	IV	0,4	DRY
86	218	800mL	S038	84	0	2,82	J	FEO	85	IV	0,15	DRY
86	88	800mL	S038	84	0	3	J	N	85	IV	0,2	DRY
86	28	800mL	S038	84	0	3,1	J	N	85	IV	0,1	DRY
67	100	800mL	S038	84	0	3,45	J	N	85	IV	0,2	DRY
68	8	800mL	S038	84	0	3,9	B	N	85	IV	0,4	DRY
87	92	800mL	S038	84	0	4,25	J	N	85	IV	2	DRY
86	71	800mL	S038	84	0	4,3	J	N	85	IV	0,25	DRY
83	22	800mL	S038	84	0	4,48	J	N	85	IV	0,15	DRY
79	71	800mL	S038	84	0	4,5	J	N	85	IV	0,4	DRY
88	100	800mL	S038	84	0	4,4	J	N	85	IV	0,1	DRY
80	41	800mL	S038	84	0	9,5	J	N	85	IV	1	DRY
60	50	800mL	S038	84	0	10,1	B	N	85	IV	0,5	DRY
67	40	800mL	S038	84	0	10,25	J	N	85	IV	0,5	DRY
77	54	800mL	S038	84	0	10,43	J	N	85	IV	1,2	DRY
76	63	800mL	S038	84	0	10,64	J	N	85	IV	0,15	DRY

12.2 Appendix B: Part of the collar table used in the database

	A	B	C	D	E	F
1	BHID	XCOLLAR	YCOLLAR	ZCOLLAR	EOH	HOLE PATH
2	BPN 870	4135.631	39008.779	606.053	146	curved
3	BPN 871	4134.978	39006.106	806.178	141.5	curved
4	BPN 872	4135.458	39006.872	806.695	111	curved
5	BPN 873	4135.697	39009.451	607.01	172	curved
6	BPN 874	4135.574	38999.362	606.2	170	curved
7	BPN 875	4136.544	39009.281	606.521	165	curved
8	BPN 876	4135.796	39009.964	606.227	184	curved
9	BPN 877	4026.412	38785.797	577.674	133	curved
10	BPN 878	4027.877	38787.668	577.666	177	curved
11	BPN 879	4036.949	38785.219	577.381	191	curved
12	BPN 880	4153.765	39063.541	606.739	178.5	curved
13	BPN 881	4148.75	39063.158	606.801	182.5	curved
14	BPN 882	4173.089	39064.148	607.618	167	curved
15	BPN 883	4177.245	39064.644	607.881	162	curved
16	BPN 884	4073.06	39001.165	580.585	270	curved
17	BPN 885	4073.21	39002.448	580.521	253	curved
18	BPN 886	4114.368	39180.112	582.217	72	curved
19	BPN 887	4108.815	39149.948	581.874	150	curved
20	BPN 888	4113.437	39149.498	581.965	112.5	curved
21	BPN 889	4089.663	39093.475	581.045	100.5	curved
22	BPN 890	4060.846	39095.415	581.054	235	curved
23	BPN 891A	3924.372	38877.72	580.379	20	curved
24	BPN 891B	3923.302	38878.446	580.451	305	curved

12.3 Appendix C: Part of the survey table used in the database creation

1	BHID	AT	DIP	BRG
2	BPN870	0	1.19	314.72
3	BPN871	0	3.52	297.77
4	BPN872	0	12.72	296.72
5	BPN873	0	15.13	316.38
6	BPN874	0	8.2	272.3
7	BPN875	0	12.83	321.82
8	BPN876	0	2.9	321.5
9	BPN877	0	3.77	283.91
10	BPN878	0	3.67	320.42
11	BPN879	191	-0.44	343.22
12	BPN880	0	-0.46	7.04
13	BPN881	0	1.05	337.61
14	BPN882	167	2.39	18.7
15	BPN883	162	2.5	40.89
16	BPN884	270	1.1	257.25
17	BPN885	253	7.35	300.27
18	BPN886	72	0.85	7.23
19	BPN887	133	0.7	329.43
20	BPN888	112.55	1.57	42.53
21	BPN889	100.5	2.92	292.7

12.4 Appendix D: Part of the geology table used in the database creation

1	BHID	FROM	TO	LITHO
2	BPN 870	0	56.6	FWS
3	BPN 870	56.6	123.6	FWC
4	BPN 870	123.6	143.3	OSU
5	BPN 870	143.3	146	HWQ
6	BPN 871	0	48.4	FWS
7	BPN871	48.4	82.8	FWC
8	BPN 871	82.8	122.2	OSU
9	BPN 871	122.2	141.5	HWQ
10	BPN 872	0	32.5	FWS
11	BPN872	32.5	52.2	FWC
12	BPN 872	52.2	71.1	OSU
13	BPN 872	71.1	75.2	HWQ
14	BPN 872	75.2	84.6	OSU
15	BPN 872	84.6	111	HWQ
16	BPN 873	0	30.5	FWS
17	BPN873	30.5	50	FWC
18	BPN 873	50	70.5	OSU
19	BPN 873	70.5	74.04	HWQ
20	BPN 873	74.04	82.01	OSU
21	BPN 873	82.01	156	HWQ

12.5 Appendix E: Validation report for the geology table

	A	B	C	D	E
1	Database Management - Database Load Report May 16	2022			
2					
3	Date : 16-May-22				
4	Database : 2520mw_konkola_east				
5	Format_file : validation report.dsc				
6					
7	==========				
8					
9					
10					
11	Loading Table : geology from file geology_nose.csv				
12	Warning: "depth_from" is not numeric				
13	Warning: "depth_to" is not numeric				
14	BHID	FROM	TO	LITHO	
15	Warning: Hole ID does not exist in the collar table				
16	BPN873	30.5	50	FWC	
17	Warning: depth_to exceeds maximum depth of (133.00) for this hole				
18	BPN 877	83.5	133.5	HWQ	
19	Warning: depth_to exceeds maximum depth of (112.50) for this hole				
20	BPN 888	102.23	112.55	HWQ	
21					
22					
23	0 records were inserted.				
24	155 records were updated.				
25	3 records were rejected.				
26					
27	Performing sample overlap checks				
28	Sample () from hole (DVN1589) with interval (6.00 - 52.50)				
29	overlaps previous sample () with interval (0.00 - 29.50)				
30	overlapping sample check complete				
31					
32					
33	Page 1 of 1				

12.6 Appendix F: Volume report of the ore shale in each block modeled

Block 1

SOLID MODELLING OBJECT REPORT
Layer Name: oreshale_lithologyblock1.dtm
Object: 8
Trisolation: 8
Validated = true
Status = solid
Trisolation Extents
X Minimum: 3743.552 X Maximum: 4061.540
Y Minimum: 39161.139 Y Maximum: 39361.455
Z Minimum: 565.971 Z Maximum: 614.504
Surface area: 91142
Volume : 464569

Block 2

SOLID MODELLING OBJECT REPORT
Layer Name: oreshale_lithologyblock2.dtm
Object: 8
Trisolation: 8
Validated = true
Status = solid
Trisolation Extents
X Minimum: 3891.205 X Maximum: 4154.806
Y Minimum: 39152.527 Y Maximum: 39311.222
Z Minimum: 566.000 Z Maximum: 605.000
Surface area: 43704
Volume : 149984

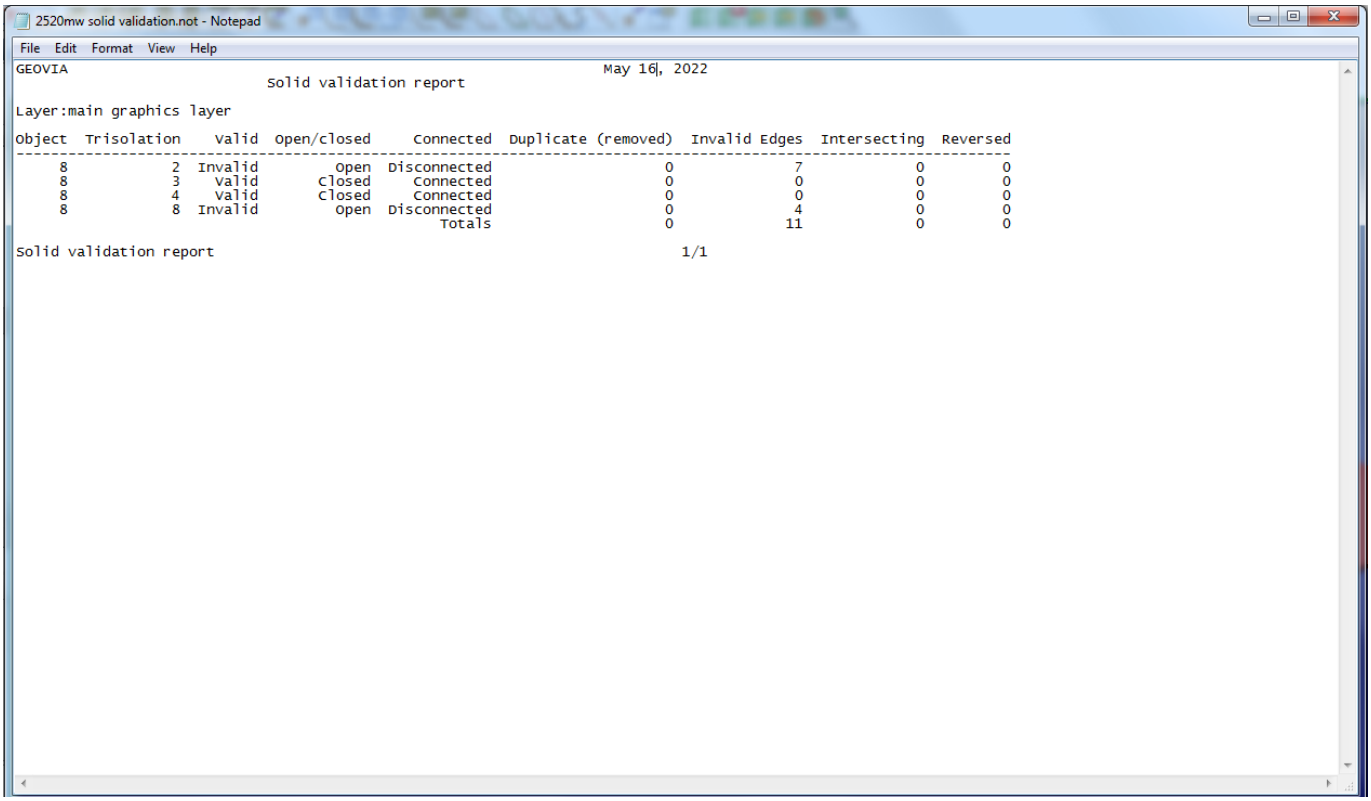
Block 3

SOLID MODELLING OBJECT REPORT
Layer Name: oreshalelithology_block3.dtm
Object: 8
Trisolation: 8
Validated = true
Status = solid
Trisolation Extents
X Minimum: 4025.319 X Maximum: 4195.614
Y Minimum: 39084.167 Y Maximum: 39276.392
Z Minimum: 565.690 Z Maximum: 627.718
Surface area: 28356
Volume : 124460

Block 4

SOLID MODELLING OBJECT REPORT
Layer Name: oreshale_block4lithology.dtm
Object: 8
Trisolation: 8
Validated = true
Status = solid
Trisolation Extents
X Minimum: 4106.647 X Maximum: 4448.012
Y Minimum: 39095.717 Y Maximum: 39277.234
Z Minimum: 563.883 Z Maximum: 629.854
Surface area: 70419
Volume : 293186

12.7 Appendix G: Validation report of the created solids for the ore shale lithology



2520mw solid validation.not - Notepad

File Edit Format View Help

GEOVIA May 16, 2022

Solid validation report

Layer:main graphics layer

Object	Trisolation	Valid	Open/closed	Connected	Duplicate (removed)	Invalid Edges	Intersecting	Reversed
8	2	Invalid	Open	Disconnected	0	7	0	0
8	3	Valid	Closed	Connected	0	0	0	0
8	4	Valid	Closed	Connected	0	0	0	0
8	8	Invalid	Open	Disconnected	0	4	0	0
				Totals	0	11	0	0

Solid validation report 1/1